Universitat Autònoma de Barcelona

Printing Technologies for Biotechnological and Environmental Sensing Applications

Roberto Pol Arcas

Universitat Autònoma
de Barcelona

Printing Technologies for Biotechnological and Environmental Sensing Applications

Roberto Pol Arcas

PhD Thesis in Chemistry

Directed by:

Dr. María del Mar Baeza Labat
Dr. Francisco Céspedes Mulero

Chemistry Departmet

Science Faculty

June 2019

Universitat Autònoma de Barcelona

PhD thesis:

Printing Technologies for Biotechnological and Environmental Sensing Applications

was presented to achieve the PhD grade by:

Roberto Pol Arcas

Dr. María del Mar Baeza and Dr. Francisco Céspedes Mulero give approval to the following PhD thesis:

Dr. María del Mar Baeza

Dr. Francisco Céspedes Mulero

All the presented work throughout this PhD thesis was performed thanks to the following financial support:

- ***Personal Investigador en Formación (PIF)*** grant awarded by the Autonomous University of Barcelona.
- **Development of a comprehensive treatment process for SOx and NOx from flue gas addressed to waste gases valorization.** (CTQ2015-69802-C2-1-R) research project from the Spanish *Ministerio de Economía y Competitividad y Fondo Europeo de Desarrollo Regional* (MINECO/FEDER, UE).

“One often meets his destiny on the road he takes to avoid it”

Master Oogway

ACKNOWLEDGEMENTS

These are the last words of the PhD thesis. There are few hours left for the delivery of the memory and there is too much to thanks to too many people. Although I am the one presenting this PhD thesis, the work shown here was performed thanks to the collaboration of a big team composed by supervisors, external collaborators and undergraduate students. The trust that supervisors have put on me (they allowed me to do a lot of crazy stuff) and their help will be always present in my mind. They have constantly helped me with any problems which appeared throughout the course of the thesis and I have learned a lot of their experience. It is important also to acknowledge someone that has contributed as a supervisor (although it does not appear as one) and thanks to him I was able to end up doing this printing technologies thesis. I encourage everyone to work with external experts opening collaborations. There are a lot of people that work on complementary areas that have tremendous knowledge that surely, improve the work that a person alone can produce and is a beautiful way to meet interesting people which finally I can call them friends. Students have helped me not only to start proving the concepts of the experiments performed, but also helped me to improve my managing skills. Moreover, although not involved in any aspect of the thesis, I cannot forget about my previous mentors that introduced me to the scientific community.

There is a lot of people that has contributed to the PhD thesis in a “different” manner. I am talking about lab mates and friends. There is one person that has gone alongside with me during the PhD thesis and has become one of my closest friends. I have met a lot of people during this period and enjoyed overmuch social activities which made the thesis completely bearable. Moreover, the cafeteria staff which have been taking care of me daily is acknowledged.

Finally, acknowledge my family which have always been by myside and guided me through the process. It has always been really fun to try to explain what I was doing at work and see their reaction.

Mire mola se merece una ola (internal joke).

TABLE OF CONTENT

ABBREVIATIONS AND SYMBOLS

3D	Three-Dimensional
3D-SSMP	3D-Printed Sulfide-Selective Microfluidic Platform
ALS	Ambient Light Sensor
BDD	Boron-Doped Diamond
CFA	Continuous Flow Analysis
DS	Drop Spacing
EDX	Energy Dispersive X-ray Spectroscopy
FIA	Flow Injection Analysis
IPSSE	Inkjet-Printed Sulfide-Selective Electrode
LED	Light-emitting diode
LOC	Lab-On-a-Chip
MTB	Methylthymol blue
PEN	Polyethylene Naphthalate
PLA	Polylactic Acid
rFIA	Reverse Flow Injection Analysis
SAOB	Sulfide Antioxidant Buffer
SEM	Scanning Electron Microscopy
SPSSE	Screen-Printed Sulfide-Selective Electrode
UASB	Upflow Anaerobic Sludge Blanket

THESIS ABSTRACT

Modern industrial activities have left wide-spread hazardous pollution in soil, air and water across the globe. Emissions of SOx coming from flue gases require treatment before their release into the environment. Conventional physic-chemical treatments used hitherto are expensive and time-consuming. Moreover, those treatments also generate wastewater that requires further processing. To overcome the SOx treatment challenge, a new approach using environmentally friendly biological method is proposed. The process is based on a selective adsorption of SOx, followed by a two-stage biological treatment. Once the SOx are adsorbed they undergo a first biocatalytic stage, in which sulfate-reducing microorganisms catalyze their conversion into hydrogen sulfide. Afterwards, a second biocatalytic stage by sulfide-oxidizing microorganisms is done, finally obtaining elemental sulfur.

A crucial point to address in this biotechnological process is the real-time quantification of sulfur species before and after each biocatalytic stage. Conventional methods, such as gravimetry, turbidimetry, nephelometry, capillary electrophoresis and ionic chromatography have been widely used for sulfur species quantification. Although those methods have been overwhelmingly implemented a few decades ago, they are not suitable of in situ real-time measurements, require trained personnel and they are costly and time consuming. Therefore, there is a need to provide new analytical systems that can replace conventional ones.

Microfluidic platforms have been extensively studied due to their possibility of replacing a fully equipped conventional laboratory. Well-known advantages of these microfluidic sensing systems include: compactness, low sample consumption, low-cost production, better overall monitoring and process control, real-time analysis and a fast response. These characteristics open the possibility of performing in situ and real-time measurements. Also, they operate in such a manner that sample pre-treatment as well as chemical assay can be performed therein. Their ergonomic and user-friendly design allows them to be easily adapted to perform a desired analysis just by simply modifying the geometry of the channels. These features make microfluidics of interest in processes that require multiple analyses at the same time.

Several microfabrication techniques (e.g., micromachining, hot embossing, injection molding, laser ablation, micromilling and soft lithography) and materials (e.g., silicon, polymers, metals, ceramics, etc.) have been used for the production of miniaturized analytical systems. Nonetheless, all these methods require trained personnel and are expensive and time

consuming. Moreover, they require further processing steps (e.g., etching, sealing, etc.) after the fabrication. Nowadays, scientists have been exploring new methodologies to produce such analytical systems in a more feasible and cheaper manner.

In this thesis, the use of printing technologies (inkjet printing, screen-printing and 3D printing) to produce analytical platforms for quantification of relevant chemical compounds in biotechnological reactors and in the environment (S^{2-}, SO_4^{2-} and NO_2^-) are promoted. Hence, the state-of-the-art of microfluidic devices and the printed analytical systems have been widely developed:

- There is a global concern about the environmental impact of pollutants derived from their widespread use and subsequent persistence in the environment. In this context, attempts to develop novel methods and technologies for detection of pollutants in real-time have attracted many attentions. The ever-increasing demand of remote autonomous field deployable analytical systems has become the driving force behind the different strategies born. Microfluidic lab-on-a-chip platforms excel, offering continuous tracking of chemical agents in an integrated miniaturized fashion. The latest developments in environmental monitoring devices and future perspectives are discussed.

- The two-step fabrication of the first inkjet-printed sulfide-selective electrode (IPSSE) is described. The two-step fabrication consists of printing a silver electrode followed by an electrochemical deposition of sulfide to produce a second kind electrode (Ag/Ag_2S). The performance of this novel device was tested using potentiometric measurements. Nernstian response (-29.4 ± 0.3 mV·decade^{-1}) was obtained within concentrations of 0.03-50 mM with a response time of ~3 s. Furthermore, river and sea-spiked environmental samples and samples from a bioreactor for sulfate reduction to sulfide were measured and compared against a commercial sensor giving no significant differences. The IPSSE described in this work showed good reproducibility and durability during daily measurements over 15 days without any special storage conditions. Considering all the current challenges in inkjet-printed ion-selective electrodes, this alternative fabrication approach opens a new perspective for mass production of all-solid-state ion-selective electrodes.

- The production of a 3D-printed microfluidic platform with integrated potentiometric detection is described. The device contains completely integrated therein a second kind sulfide-selective electrode (Ag/Ag_2S) and a pseudo-reference electrode (Ag/AgCl). This could be accomplished by splitting the 3D printing stage in two and screen printing the electrodes. Then, the electrodes were morphologically characterized while the device was characterized in terms of its analytical response. Furthermore, tap/river/sea-spiked water samples and wastewater from a biotechnological process were measured and compared against a commercial sensor giving no significant differences. Considering all the current challenges in the fabrication of 3D-printed microfluidic platforms with electrochemical detection for environmental and biotechnological screening applications, this appealing approach could constitute a new paradigm in the production of functional monitoring devices.

- A microfluidic system was designed for sulphate ion determination in wastewater from a biotrickling filter operating in reverse flow injection analysis. This microfluidic system integrates the reaction, conditioning and detection in a three-platform system fabricated by means of 3D printing. The sensing working principle relied on a colorimetric change caused by the displacement of barium by its precipitation with sulphate in a barium ion-containing complex. The performance of this well-known colorimetric method (Methylthymol blue method), which has been widely used in batch analysis, is now tested in continuous flow. The analytical performance revealed a linear behavior for concentrations between 10- 80 $mg \cdot L^{-1}$ of sulphate ion and a limit of detection of 8 $mg \cdot L^{-1}$. These new microfluidic platforms system for sulphate monitoring in real-time could find uses not only in biotechnological processes, but also in environmental and biomedical fields.

- Nitrogen-based chemicals represent one of the most important family compounds in freshwater and marine ecosystems. Nitrogen cycle is responsible of spread nitrogen compounds all over the environment in an equilibrium manner. Industrial human's activities have harshly contributed to the disruption of nitrogen cycle and its consequences have severely affected earth ecosystems. Tracking the chemicals involved in the nitrogen cycle have become a crucial point to fight against eutrophication and global water acidification. A smartphone readout-based system has been developed to determine the concentration of nitrite ion (the nitrogen compound

that possess higher toxicity) in environmental samples. The device was fabricated by means of 3D printing to allow easy design modification to fit any smartphone. Moreover, the system took advantage of the less explored potential of ambient light sensor contained within the smartphones. Finally, "ALSens" application was developed to be used by non-trained personnel to not only determine nitrite concentration but also to automatically send relevant parameters (analyte, day, hour, location and concentration) of the assay for tracking purposes to an open online database allowing a worldwide mapping of nitrite ion concentration. Considering the devastating implications of nitrogen cycle disruption, these novel systems for nitrite screening will suddenly become a global monitoring standard approach.

RESUMEN

Las actividades industriales han dejado contaminación en el suelo, el aire y el agua en todo el mundo. Las emisiones de SOx provenientes de gases de combustión requieren tratamiento antes de su liberación al medio ambiente. Los tratamientos fisicoquímicos convencionales utilizados hasta ahora son costosos y requieren mucho tiempo. Además, esos tratamientos también generan aguas residuales que requieren un procesamiento adicional. Para superar el desafío del tratamiento de SOx, se propone un nuevo enfoque que utiliza un método biológico respetuoso con el medio ambiente. El proceso se basa en una adsorción selectiva de SOx, seguida de un tratamiento biológico de dos etapas. Una vez adsorbidos los SOx, se someten a una primera etapa biocatalítica, en la que los microorganismos reductores de sulfato catalizan su conversión en sulfuro de hidrógeno. Posteriormente, se realiza una segunda etapa biocatalítica por microorganismos oxidantes de sulfuro, obteniendo finalmente azufre elemental.

Un punto crucial que tratar en este proceso biotecnológico es la cuantificación en tiempo real de las especies de azufre antes y después de cada etapa biocatalítica. Los métodos convencionales, tales como la gravimetría, la turbidimetría, la nefelometría, la electroforesis capilar y la cromatografía iónica se han utilizado para la cuantificación de especies de azufre. Aunque esos métodos se han implementado de manera abrumadora hace unas décadas, no son adecuados para mediciones *in situ* y en tiempo real, requieren personal capacitado, son costosos y consumen mucho tiempo. Por lo tanto, existe la necesidad de proporcionar nuevos sistemas analíticos que puedan reemplazar a los convencionales.

Las plataformas microfluídicas se han estudiado debido a su posibilidad de reemplazar un laboratorio convencional totalmente equipado. Las ventajas bien conocidas de estos sistemas de detección incluyen: compacidad, bajo consumo de muestra, producción de bajo coste, mejor monitoreo y control de procesos, análisis en tiempo real y una respuesta rápida. Estas características abren la posibilidad de realizar medidas *in situ* y en tiempo real. Además, funcionan de tal manera que el pretratamiento de la muestra y el ensayo químico se pueden realizar en su interior. Su diseño ergonómico y fácil de usar les permite adaptarse fácilmente para realizar el análisis deseado simplemente modificando la geometría de los canales. Estas características hacen que la microfluídica sea de interés en procesos que requieren múltiples análisis al mismo tiempo.

Para la producción de sistemas analíticos miniaturizados se han utilizado varias técnicas de microfabricación (por ejemplo, micromaquinado, estampado en caliente, moldeo por inyección, ablación por láser, micromilling y litografía) y materiales (por ejemplo, silicio, polímeros, metales, cerámica, etc.). No obstante, todos estos métodos requieren personal capacitado, son costosos y requieren mucho tiempo. Además, requieren más pasos de procesamiento (por ejemplo, grabado químico, sellado, etc.) después de la fabricación. Hoy en día, los científicos han estado explorando nuevas metodologías para producir tales sistemas analíticos de una manera más factible y más barata.

En esta tesis, se promueve el uso de tecnologías de impresión (impresión por chorro de tinta, serigrafía e impresión 3D) para producir plataformas analíticas para la cuantificación de compuestos químicos relevantes en reactores biotecnológicos y en el medio ambiente (S^{2-}, SO_4^{2-} and NO_2^-). Por lo tanto, el estado del arte de los dispositivos microfluídicos y los sistemas analíticos impresos se han desarrollado ampliamente:

- Existe una preocupación mundial sobre el impacto ambiental de los contaminantes derivados de su uso generalizado y subsiguiente persistencia en el medio ambiente. En este contexto, los intentos de desarrollar nuevos métodos y tecnologías para la detección de contaminantes en tiempo real han atraído mucha atención. La creciente demanda de sistemas analíticos de campo autónomos con control remoto se ha convertido en la fuerza impulsora detrás de las diferentes estrategias nacidas. Las plataformas microfluídicas de laboratorio en un chip son excelentes y ofrecen un seguimiento continuo de los agentes químicos de forma miniaturizada integrada. Se discutirán los últimos desarrollos en dispositivos de monitoreo ambiental y perspectivas futuras.

- Se describe la fabricación en dos etapas del primer electrodo selectivo de sulfuro impreso por inyección de tinta (IPSSE). La fabricación en dos pasos consiste en imprimir un electrodo de plata seguido de una deposición electroquímica de sulfuro para producir un electrodo de segunda especie (Ag/Ag_2S). El rendimiento de este nuevo dispositivo se probó utilizando medidas potenciométricas. La respuesta Nernstiana (-29.4 ± 0.3 mV · década^{-1}) se obtuvo en concentraciones de 0.03-50 mM con un tiempo de respuesta de ~ 3 s. Además, se midieron las muestras ambientales de río y mar, y las muestras de un biorreactor para la reducción de sulfato a sulfuro y se compararon con un sensor comercial sin que mostrasen diferencias significativas. El IPSSE descrito en este trabajo mostró una buena reproducibilidad y durabilidad durante las medidas

diarias a lo largo de 15 días sin condiciones especiales de almacenamiento. Teniendo en cuenta todos los desafíos actuales en electrodos selectivos de iones impresos por inyección de tinta, este enfoque alternativo de fabricación abre una nueva perspectiva para la producción en masa de electrodos selectivos de iones de estado sólido.

- Se describe la producción de una plataforma de microfluidos impresa en 3D con detección potenciométrica integrada. El dispositivo contiene completamente integrado un electrodo selectivo de sulfuro de segunda especie (Ag/Ag_2S) y un electrodo de pseudo-referencia (Ag/AgCl). Esto se lograrse dividiendo la etapa de impresión 3D en dos e imprimiendo los electrodos utilizando una máscara. Los electrodos se caracterizaron morfológicamente, mientras que el dispositivo se caracterizó en términos de su respuesta analítica. Además, se midieron las muestras de agua del grifo/río/mar y aguas residuales de un proceso biotecnológico y se compararon con un sensor comercial sin mostrar diferencias significativas. Teniendo en cuenta todos los desafíos actuales en la fabricación de plataformas microfluídicas impresas en 3D con detección electroquímica para aplicaciones de detección ambiental y biotecnológica, este enfoque atractivo podría constituir un nuevo paradigma en la producción de dispositivos funcionales de monitoreo.

- Se diseñó un sistema de microfluidica para la determinación de iones de sulfato en aguas residuales de un filtro de goteo que funciona por análisis de inyección de flujo inverso. Este sistema microfluídico integra la reacción, el acondicionamiento y la detección en un sistema de tres plataformas fabricadas mediante impresión 3D. El principio de funcionamiento de la detección se basó en un cambio colorimétrico causado por el desplazamiento de bario por su precipitación con sulfato en un complejo que contiene ion bario. El rendimiento de este método colorimétrico bien conocido (método del azul de metiltimol) se prueba en flujo continuo. El rendimiento analítico reveló un comportamiento lineal para concentraciones entre 10-80 $mg \cdot L^{-1}$ de ion sulfato y un límite de detección de 8 $mg \cdot L^{-1}$. Este nuevo sistema de plataformas microfluídicas para el monitoreo de sulfatos en tiempo real podría encontrar usos no solo en procesos biotecnológicos, sino también en medioambiente y biomedicina.

- Los productos químicos basados en nitrógeno representan uno de los compuestos familiares más importantes en los ecosistemas marinos y de agua dulce. El ciclo del

nitrógeno es responsable de la propagación de compuestos de nitrógeno en todo el medio ambiente de manera equilibrada. Las actividades industriales han contribuido duramente a la interrupción del ciclo del nitrógeno y sus consecuencias han afectado gravemente a los ecosistemas terrestres. El seguimiento de los productos químicos involucrados en el ciclo del nitrógeno es crucial para luchar contra la eutrofización y la acidificación global del agua. Se ha desarrollado un sistema basado en la lectura de teléfonos inteligentes para determinar la concentración de ion nitrito (el compuesto de nitrógeno que posee mayor toxicidad) en muestras ambientales. El dispositivo fue fabricado por medio de impresión 3D para permitir una fácil modificación del diseño para adaptarse a cualquier teléfono inteligente. Además, el sistema aprovechó el potencial inexplorado del sensor de luz ambiental contenido en los teléfonos. Finalmente, la aplicación "ALSens" fue desarrollada para ser utilizada por personal no capacitado, no solo para determinar la concentración de nitrito, sino también para enviar automáticamente los parámetros relevantes (analito, día, ubicación, concentración) del ensayo con fines de seguimiento a una base de datos online. Base de datos que permite un mapeo mundial de la concentración de iones de nitrito. Teniendo en cuenta las consecuencias devastadoras de la interrupción del ciclo del nitrógeno, estos nuevos sistemas para la detección de nitritos se volverán un estándar de monitoreo global.

CHAPTER 1

Introduction

1.1. Analytical chemistry

Information is power "*scientia potentia est*". This term has been widely discussed in the society from several points of view. It is true that information gives you the power to act accordingly to a situation and therefore take advantage. However, bare information without the knowledge to process it does not constitute a benefit.[1]

Analytical chemistry is the branch of chemistry that uses devices or instruments to separate, identify and quantify matter. The information given by an analytical assay with the corresponding knowledge allows scientist to act if required. For instance, a bad treated industry wastewater that is poured to a river may contain pollutants that upon tracking them throughout the river might help to maintain a decontaminated environment.[2] Nowadays, the importance of analytical chemistry is increasing as it crucial to solve industrial, environmental, biomedical and social challenges.[3,4,5] Considering that fact, there is a growing demand for analytical information obtained through autonomous, robust and transportable analysis devices. Consequently, there is a growing demand on the production of functional platforms that present high repeatability, reproducibility, selectivity/specificity, robustness and low detection limits.

For the last 20 years two complementary paths have been followed in terms of analytical device production. The first path designs bulky and expensive equipment which present high versatility and can be used to analyze an enormous number of samples coming from completely different sources, whereas the second path relies on the production of miniaturized devices that accomplish the quantification of a key parameter and can be used by non-skilled personnel in remote areas.

1.2. Sensors

Chemical sensors are devices that can transduce chemical information of a sample into a useful analytical signal. This kind of devices are composed by two basic elements (Figure 1.1). The first is a recognition element or receptor which interacts with the target analyte and the second is the transducer which transforms the changes produced in the receptor (primary signal) to a quantifiable signal (secondary signal). Analyte is selectively recognized by the

receptor which produces a primary signal that is transformed to a secondary signal readable, commonly electrical one, by the transducer.[6]

Therefore, depending on the receptor and the transduction they can be classified.

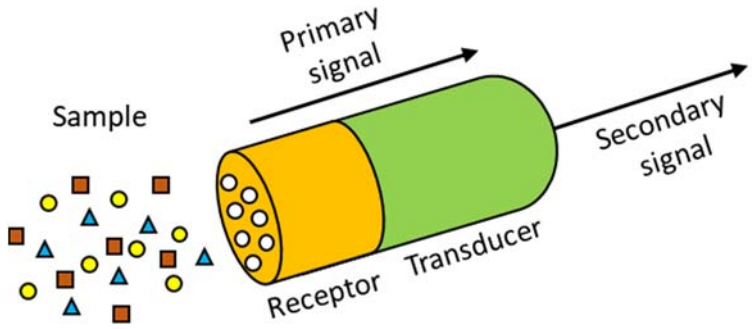

Figure 1.1. Scheme of a chemical sensor.

Receptor can be classified in three different kinds depending on their nature:

a) **Physical:** There are no reactions involved in the detection, in other words there is only a change in a physical property. For instance, piezoelectric sensors suffer a change in the potential when an external pressure is applied and inside out.

b) **Chemical:** The signal is produced by a chemical reaction/interaction. For instance, ionophores (host) interaction with ions (guest) produce a change in a potential.

c) **Biochemical:** The receptor comes from a biological source. For instance, an aptamer that interacts with a molecule producing a change in the charge transfer resistance.

The sensors are classified according to the type of transducer used. Thus, ttransduction can be classified in five kinds depending on their mechanism:[7]

a) **Optical sensors:** They measure changes regarding the optical properties such as absorbance, reflectance, fluorescence, luminescence and dispersion.

b) **Electrochemical sensors:** They measure electrical outputs produced by a chemical reaction or interaction that modifies the potential or the intensity measured.

c) **Electrical sensors:** They measure changes in the electrical properties of the sample or the analyte like conductivity or capacitance.

d) **Piezoelectrical sensors:** They measure an electrical potential change produced by a pressure applied to the sensor.

e) **Thermal sensors:** They measure changes in temperature caused by the reaction produced by the analyte.

f) **Magnetic sensors:** They measure paramagnetic properties of the species involved in the recognition.

1.2.1. Optical sensors

Generally, optical sensors working principle relied on the interaction between a defined electromagnetic radiation with the sample in which the absorption can be correlated with the analyte in solution.[8] For instance, a solution that contains copper (II) ions presents a blue color which means that absorbs the complementary color, orange. Therefore, the higher the concentration of copper (II) the intense blue will be seen, and a higher absorbance will present which can be directly correlated to the concentration.

1.2.1.1. Electromagnetic transitions

There are three basic phenomena by which a molecule can absorb radiation; they all consist on raising the internal energy of the molecule to a higher state and the increment of energy is proportional to the absorb radiation (hv).[9] The three energetic levels are quantified and discrete (Figure 2.1). In rotational transitions, molecules rotate through several axis which corresponds to the near infrared and microwave part of the spectrum. In vibrational transitions, molecules vibrate through several axis which corresponds to radiation absorption of the medium and far infrared part of the spectrum. Finally, electronic transitions are found in the ultraviolet and visible (UV-Vis) part of the spectrum related with radiation absorption in this zone.

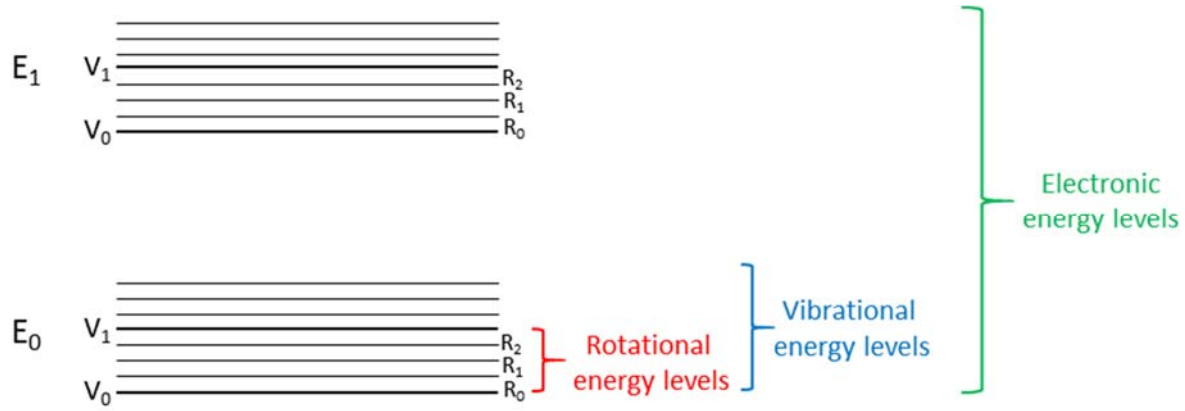

Figure 1.2. Energetic level diagrams of electromagnetic radiation transitions caused from infrared to ultraviolet range radiation absorption

Electronic transitions are caused by the absorption of radiation of specific groups, bond or functional group of a molecule. Electrons in a molecule can be classified in four groups:

a) **Kernell:** They are electrons of the core and present high excitation energies and they do not contribute to the absorption in the UV-Vis region.

b) **Sigma:** They are electrons present in single bonds, like saturated carbons. They present high excitation energies and they do not contribute to the absorption in the UV-Vis region.

c) **Non-bonding electrons:** Their bonding energy (N, O, S and halogens) is lower and they can be exited in the UV-Vis region.

d) **π:** They represent double and triple bonds, they can be easily exited and are the responsible of most of the UV-Vis region absorption.

1.2.1.2. Beer-Lambert law

The amount of monochromatic radiation that absorbs a sample obey the well-known Beer-Lambert law.[10] Although the most common term used for optical assays is absorption the equipment measure transmittance (i.e. the difference between incident and transmitted radiation through a path). Hence, the transmittance can be calculated by (Equation 1.1):

$$T = \frac{P}{P_0} \qquad \text{(Equation 1.1)}$$

Where T is transmittance, P is the transmitted radiation, P_0 is the incident radiation. The equation can also be correlated with absorbance by (Equation 1.2):

$$A = -\log T \qquad \text{(Equation 1.2)}$$

Moreover, absorbance is directly proportional to the concentration of the light-absorbing specie (Equation 1.3).

$$A = \epsilon bc \qquad \text{(Equation 1.3)}$$

Where A is the absorbance, ϵ is the molar absorptivity (L/mol·cm), b is the optical path (cm) and c (mol/L) is the analyte concentration. Molar absorptivity is a feature of a substance that tells the amount of light absorbed at a defined wavelength. Therefore, considering that molar absorptivity and optical path are constant, the absorbance can be correlated with a linear calibration plot with the concentration of the chromophore, being able to be used for quantification of analytes.

1.2.2. Electrochemical sensors

Electrochemical sensors rely on measuring voltage, charge or intensity on an electrochemical cell with the objective of gathering information about an analyte's concentration.[11] As a matter of fact, a chemical cell is composed of two or three electrodes (Figure 1.3), depending on the required configuration for measurement techniques used.

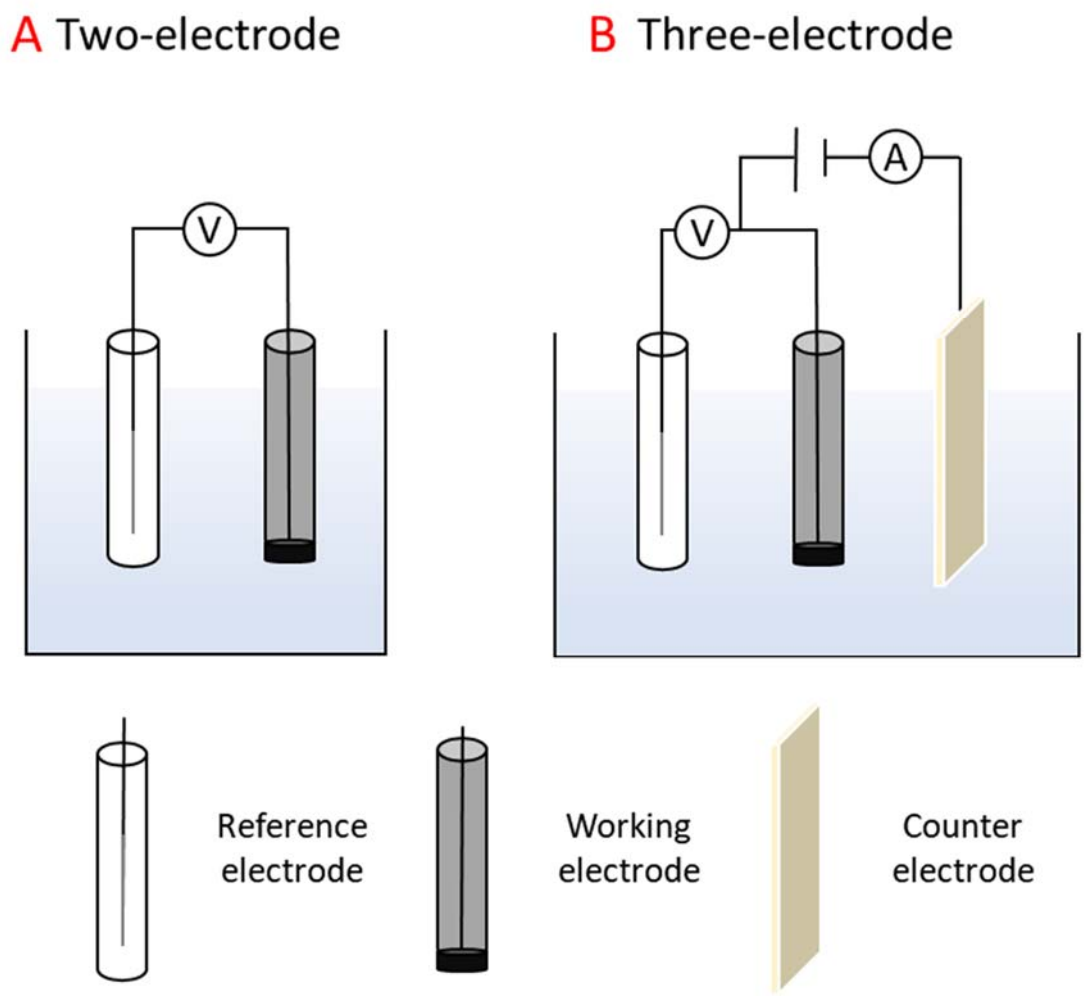

Figure 1.3. Scheme of the cells used for potentiometric measurements (A: two-electrode system) and for amperometric measurements (B: tree-electrode systems).

1.2.2.1. Potentiometric

Electrochemical cells used for potentiometric measurements are galvanic cells. In potentiometry cells use a two-electrode configuration system (Figure 1.3A). Therefore, they work under high resistance condition and no electrical current. A schematic classification of the potentiometric sensor regarding the sensing phase boundary is shown in Figure 1.4. Hence, working electrodes are classified in: metallic and membrane electrodes. That last group is also called ion-selective electrodes and the main difference with metallic's is that no redox reaction takes place during measurement. Membranes can either be glassy, crystalline or liquid ion-exchanger resins.

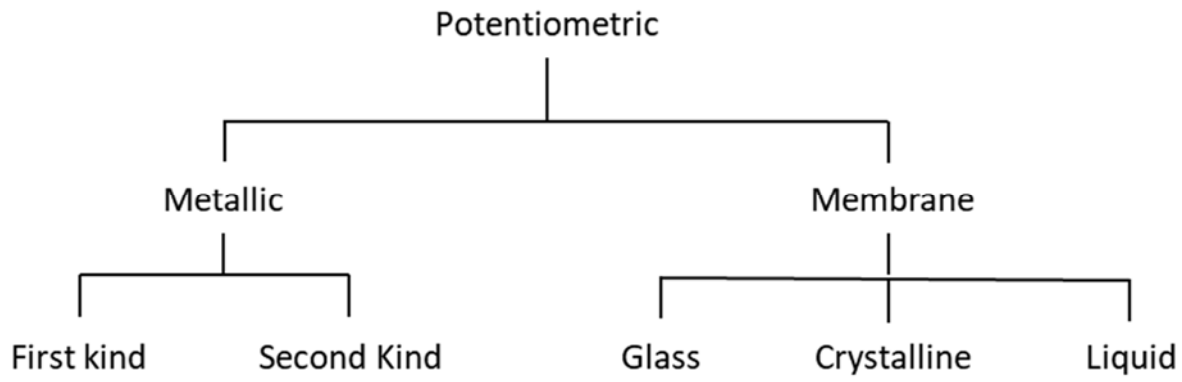

Figure 1.4. Classification of potentiometric sensors depending on the receptor phase boundary.

A cell's measured potential (E_{cell}) is defined by the difference in potential between a cathode, anode and the liquid union potential (U, Equation 1.4). The indicator electrode (E_{ind}) acts as the cathode while the reference (E_{ref}) corresponds to the anode:

$$E_{cell} = E_{ind} - E_{ref} + U \qquad \text{(Equation 1.4)}$$

Considering that the effect of the liquid union potential is minimized, and the potential by the reference electrode is constant we can assume that the potential of the cell is proportional to the indicator potential (half-cell potential) which is correlated with the activity of the ionic species involved by the well-known Nernst equation. For metallic electrodes the response is based on redox process defined by Nernst equation. In the case of membrane electrodes (glass, crystalline and liquid) the response is based on ion exchange into the membrane.[12] In this kind of electrodes, the response is based on Nernst-Nicolski o Nikolski-Eisenman. Consequently, for metallic electrodes used in this thesis, the response is based on a redox process and for the half-cell:

$$aOx + ne^{-} \leftrightarrow bRed$$

The potential measured follows the Nernst equation by (Equation 1.5):

$$E = E^{0} - \frac{RT}{nF} ln \frac{\{Red\}^{b}}{\{Ox\}^{a}} \qquad \text{(Equation 1.5)}$$

Where the E^0 is the standard potential, R is the gas constant (8.314 J/K·mol), T is the temperature (298.15 K), n is the number of electrons involved in the redox process and F is the Faraday constant (96485 C/mol).

Alternatively, converting the natural logarithm into the base 10 logarithm gives the frequently used form of the Nernst equation (Equation 1.6):

$$E = E^0 - \frac{0.05916}{n} log \frac{\{Red\}^b}{\{Ox\}^a} \qquad \text{(Equation 1.6)}$$

Metallic first kind electrodes: Electrodes of the first kind consist of a metal wire, which is in contact with a solution containing the cations of the metal. Charged particles (ions) are exchanged across the phase boundary. Hence, the electrode reaction can be considered as an ion-transfer reaction:

$$M^{n+} + ne^- \leftrightarrow M^0$$

Since the metal does not possess a charge its present unit activity. Therefore, the potential for the hall-cell observed follows (Equation 1.7):

$$E = E^0_{M^{n+},M} + \frac{RT}{nF} ln\{M^{n+}\}^n \qquad \text{(Equation 1.7)}$$

Metallic second kind electrodes: Metallic second kind electrodes consist of a metal wire coupled to a precipitation equilibrium between insoluble salt formed by metal cation and anion. This salt is in contact with a solution containing the anions of the metal salt. Hence, the electrode reaction consists of a combination of a redox reaction and a precipitation:

$$Redox: M^{n+} + ne^- \leftrightarrow M^0$$
$$Precipitation: MmXx_{(s)} \leftrightarrow mM^{n+} + xX^{n-}$$
$$\textbf{Combination: } MmXx_{(s)} + ne^- \leftrightarrow M^0 + xX^{n-}$$

In this case, the activity of the ions (X^{n-}) in solution directly depends on the solubility product and the potential observed follows (Equation 1.8):

$$E = E^{0}_{MmXx,M} - \frac{RT}{nF} ln\{X^{n-}\}^{x} \qquad \text{(Equation 1.8)}$$

Glass membrane electrodes: Glass is based on silicates spread in an amorphous way which contains several ions. Its permeability to ions such as H^+, Na^+ and K^+ allows them to create a potential difference across its phase boundary reliant on the ion's activity. Therefore, by slightly modifying the glass composition the membrane can show selectivity to the aforementioned ions.

Crystalline membrane electrodes: Crystalline membrane electrodes, also called solid state electrodes, are based on an ionic solid with a very low solubility product. They rely on the crystal defects in the framework and possesses ionic conductivity. They potential changes are caused by the interaction with the ions that can be exchanged (or added to the vacancies) with the ionic solid lattice.

Liquid membrane electrodes: Liquid membrane electrodes present a polymeric matrix which contains a molecule (ionophore) that has some selectivity to an ion. Therefore, the potential difference generated between the test solution and the inner polymeric membranes can be correlated with the ion activity.

1.2.2.2. Amperometric

Amperometric-detection based sensors measure the current intensity resulting from an electrochemical reaction produced at the working electrode surface caused by applying a particular potential.[13] In amperometry, use a three-electrode configuration system (Figure 1.3B). In the working electrode (or polarizable electrode) takes place the electrochemical reaction, whereas the reference electrode ensures the potential applied to the working electrode by the counter electrode (which closes the electrical circuit).

Unlike potentiometric sensors, amperometric sensors selectivity is defined by the potential applied. Any specie that presents redox activity closer to the target analyte (or closer to 0 V) will be potentially an interference. Moreover, their response is dependent of several factors such as, electroactive area size, morphology and distribution of electroactive area (for instance, in microelectrode), electron transference speed, among others.

1.2.2.3. Impedimetric

Impedimetric sensors measure the changes in the charge transfer resistance resulting from a chemical interaction with the recognition element (commonly a biomolecule).[14] Therefore, they exploit the change in dielectric properties and/or thickness of the dielectric layer at the electrolyte-electrode interfaces. Alike amperometric sensors, they also use a three-electrode configuration system although some scientists only use two-electrode system (working and counter). When using a three-electrode system, all the voltage applied is falling on the working electrode whereas in two-electrode system if the counter is polarizable of with similar polarizability to the working the signal is a composition of response from both electrodes.

1.3. Analysis automatization by flow methodologies

Traditionally, monitoring (i.e. continuous or repeated observation, measurement, and evaluation of health and/or environmental or technical data for defined purposes, according to prearranged schedules in space and time, using comparable methods for sensing and data collection) was performed by sampling in a remote area, transport the samples and measure them in laboratory facilities. This old-fashion methodology presents several drawbacks. Samples cannot be measured online, and the concentration of unstable analyte can change from sampling to analysis. Moreover, there is a limit of samples that can be collected and in a reasonable small period. Also, it requires personnel collecting samples. In addition, this methodology not only presents higher total analysis time but also severely increases the cost of the analyses. Finally, it does not allow obtaining information *in situ* or in real time. Aspects of this problems were solved by the appearance of flow analyses, easily automated, transportable and robust.

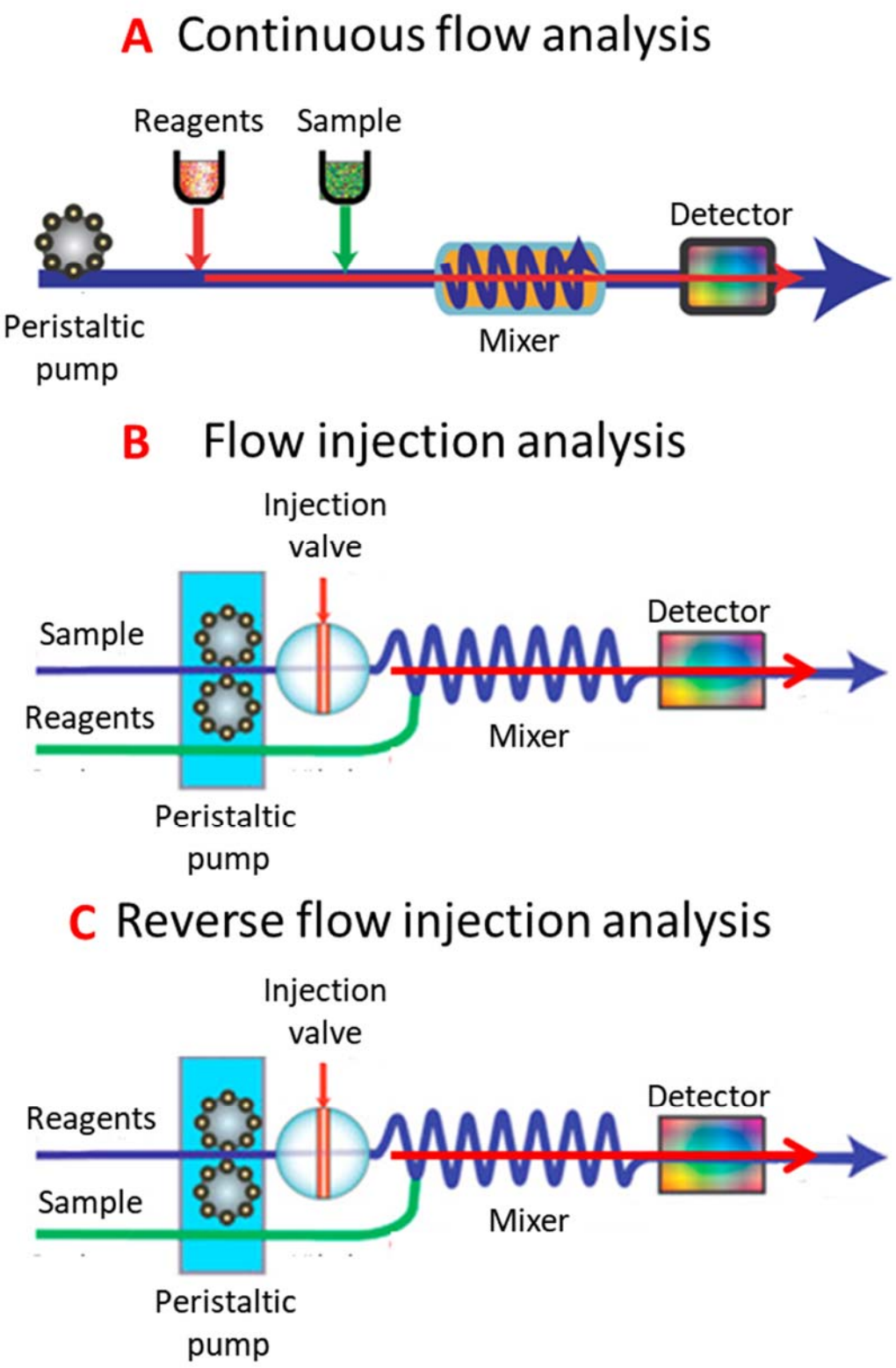

Figure 1.5. Scheme of the most common flow systems analysis and their respective components; continuous flow (A), a classical flow injection in which the sample is injected (B) and reverse flow injection in which the reagent is injected (C).

Flow analyses (Figure 1.5) can integrate the different steps of the analytical process in an autonomous way. Sampling, sample pretreatment and recognition can be automatedly performed giving online information of the desired samples. This kind of analyses are suitable for applications that requires constant analytical information for monitoring or control of a process. Therefore, their potential for being applied in environmental quality monitoring and biotechnological process control is astonishing. Moreover, they can be modified to be easily adapted to different analytical purposes. Finally, they can be classified in different flow analysis methodologies regarding the fluid management devices applied. Among others, the most common ones are: continuous flow analysis, flow injection analysis and sequential injection analysis.

1.3.1. Continuous flow analysis

Continuous flow analysis (CFA) can be understood as a process in which the analyte concentration is measured uninterruptedly in a stream. Solutions containing the sample and the reagents are constantly being pumped with a peristaltic pump to the mixer and the detector giving online *in situ* information. This methodology is the most flexible to perform all the required operations in a chemical assay. Moreover, continuous flow analysis is made up with just few instrumentations (in most cases just a bare pump) becoming much less complex and easier to use than classical batch analyses. However, CFA presents a disadvantage; high reagent and sample consumption for monitoring in long period of times.

1.3.2. Flow injection analysis

Flow injection analysis (FIA) is based on the injection of a liquid sample into a moving, non-segmented continuous carrier stream of a suitable reagent.[15] This methodology has received much attention during the past decades thanks to its capability to reduce costs for daily analysis that can be performed with a time-lapse rather than constant information. Additionally, the capability of FIA to control in a high reproducible manner the sample volume used, the reaction time and the mixing conditions has allowed the design of novel analytical methods unviable by batch conditions. However, although FIA reduces costs compared to CFA, it requires further instrumentation (at least an injection valve), which can introduce further problems to the assay. For instance, the change of position of a 6-way vale could introduce relevant noise to

potentiometric measurements. On the other hand, it has the advantage of allowing the automation of the analysis and reducing sample consumption.

1.3.3. Reverse flow injection analysis

In some situations, a modification of the FIA is performed to adapt the assay to real conditions. For instance, in environmental samples such as river, sea or lakes, the amount of sample is enormous. In this kind of cases, were sample waste does not present a drawback, the reagent is injected whereas the sample is used as a carrier; this modification receives the name of reverse flow injection analysis (rFIA). This strategy presents the advantage of reducing the reagent consumption and minimize the generation of waste.

1.4. Miniaturization

Miniaturization (i.e. manufacture ever smaller devices) of analytical systems constitutes a great advance with respect to old-fashion systems.[16] Miniaturized systems reduce sample and reagent consumption, response time and cost by analysis.[17,18] On the other hand, they increase the automatization rate, portability and minimize waste generation which makes them appealing as green chemistry. Besides, with the partial or total automatization of an analytical system they reduce laboratory assembly and trainer personnel decreasing operational errors. A tremendous number of microsystems which integrates analytical operations such as, mixers, filtrations, reactions, separations and detections are extensively being developed.[19,20,21]

Moreover, there are a wide variety of materials that can be used depending on the final application. Glass have been extensively used thanks to its transparency for optical assays. However, prototyping of glass remains a challenge. Alternatively, transparent polymers have been exploited for optical assays such as, polymethyl methacrylate, polydimethylsiloxane, polycarbonate and cyclic olefin copolymer.[22] Additionally, other materials like low temperature co-fired ceramics which allow high temperature assay have also been used for microfluidic architectures.[23] On the other hand, the conductive polymers have also been extensively studied for miniaturized electronics.[24]

1.5. Device fabrication methodologies

With the ever-increasing demand of autonomous microanalytical system, novel method for low-cost fabrication of functional devices have been developed by the scientific community. Although traditional fabrication methods give impressive reliable sensing platforms, they are complex, expensive and require trained stuff.[22]

1.5.1. Traditional

1.5.1.1. Photolithography

Photolithography is the technique used to transfer copies of a master pattern onto the surface of a solid material (commonly silicon wafer).[25] Is the most used technique for the fabrication of integrated circuits thanks to its impressive reproducibility. Performance of a photolithographic process is determined by its resolution, the minimum feature size that can be transferred with high fidelity; the registration, how accurately patterns on successive masks can be aligned; and throughput, the number of wafers that can be transferred per hour. Photolithography and pattern transfer involve a set of consecutive steps[26] that are summarized in Figure 1.6. Generally, photolithography starts with a silicon wafer which presents a partial oxidation of its surface. Then a layer of photoresistor which polymerizes under a certain light condition (UV in most cases) is applied. Afterwards, a mask with the desired motif is aligned on top, and the light source is applied polymerizing the photoresistor selectively. Finally, an etching/cleaning is applied to get rid of the unpolymerized photoresistor. In other cases, a further treatment is applied to also eliminate the SiO_2 layer. On top of that, the use of different photoresistor and different layers allows this technology to produce high complex architectures. Therefore, photolithography is the established technique to produce electronic chips for computer, smartphones or other electronic-dependent devices. However, its cost and the required facilities to produce electronics by this means makes photolithography a bad approach for rapid prototyping at research labs.

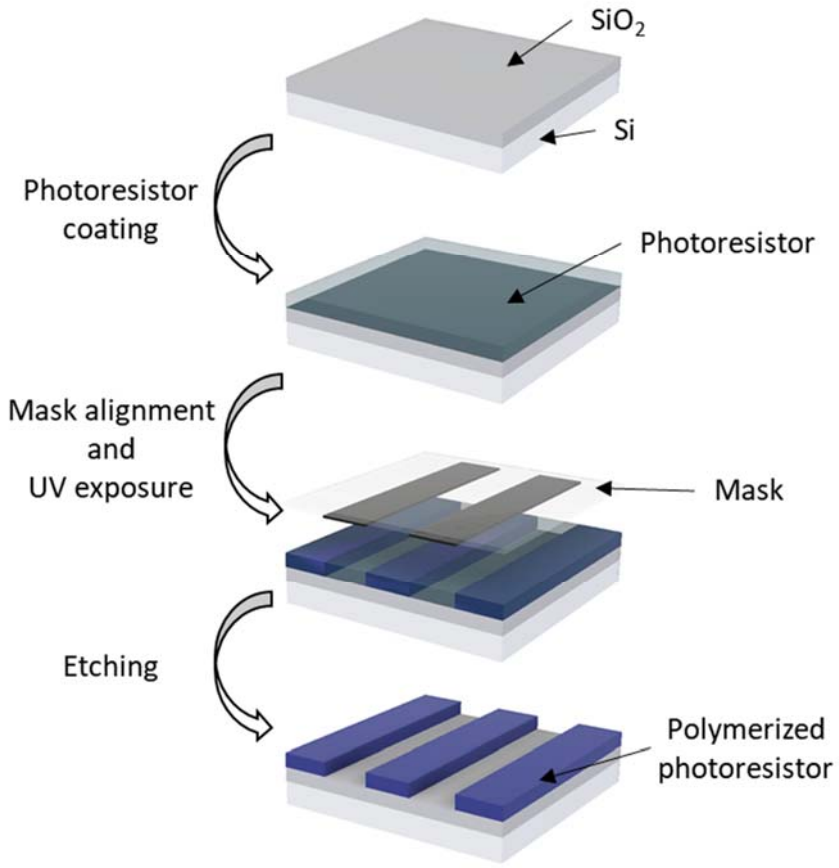

Figure 1.6. Basic photolithography process. This example incudes Photoresistor coating, mask alignment, exposure and etching.

1.5.1.2. Laser ablation/Mechanical milling

Laser ablation is the process of removing material from a solid surface by irradiating it with a laser beam (Figure 1.7A).[27] The material is heated by the absorbed laser energy and evaporates or sublimates. Applying different laser intensities and pulses a pattern with a defined length can be produced. Mechanical milling works alike laser ablation but using a drill (Figure 1.7B).[28] Hence, using different drills and different conditions a particular path with a defined length can be produced. Both technologies are commonly used for producing either microfluidic platforms or to produce microelectrodes.

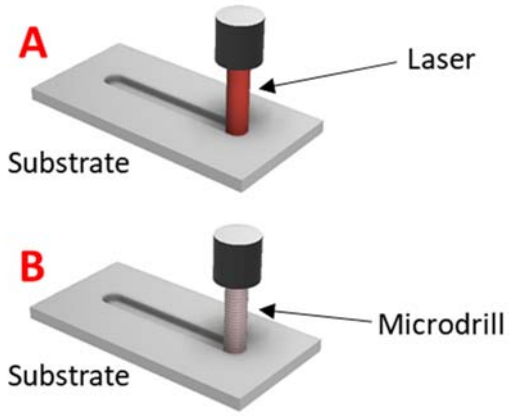

Figure 1.7. Schematic images of the path produced by laser ablation (A) and mechanical milling (B).

1.5.1.3. Injection molding and Hot embossing

Injection molding is a manufacturing technique that produces parts by injecting molten material into a mold (Figure 1.8).[29] Injection moulding can be performed several kinds of materials.[30] Material used for the part production is fed into a container, mixed or heated (using a helical shaped screw and a cylinder liner as heater), and injected (controlling the quantity of material) into a mould cavity, where it cools and hardens to the configuration of the cavity. This technique is frequently used by the industry; when an optimal shape of a material is found a mould is fabricated and an industrial scale production starts. However, this technology can be also used to produce microfluidic platforms.

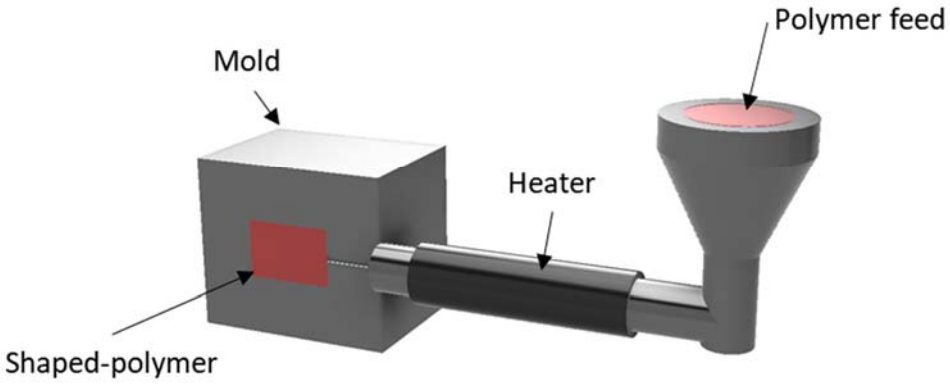

Figure 1.8. Schematic image of an injection moulding machine.

Hot embossing alike injection molding is a technology that relies on heating a polymer and apply pressure to define a material form (Figure 1.9). A polymeric material is placed between a positive and a negative part and the pressure is applied whereas molds are heated up; then they cool down and the part is extracted.[31] This technology find uses in a wide variety of situations for analytical purposed, from production to optical diffraction patterns to microfluidics.

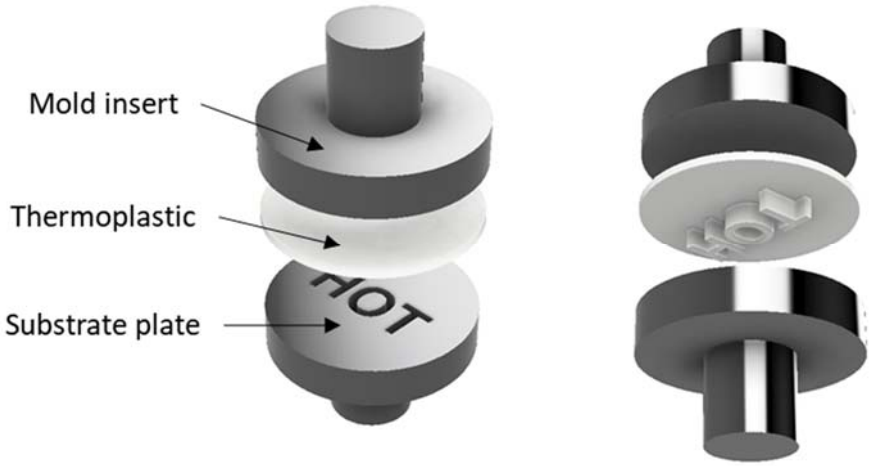

Figure 1.9. Schematic representation of the hot embossing process.

1.5.2. Printing technologies

Nowadays, printing technologies have emerged as the alternative to traditional manufacturing processes.[32] They can fabricate in a high repeatable manner at a low-cost and therefore, have been stablish as the standard fabrication methodology for miniaturized sensors or sensing platforms. There are many different printing technologies that can be classified depending on the deposition method. However, only few of them have been widely exploited by the scientific community.

1.5.2.1. Screen printing

Screen printing technology have been used for many different applications since thousands of years ago. Screen printing is a technique whereby a mask is used to selectively transfer a motif onto a substrate.[33] A squeegee is moved across the screen to fill the open mask apertures

with ink. Combining several layers with different materials, this technique has been mainly used for mass production of general three-electrode systems. In most cases, two carbon paths are printed as working and auxiliary electrodes; then, a silver/chlorine silver tip (Ag/AgCl) is printed as reference electrode, and finally an insulator is used to define the electroactive area. Once the basic three-electrode systems are obtained a modification of the working electrode allows the systems to improve the analytical response.

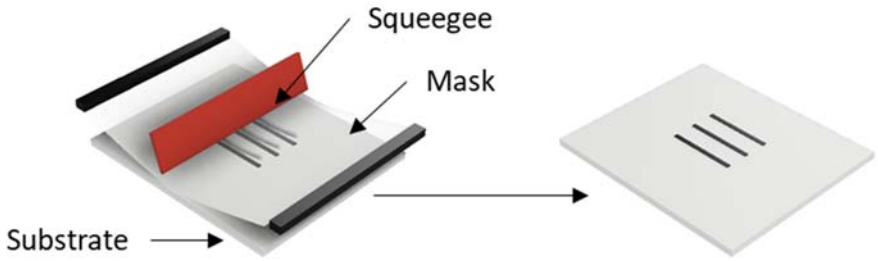

Figure 1.10. Schematic representation of the screen-printing process.

1.5.2.2. Inkjet printing

Inkjet printing constitutes a contactless, additive process with the capability to deposit microdroplets of ink on a substrate following a digitalized predefined pattern (Figure 1.11). Works alike a common office printer but the printers presents higher versatility in terms of wave function of the piezoelectric used to deliver the drops from the cartridge.[34] Ink formulations are composed by materials that can be dispersed, suspended or dissolved in a liquid with defined properties (viscosity, surface tension and boiling point). In fact, electrically conductive paths can be inkjet-printed from a wide variety of materials, from metals to conductive, semiconductive and dielectric polymers.[35]

a) **Conductive patterns** are mostly printed using inks based on metal nanoparticles, organometallic compounds, and carbon nanostructures. Metal inks based on nanoparticles are commonly employed as conductive elements in electronics due to its reliable and stable conductivity. The selection of conducting material depends on the final application of the device. Silver ink is the most used by the community due to their low

sintering temperature and they resistance to mechanical stress after sintering reaching applications that require flexible electronics.

b) **Semiconducting materials** find a wide range in application in printed electronics. Depending on the target application (range of conductivity required and mechanical stress), inorganic or organic semiconductors can be printed.

c) **Dielectrics materials** are passive materials which are used in many types of devices. Among others, dielectric materials are formed by inorganic, polymeric or hybrid materials. They are mostly used in the production of sensors to define the electroactive area and to insulate the electrical path.

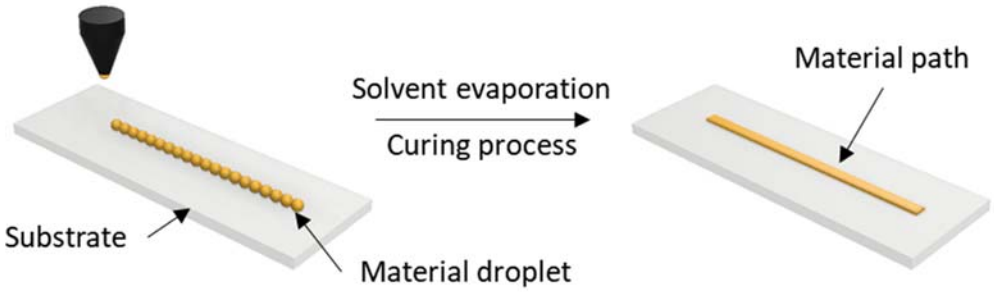

Figure 1.11. Schematic representation of the inkjet printing process and the post-processing step.

1.5.2.3. 3D printing

3D-printing refers to additive manufacturing techniques, which can create three-dimensional solid layer-by-layer under precise digital control.[36] Among these techniques, the ones that are most relevant to analytical device fabrication are fused deposition modelling, stereolithography and selective laser sintering.

a) **Fused deposition modelling:** In fused filament fabrication, a spool of filament is loaded into the printer and then fed to the extrusion head, which is equipped with a heated nozzle (Figure 1.12).[37] Once the nozzle reaches the desired temperature, a motor drives the filament through it melting the polymer. The printer moves the extrusion head, laying down melted material at precise locations, where it cools and solidifies. When a layer is

finished, the build platform moves down, and the process repeats until the part is complete. This 3D-printed technology is the most used one thanks to its low cost and versatility.

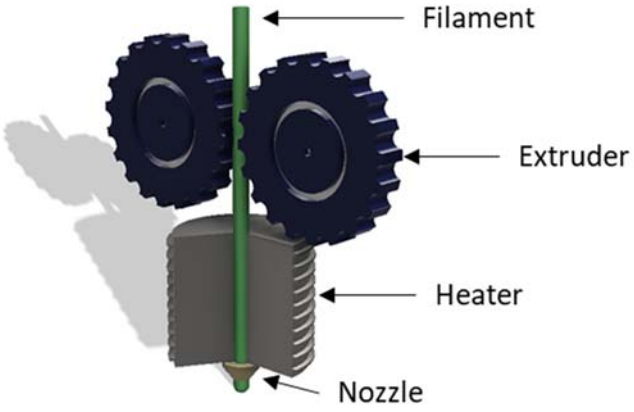

Figure 1.12. Scheme of the fused filament fabrication printing head containing extruder and heater.

b) **Stereolithography and digital light processing:** Stereolithography and digital light processing are similar processes that both use a light source to solidify the liquid resin in a layer-by-layer manner (Figure 1.13).[38] Stereolithography uses a single-point laser to cure the resin, while digital light processing uses a digital light projector to flash a single image of each layer all at once. This printing technology presents tremendous resolution and produces highly detailed parts. However, the cost of the printer and the polymer used is also higher.

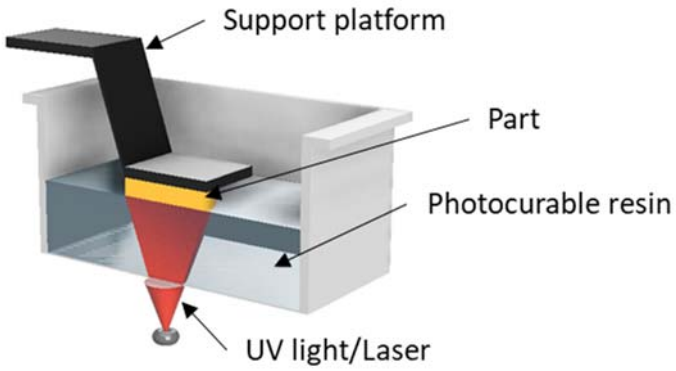

Figure 1.13. Schematic representation of the stereolithography and digital light processing.

c) **Selective laser sintering:** Selective laser sintering process relies on using a laser beam to sinter polymeric or metal particles (Figure 1.14).[39] A recoating roller deposits a very thin layer of powder onto the build platform and the laser selectively sinters the particles binding them together. When the entire cross-section is scanned, the building platform moves down one layer and the process repeats.

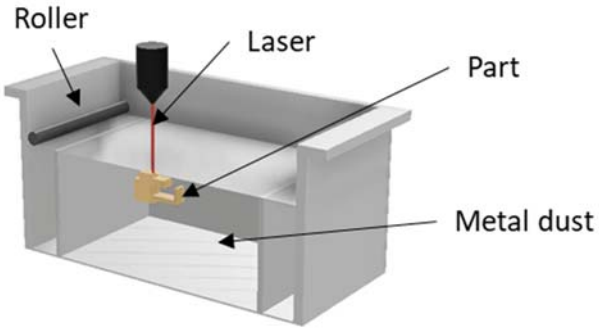

Figure 1.14. Schematic representation of a selective laser sintering machine.

1.6. References

(1) Al-Lozi, E.; Papazafeiropoulou, A. *Intention-Based Models: The Theory of Planned Behavior Within the Context of IS*; 2011.

(2) Pol, R.; Céspedes, F.; Gabriel, D.; Baeza, M. Microfluidic Lab-on-a-Chip Platforms for Environmental Monitoring. *TrAC - Trends Anal. Chem.* **2017**, *95*, 62–68.

(3) Das, S.; Sen, B.; Debnath, N. Recent Trends in Nanomaterials Applications in Environmental Monitoring and Remediation. *Environ. Sci. Pollut. Res.* **2015**, *22* (23), 18333–18344.

(4) Zhang, D.; Fu, H. Z.; Ho, Y. S. Characteristics and Trends on Global Environmental Monitoring Research: A Bibliometric Analysis Based on Science Citation Index Expanded. *Environ. Sci. Pollut. Res.* **2017**, *24* (33), 26079–26091.

(5) Nechushtai, R.; Elit, M.; Systems, S. M. United States Patent, 2001.

(6) Turner, A. P. F.; Karube, I.; Wilson, G. S. *Biosensors : Fundamentals and Applications*; New York, 1987.

(7) ADAM HULANICKI, S. G. and F. I. Chemical Sensors Definitions and Classification. *Pure&App/. Chern.* **1991**, *63* (9), 1247–1250.

(8) Aizawa, M. Optical Chemical Sensors. *Mater. Japan* **2011**, *34* (11), 1233–1237.

(9) Pavia, D. L.; Lampman, G. M.; Kriz, G. S. *Introduction to Spectroscopy*; Bellingham, 2001.

(10) Swinehart, D. F. The Beer-Lambert Law. *J. Chem. Educ.* **2009**, *39* (7), 333.

(11) Wang, J. *Analytical Electrochemistry, Third Edition*; 2006.

(12) Bakker, E.; Pretsch, E. Modern Potentiometry. *Angew. Chemie - Int. Ed.* **2007**, *46* (30), 5660–5668.

(13) Amperometric Detection Method https://goldbook.iupac.org/html/A/A00301.html.

(14) Muñoz, J.; Montes, R.; Baeza, M. Trends in Electrochemical Impedance Spectroscopy Involving Nanocomposite Transducers: Characterization, Architecture Surface and Bio-Sensing. *TrAC - Trends Anal. Chem.* **2017**, *97*, 201–215.

(15) Hansen, E. H.; Růžička, J. Flow Injection Analyses. Part I. A New Concept of Fast Continuous Flow Analysis. *Anal. Chim. Acta* **1975**, *78* (1), 145–157.

(16) Manz, A.; Graber, N.; Widmer, H. M. Miniaturized Total Analysis Systems: A Novel Concept for Chemical Sensing. *Sensors Actuators, B Chem.* **1990**, *1*, 244–248.

(17) Madou, M.; Florkey, J. From Batch to Continuous Manufacturing of Microbiomedical Devices. *Chem. Rev.* **2000**, *100* (7), 2679–2692.

(18) Desmet, G.; Eeltink, S. Fundamentals for LC Miniaturization. *Anal. Chem.* **2013**, *85* (2), 543–556.

(19) Soleymani, L.; Li, F. Mechanistic Challenges and Advantages of Biosensor Miniaturization into the Nanoscale. *ACS Sensors* **2017**, *2* (4), 458–467.

(20) Zhang, C.; Xing, D. Single-Molecule DNA Amplification and Analysis Using Microfluidics. *Chem. Rev.* **2010**, *110* (8), 4910–4947.

(21) Gong, M. M.; Sinton, D. Turning the Page: Advancing Paper-Based Microfluidics for Broad Diagnostic Application. *Chem. Rev.* **2017**, *117* (12), 8447–8480.

(22) Nge, P. N.; Rogers, C. I.; Woolley, A. T. Advances in Microfluidic Materials, Functions, Integration, and Applications. *Chem. Rev.* **2013**, *113* (4), 2550–2583.

(23) Baeza, M.; López, C.; Alonso, J.; López-Santín, J.; Álvaro, G. Ceramic Microsystem Incorporating a Microreactor with Immobilized Biocatalyst for Enzymatic Spectrophotometric Assays. *Anal. Chem.* **2010**, *82* (3), 1006–1011.

(24) Nambiar, S.; Yeow, J. T. W. Conductive Polymer-Based Sensors for Biomedical Applications. *Biosens. Bioelectron.* **2011**, *26* (5), 1825–1832.

(25) King, M. C. *Principles of Optical Lithography*; 2014.

(26) Berkowski, K. L.; Plunkett, K. N.; Yu, Q.; Moore, J. S. Introduction to Photolithography:

Preparation of Microscale Polymer Silhouettes. *J. Chem. Educ.* **2009**, *82* (9), 1365.

(27) Wlodarczyk, K. L.; Carter, R. M.; Jahanbakhsh, A.; Lopes, A. A.; Mackenzie, M. D.; Maier, R. R. J.; Hand, D. P.; Maroto-Valer, M. M. Rapid Laser Manufacturing of Microfluidic Devices from Glass Substrates. *Micromachines* **2018**, *9* (8), 1–14.

(28) Dr. Liz Katherine Rincon Ardila; Dr. Luciana Wasnievski da Silva de Luca Ramos; Prof. Dr. Erik Gustavo Del Conte; Prof. Dr. Alvaro José Abackerli; Tiago Cacossi Picarelli; Felipe Alves de Oliveira Perroni; Prof. Dr.-Ing. Klaus Schützer; Dipl.-Ing. Jan Mewis; Prof. Dr. h. c. Dr.-Ing. Eckart Uhlmann. Micro-Milling Process for Manufacturing of Microfluidic Moulds. *Proc. 23rd ABCM Int. Congr. Mech. Eng.* **2016**, No. December.

(29) Attia, U. M.; Marson, S.; Alcock, J. R. Micro-Injection Moulding of Polymer Microfluidic Devices. *Microfluid. Nanofluidics* **2009**, *7* (1), 1–28.

(30) Su, X.; Berthier, E.; Zhang, T.; Lee, U. N.; Guckenberger, D. J.; Theberge, A. B.; Dostie, A. M. Fundamentals of Rapid Injection Molding for Microfluidic Cell-Based Assays. *Lab Chip* **2018**, *18* (3), 496–504.

(31) Goral, V. N.; Hsieh, Y. C.; Petzold, O. N.; Faris, R. A.; Yuen, P. K. Hot Embossing of Plastic Microfluidic Devices Using Poly(Dimethylsiloxane) Molds. *J. Micromechanics Microengineering* **2011**, *21* (1).

(32) Gates, B. D.; Xu, Q.; Stewart, M.; Ryan, D.; Willson, C. G.; Whitesides, G. M. New Approaches to Nanofabrication: Molding, Printing, and Other Techniques. *Chem. Rev.* **2005**, *105* (4), 1171–1196.

(33) Metters, J. P.; Kadara, R. O.; Banks, C. E. New Directions in Screen Printed Electroanalytical Sensors: An Overview of Recent Developments. *Analyst* **2011**, *136* (6), 1067–1076.

(34) Moya, A.; Gabriel, G.; Villa, R.; Javier del Campo, F. Inkjet-Printed Electrochemical Sensors. *Curr. Opin. Electrochem.* **2017**, *3* (1), 29–39.

(35) Hoath, S. D. *Fundamentals of Inkjet Printing: The Science of Inkjet and Droplets*; 2016.

(36) Gross, B.; Lockwood, S. Y.; Spence, D. M. Recent Advances in Analytical Chemistry by 3D Printing. *Anal. Chem.* **2017**, *89* (1), 57–70.

(37) Zein, I.; Hutmacher, D. W.; Tan, K. C.; Teoh, S. H. Fused Deposition Modeling of Novel Scaffold Architectures for Tissue Engineering Applications. *Biomaterials* **2002**, *23* (4), 1169–1185.

(38) Patel, D. K.; Sakhaei, A. H.; Layani, M.; Zhang, B.; Ge, Q.; Magdassi, S. Highly Stretchable and UV Curable Elastomers for Digital Light Processing Based 3D Printing. *Adv. Mater.* **2017**, *29* (15), 1–7.

(39) Beaman, J.; Agarwala, M.; Barlow, J.; Marcus, H.; Bourell, D. Direct Selective Laser Sintering of Metals. *Rapid Prototyp. J.* **2002**, *1* (1), 26–36.

CHAPTER 2

Objectives

2.1. Context

Prior to state the main objective of this PhD thesis and its partial goals to accomplish, a brief description of the context (research project) will help readers to understand the importance of this though work. Therefore, the following fragment has been directly extracted from the MINECO project CTQ2015-69802-C2-1-R:

"*Emissions of SOx and NOx from flue gases require treatment before release into the atmosphere according to the current legislation. Physical-chemical treatments used so far are expensive and generate effluents that require further processing. This project faces the challenge of developing a comprehensive treatment process for SOx and NOx from flue gases by economical, robust and environmentally friendly biological methods that also consider the reuse of energy and resources in process development as well as residues valorization.*

The proposed process is based on i) a first double stage for selective absorption of SOx and NOx, ii) a second biological step catalyzed by sulfate-reducing microorganisms for reducing the sulfate/sulfite mixture from the first absorption stage to hydrogen sulfide, and iii) a third biological stage catalyzed by sulfide-oxidizing microorganisms for the oxidation of hydrogen sulfide to elemental sulfur and its subsequent recovery (Figure 1)."

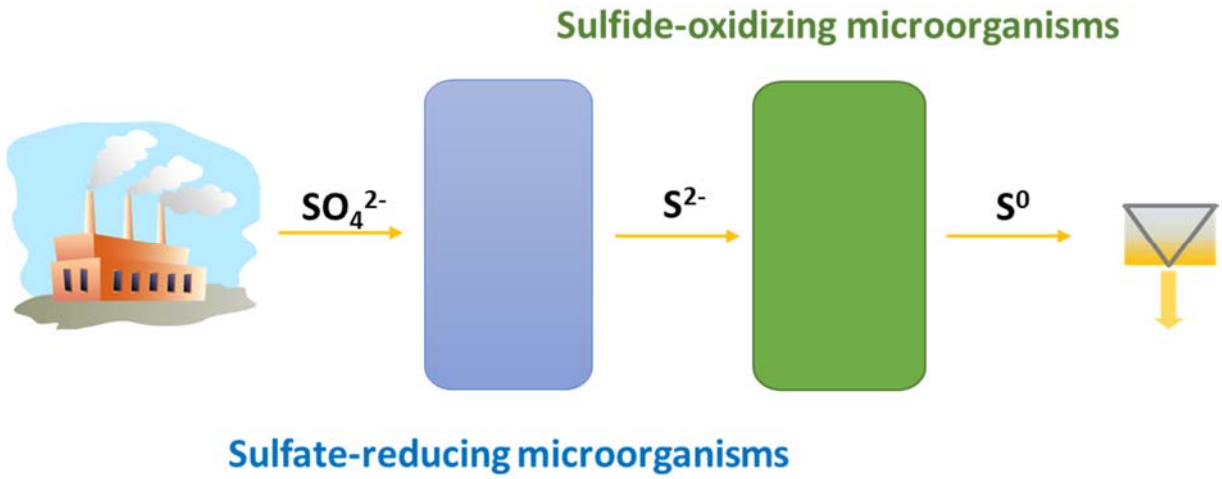

Figure 2.1. General scheme of the proposed process for transformation of SOx gases into elemental sulfur.

2.2. Objectives

One-line pitch objective: Fabrication of functional devices for monitoring chemicals involved in biotechnological processes.

The main objective of this research is the fabrication of sensing devices to measure sulfide and sulfate in an autonomous way to control the proper functioning of an upflow anaerobic sludge blanket reactor. This interesting objective was split in several specific objectives:

- Extensive study and comprehension of the state-of-the-art on the latest developments in the fabrication technologies of microfluidic devices for monitoring relevant chemicals species in the environment. Consequently, decide the better alternative to fabricate the required sensing platforms.

- Acquire the know-how of the requirements of cost-efficient printing technologies (inkjet printing, screen-printing and 3D printing) to develop devices based on different detection techniques depending on the target to monitor.

- Use of inkjet printing technology to produce an electrode for sulfide ion monitoring in batch-like conditions.

- Implementation of a two-electrode potentiometric system inside a microfluidic 3D-printed platform with sample pretreatment enclosed for on-line quantification of sulfide ion from the upflow anaerobic sludge blanket reactor.

- Development of an optical-based detection chamber in a fused filament fabrication 3D-printed microfluidic system which integrates two consecutive reactions traditionally used in the quantification of sulfate ion.

- Extend the printing technologies for fabrication of sensors for other relevant parameters to control in the biotechnological reactor for alternative treatment processes.

CHAPTER 3

Methods

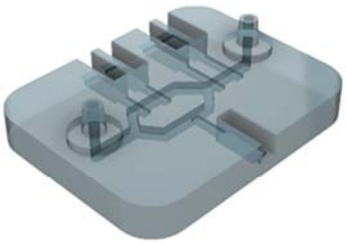

From design

to platform

3.1. Foreword

Methods section will extensively cover some major points that can be found through the experimental body of the thesis. First, an extensive description of the targeted biotechnological reactors and aquariums. Then, a comprehensive guideline for production of microfluidic platforms by means of 3D printing (steps to follow, design, slicer, troubleshooting…). Finally, a description of how to proceed with common analytical statistics. On the other hand, each experimental chapter (Chapters 5-8) will include its own materials and method section covering the specific experiments performed.

It is important to clarify that this section is composed in such a manner that helps future young researcher that start from scratch to easily catch up in the ongoing analytical trends (3D revolution).

3.2. Three-dimensional printing

3.2.1. General knowledge

Theoretical concepts regarding 3D printing have been well covered in Introduction chapter. Herein, a comprehensive guide to explain the know-how of the technique will be described. It is important to clarify that although the aim of printing technologies is to be affordable and easy-to-use for end users (they only require the end user to press the "print" button) there is a previous long complex process that requires a trained person. Thus, this complex process will be completely explained hereunder.

The overall 3D printing process can be split in three different stages; modeling, slicing and printing (Figure 3.1). Each one of these stages has its own importance in the quality of the final device and understanding the potential of the printer that is going to be used is the key factor. A mistake in a simple parameter of one of the stages can undergo into a printing failure.

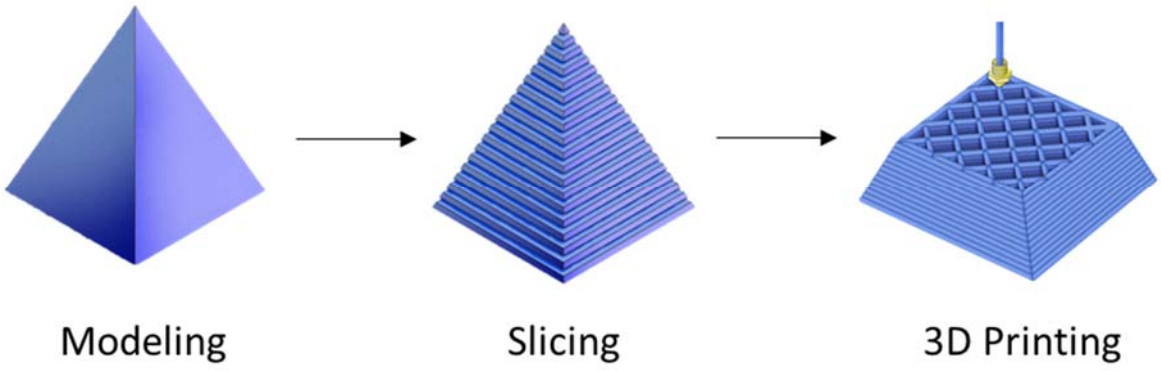

Figure 3.1. Scheme of the different stages of 3D printing: Modeling, slicing and 3D printing.

Prior to the description of the stages it is important to understand that each printer has a defined quality in terms of positive and negative resolutions (Figure 3.2). Therefore, if our printer has a negative resolution of 100 μm there is no possible way to produce channels smaller than that. In the same way, if our printer has a positive resolution of 4 μm there is no possible way to have walls smaller than that. Once we have determined the information of the resolution of the printer, then, the modeling stage can begin. Modeling can be understood as the production of a 3D structure using a software. The software used for this purpose are called

computer-aided design (CAD) software. There are a lot of modeling software available (some free) that can operate under 3D conditions (SolidWorks, OneShape, Fusion360…). Once the model is finished, in order to proceed the model needs to be saved in a ".STL" extension. This extension is the global language for 3D model to be recognized by the slicer software. The function of the slicer is to decompose the 3D in a layered fashion converting it to G-code. Once again, there are a lot of slicer software available. However, when purchasing a 3D printer, the company usually provides a defined software for the printer acquired. Finally, the file can be send it and printed.

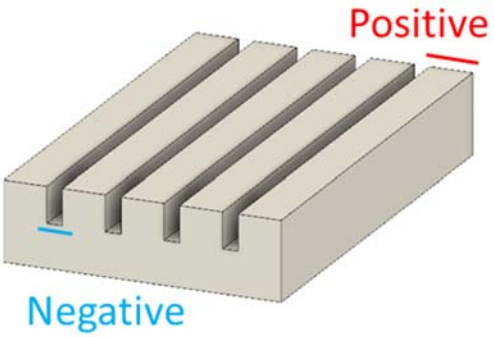

Figure 3.2. Scheme of positive and negative parts of a 3D printing microfluidic device.

The following sections will explain for non-expert readers the functioning of both required 3D software (modeling and slicing) and finally give an example of the production of a 3D printed microfluidic platform step by step.

3.2.2. Modelling software

The modeling software that has been used throughout the entire PhD thesis is Fusion360 (Autodesk®) and therefore, will be used as a standard to explain modeling software.[1] However, moving from one software to another will not require any effort as all of them work alike. This software was chosen to take advantage of one of its huge number of features: cloud tool for collaborative product development. This important feature helped with collaborative device development between our students; allowing us to share and design a single device from different computers.

3.2.2.1. User interface

The user interface can be broken up into 8 areas (Figure 3.3):

1. **Application bar:** Used for data management and collaboration. Create a New Design, Save, Export, and 3D Print. Save an untitled design or save the changes to a design as a new version and undo/redo operations.

2. **Profile and Help:** In profile you can control your profile and account settings or use the help menu to continue your learning or get help in troubleshooting.

3. **Toolbar:** Use the Toolbar to select the workspace you want to work in, and the tool you want to use in the workspace selected.

4. **Browser:** The browser lists objects in your design. Use the browser to make changes to objects and control visibility of objects.

5. **Canvas:** Canvas contains the 2D/3D design that you are doing.

6. **Viewcube:** Use the *viewcube* to orbit your design or view the design from standard view positions.

7. **Navigation bar and display settings:** The navigation bar contains commands used to zoom, pan, and orbit your design. The display settings control the appearance of the interface and how designs are displayed in canvas.

8. **Timeline:** The timeline lists operations performed on your design. Right-click operations in the timeline to make changes. Drag operations to change the order they are calculated.

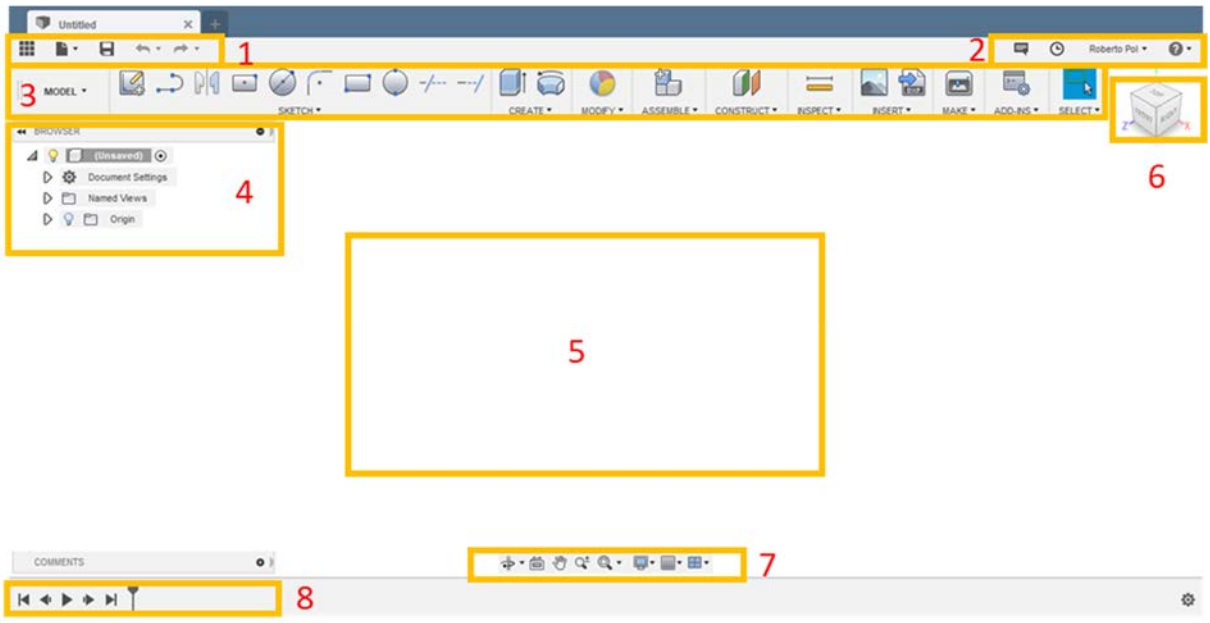

Figure 3.3. Fusion360 user interface: Application bar (1), profile and help (2), toolbar (3), browser (4), canvas (5), viewcube (6), navigation bar and display settings (7) and timeline (8).

To help readers to become familiar with 3D modeling we will describe area 3 (the key area) and go into more details with how to use it in the following sections.

3.2.2.2. Sketch (2D)

To design the microfluidic devices there was no need to use all the sketch options (find the most important ones underlined). However, it is important to know all the possibilities that the modeling software offers to be able to design non-usual microfluidic shapes. Moreover, some procedure used could be replaced by using another option. For instance, fillet works alike center point arc. The following options can be found in sketch menu:

- **Create sketch:** Enters sketch mode and create a sketch on a selected plane or face.

- **Line:** Creates a line or an arc: select a start and endpoint to draw a line segment; click and drag the endpoint of a segment to create and arc.

- **Rectangle:** Two-point rectangle: creates a rectangle using two points for the diagonal corners. Three-point rectangle: creates a rectangle using three points to define width,

direction and height. Center rectangle: creates a rectangle using two points to define the corner and the center.

- **Circle:** Center diameter circle: creates a circle using the center point and the diameter. Two-point circle: creates a circle defined by two points. Three-point circle: creates a circle defined by three points. Two-tangent circle: creates a circle tangent to two sketch lines. Three-tangent circle: creates a circle tangent to three sketch lines.

- **Arc:** Three-point arc: creates an arc using three points. Center point arc: creates an arc using a center point tangent to the other two. Tangent arc: creates an arc with tangency.

- **Polygon:** Circumscribed polygon: creates a polygon using the center point and the midpoint of one edge. Inscribed polygon: creates a polygon using the center point and a vertex. Edge polygon: creates a polygon by defining a single edge and the position of the polygon.

- **Ellipse:** Creates an ellipse defined by a center point, major axis and a point of the ellipse.

- **Slot:** Center to center slot: creates a linear slot defined by placement and distance of slot arc centers and by slot width. Overall slot: creates a linear slot defined by orientation, length and width. Center point slot: creates a linear slot defined by a center point, location of slot arc centers and by slot width. Three-point arc slot: creates a slot arc defined by a three-point center arc and slot width. Center two-point arc slot: creates an arc slot defined by a center point, two-point center arc and slot width.

- **Spline:** Fit point spline: creates a spline through the selected fit points. Control point spline: creates a spline driven by the selected control points.

- **Conic curve:** Creates a curve driven by endpoints and Rho value; depending on the rho value, the curve can be elliptical, parabolic or hyperbolic.

- **Point:** Creates a sketch point.

- **Text:** Inserts text into the active sketch.

- **Fillet:** Places an arc of a specified radius at the intersection of two lines or arcs.

- **Trim:** Trims a sketch curve to the nearest intersecting curve or geometry boundary.

- **Extend:** Extends a curve to the nearest intersecting curve or geometry boundary.

- **Break:** Break curve entities into two or more sections.

- **Sketch scale:** Scales sketch geometry to a specific value.

- **Offset:** Copies the selected sketch curves a specific distance from the original one.

- **Mirror:** Mirrors the selected sketch curves about the selected sketch line.

- **Circular pattern:** Duplicates selected sketch curves in an arc or a circular pattern.

- **Rectangular patterns:** Duplicates sketch curves in rows and columns.

3.2.2.3. Create (3D)

Once the sketch of the microfluidic platform has been finished, it time to move on to create the 3D structure. Inside the "Create menu" there are a lot of different options. However, only few of them have usage in terms of microfluidic fabrication. The following three useful options can be found in "Create menu":

- **Extrude:** Adds depth to a closed sketch profile or a planar face.

- **Revolve:** Revolves a closed sketch profile or a planar face around a selected axis.

- **Thread:** Adds internal or external threads to cylindrical geometry.

3.2.2.4. Modify

Modify has many options that can be use in a wide variety of situations. However, none of them are relevant in the production of microfluidic platforms. Nonetheless, it is important to ensure that in the appearance option is selected one of the glass materials (transparent/translucent); otherwise, channels will remain unseen.

3.2.2.5. Construct

There are some situations that will require the construction of one plane or an axis to proceed with the design. The following options can be found in "Construct menu":

- **Circular pattern:** Duplicates selected sketch curves in an arc or a circular pattern.

- **Rectangular patterns:** Duplicates sketch curves in rows and columns.

3.2.3. Modeling a simple microfluidic Y-shaped mixer

There are different pathways to finally design a microfluidic platform. In this section, we will show just an example. Nonetheless, diverse strategies can be used to produce the same platform. In every case, first we need to draw a 2D sketch and then create the third dimension.

3.2.3.1. Sketch

1. Create a sketch and choose the base plane (Figure 3.4-1).

2. Chose the size of the microfluidic platform using sketch option two-point rectangle (Figure 3.4-2).

3. Use fillet option in each corner (Figure 3.5-3); the importance of fillet will be explained in 3.4.6. troubleshooting.

4. Start drawing the microfluidic channels using line option (Figure 3.5-4).

5. Use mirror option (as many times as needed) to save some time drawing the mixing corners (Figure 3.6-5).

6. Draw the circles for inlets and outlet using two-point circle option (Figure 3.6-6).

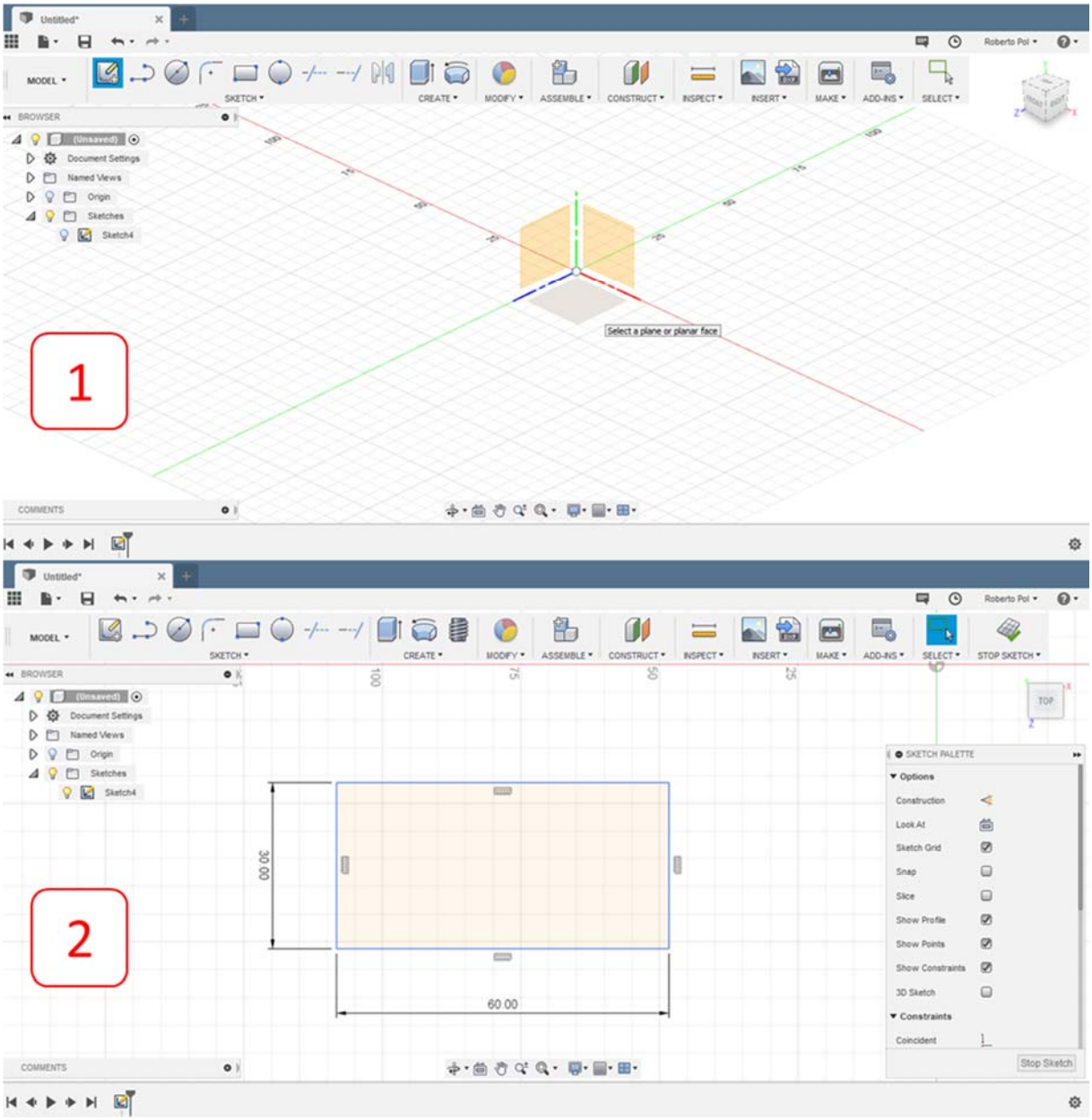

Figure 3.4. Creating a sketch (1) and drawing a rectangle (2).

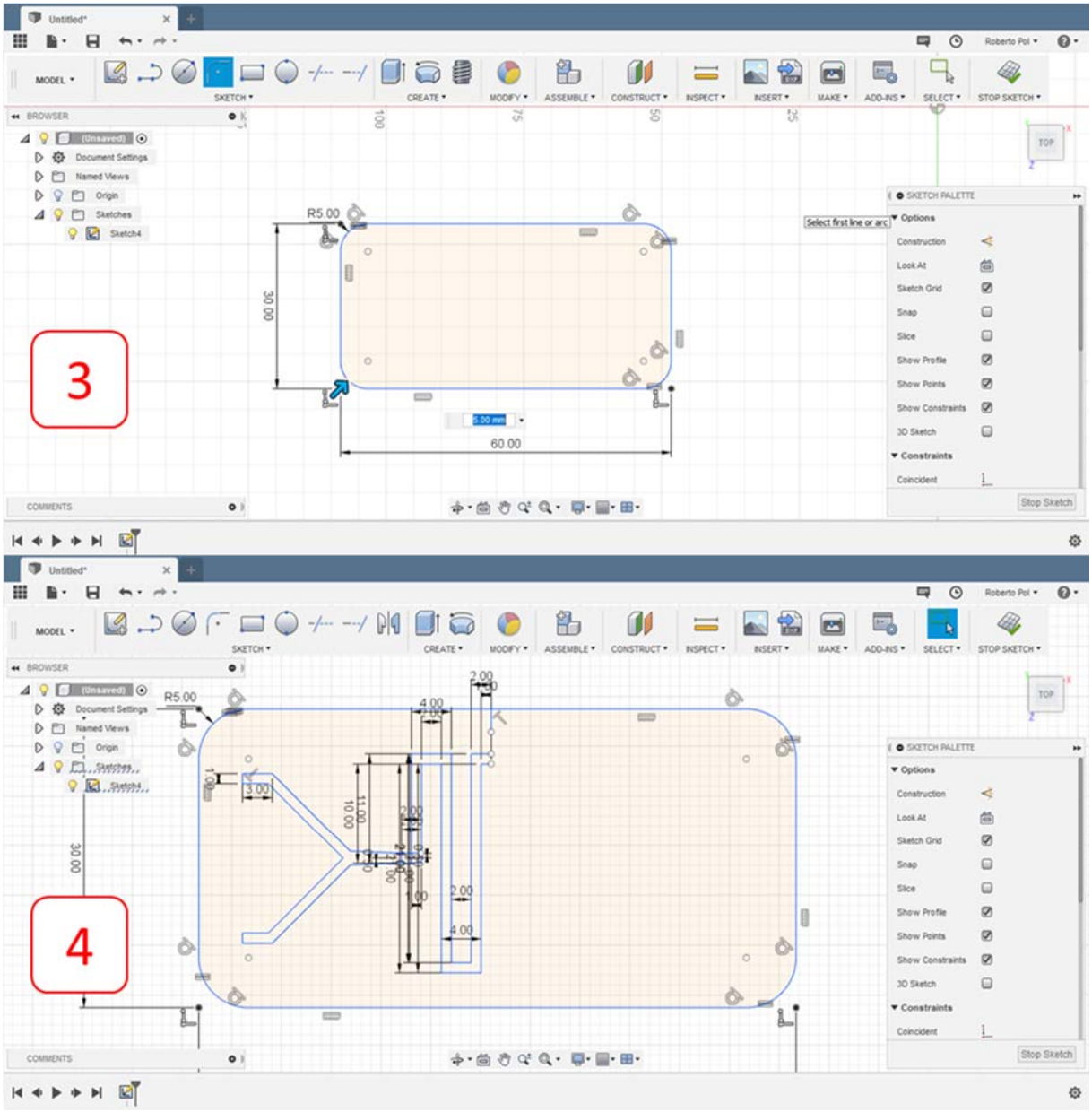

Figure 3.5. Rounding corners (3) and drawing the microfluidic path (4).

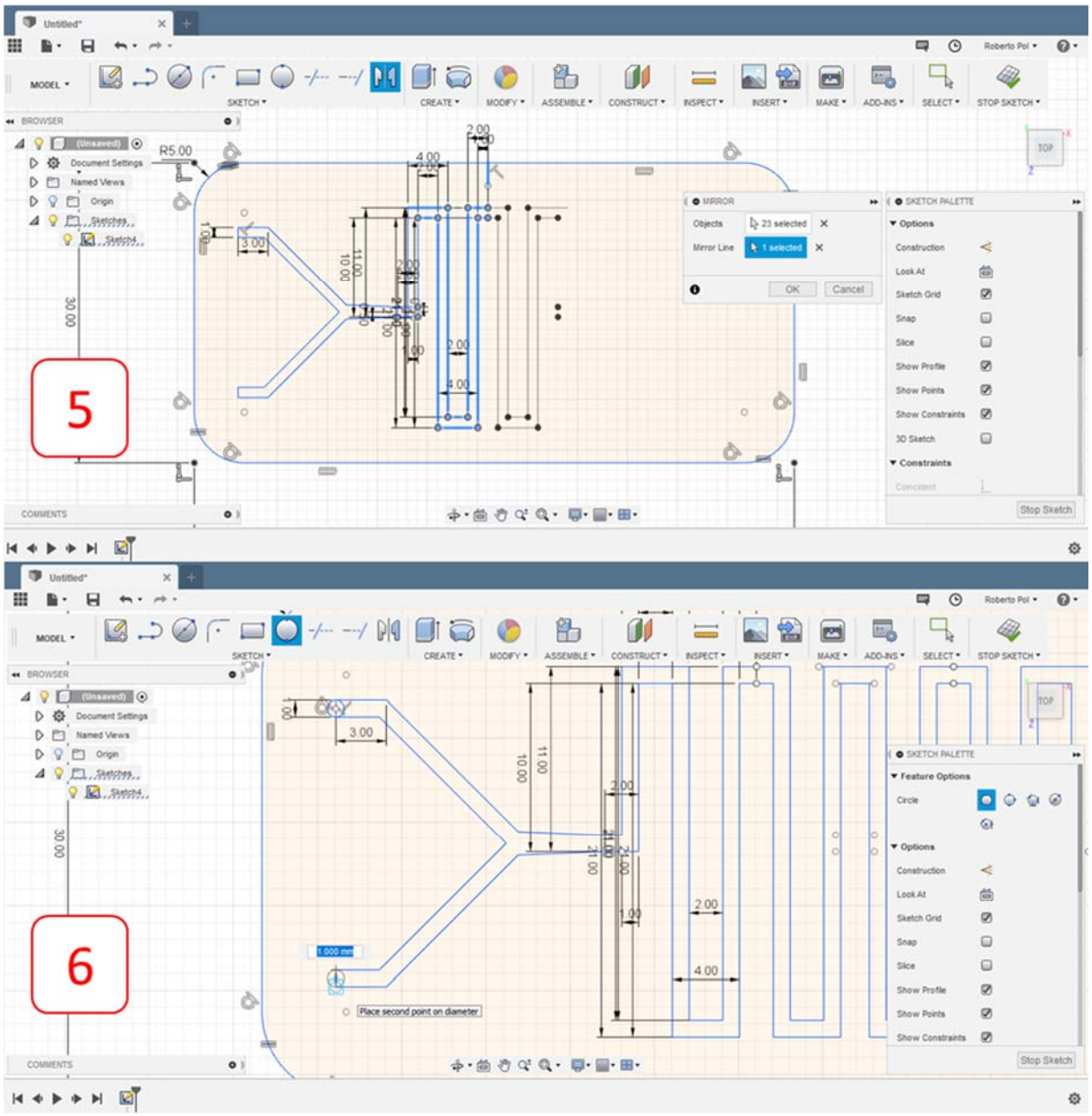

Figure 3.6. Taking advantage of mirror feature to automatically end the path (5) and drawing circle on inlets and outlet (6).

3.2.3.2. Create

Once all the 2D sketch is finished its time to give it the third dimension. For this step of the modelling software, the option extrude will be used constantly. It is important to play with show/hide options in “Browser menu”.

1. Open extrude option, select all the sketch and give the microfluidic system a defined thickness (Figure 3.7-1).

2. Open extrude option and select the microfluidic path (Figure 3.7-2). In the extrude menu chose the following:

- Start: offset plane.
- Offset: half of the thickness of the microfluidic system.
- Direction: symmetric.
- Measurement: both will work properly.
- Distance: the height of the microfluidic channel (beware measurement option).
- Operation: cut.

3. Open extrude option and select the inlets and outlets (Figure 3.8-1). In the extrude menu chose the following:

- Start: offset plane.
- Offset: half of the thickness of the microfluidic system – half of the channel height.
- Direction: one side.
- Extend: all.
- Operation: cut.

3.2.3.3. Save

The model needs to be saved in ".stl extension" to be readable for the slicer. To save it in this extension simple right click on top of the generated body on browser menu and chose to save as ".slt" and a new menu will appear. Just set high refinement and save the microfluidic system (Figure 3.8-2).

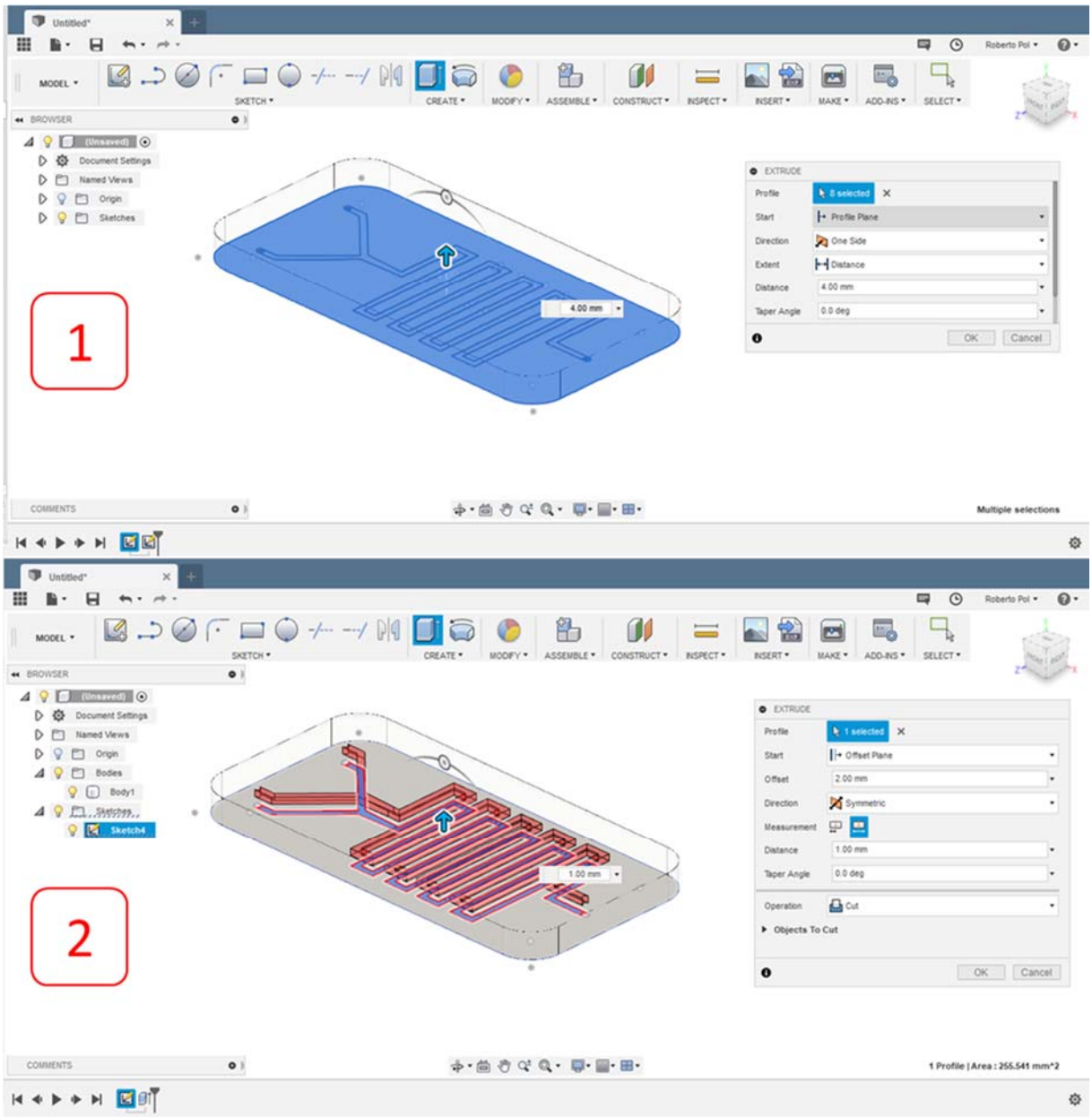

Figure 3.7. Extruding the thickness (1) and cutting the channel (2) of the microfluidic platform.

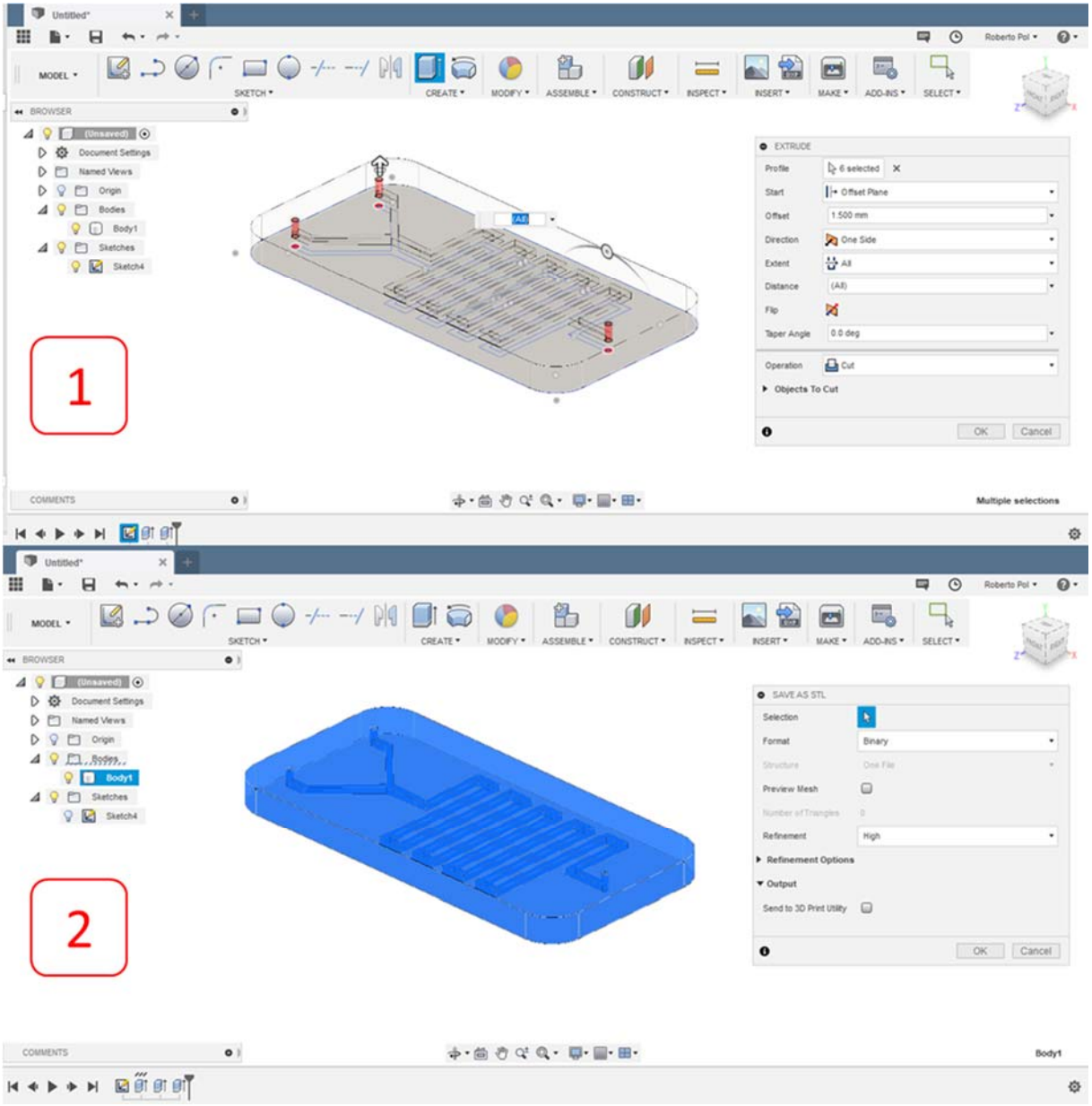

Figure 3.8. Cutting inlets and outlet (1) and saving in ".stl format".

3.2.4. Slicing software

The slicer software that has been used throughout is CuraBCN3D v. 0.1.5 and therefore, will be used as a standard to explain modeling software. Unlike modeling software, using one slicer or another is crucial when producing the microfluidic devices. 3D printing slicing software controls every aspect of your 3D print. It translates 3D models into instructions your printer understands. Therefore, better instructions mean better prints, so a simple software upgrade makes all the difference.

3.2.4.1. User interface

The user interface can be broken up into 6 areas (Figure 3.9):

1. **Menu bar:** used for data management and define printer settings.

2. **Data management:** used for loading 3D printing files, 3D printing settings profiles and transform the model into G-code.

3. **Orientation/Size:** orientates the model to be printed in the most efficient way. Also used to rescale or mirror it.

4. **Canvas:** canvas contains the 3D model.

5. **Printing settings:** define all parameters regarding printing quality, materials and filaments.

6. **View mode:** 3D model can be visualized with different tools to ensure the best parameters.

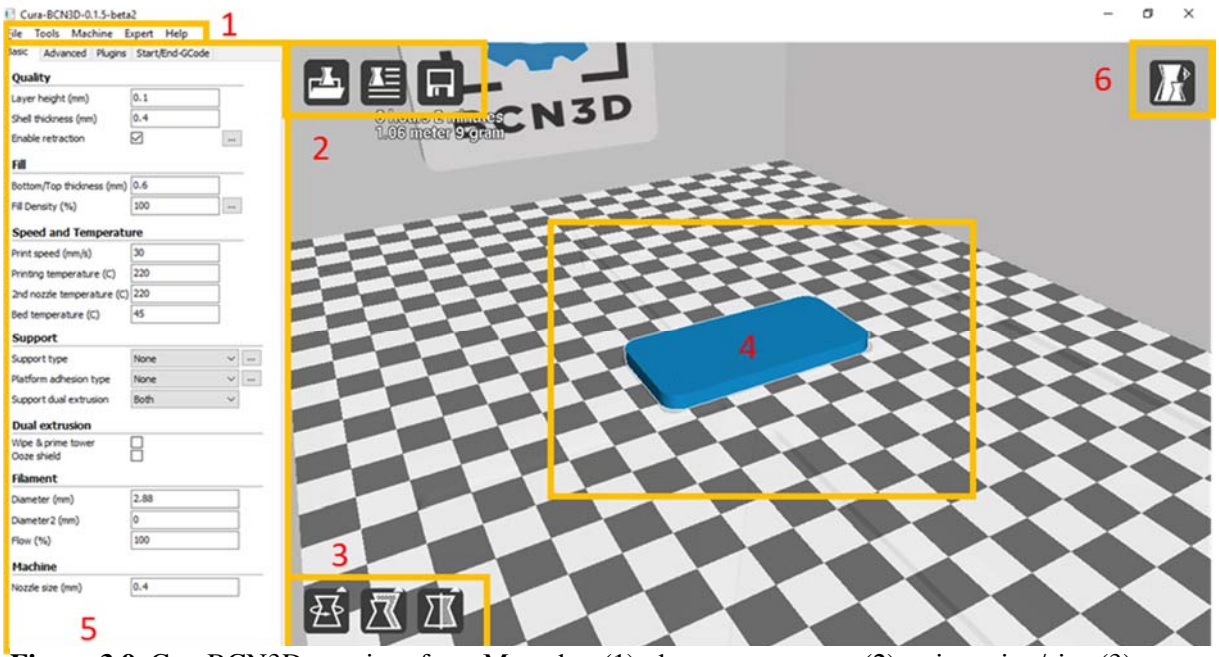

Figure 3.9. CuraBCN3D user interface: Menu bar (1), data management (2), orientation/size (3), canvas (4), printing settings (5), viewmode (6).

To help readers to become familiar with 3D slicing we will describe area 5 and go into more details with how to set it in the following sections.

3.2.4.2. Printing settings

Hereunder, we will discuss the most important printing settings.

- **Layer height:** layer height of each one of the Z layers. Higher values produce faster prints in lower resolution, lower values produce slower prints in higher resolution.

- **Shell thickness:** the thickness of the walls in the horizontal direction. This value divided by the wall line width defines the number of walls.

- **Enable retraction:** retract the filament when the nozzle is moving over a none-printed area.

- **Bottom/Top thickness:** this controls the thickness of the bottom and top layers, the amount of layer put down is calculated by the layer thickness and this value.

- **Fill density (%):** this control how densely filled the inside of your print will be.

- **Print speed:** the speed at which printing happens.

- **Printing temperature:** temperature used for printing; defined by the material used.

- **Bed temperature:** temperature used for the heated printer bed; defined by the material used.

- **Platform adhesion type:** different options that help to improve both priming your extrusion and adhesion to the build plate. Brim adds a single layer flat area around the base of your model to prevent warping. Raft adds a thick grid with a roof below the model. Skirt is a line printed around the model but not connected to it.

- **Filament; diameter:** adjusts the diameter of the filament used.

- **Nozzle size:** the nozzle size is used to calculate the line width of the infill and to calculate the amount of outside wall lines and thickness.

- **Retraction; Speed: s**peed at which the filament is retracted, a higher retraction speed works better but a very high speed can lead to filament grinding.

- **Retraction; distance:** distance at which the filament is retracted.

3.2.5. Slicing the microfluidic Y-shaped mixer

Each slicer and each printer will have its very own optimized parameters. Here we will show the ones that gave good printing quality for our purpose and briefly explain why.

First, the model needs to be loaded to the canvas and provide the best orientation. Through several tests, we found that the best orientation was flat with a 15º rotation (Figure 3.10); the importance of rotation will be explained in 3.4.6. troubleshooting. Finally, the parameters can be selected:

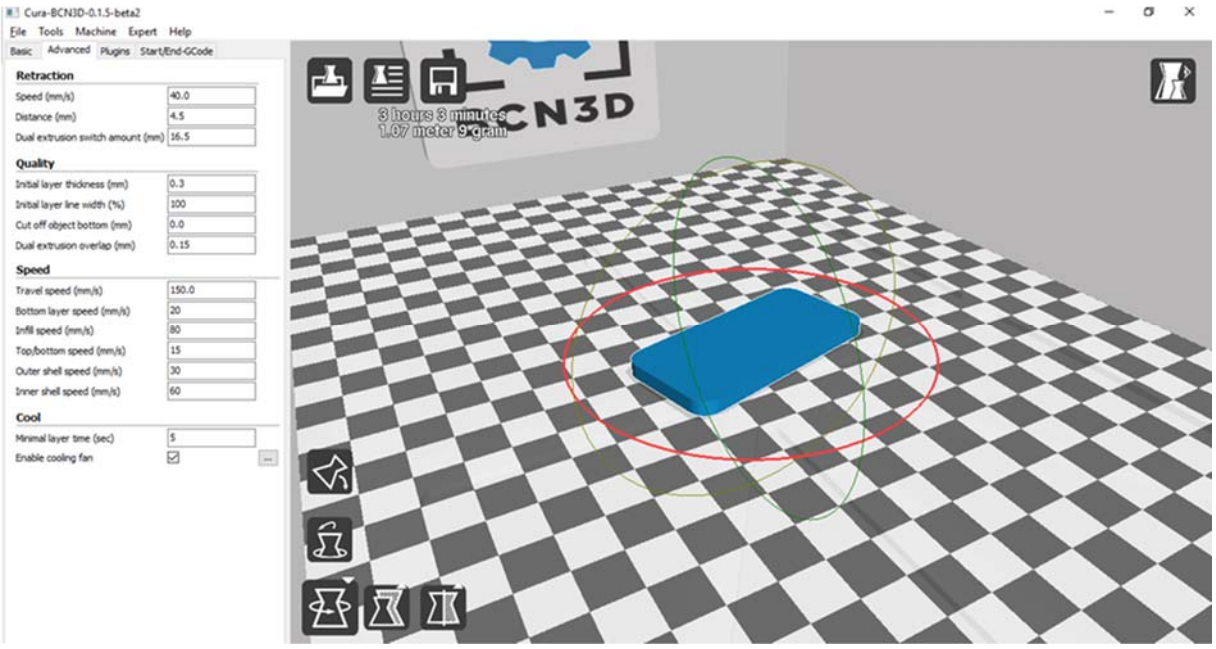

Figure 3.10. Optimal printing orientation.

- **Layer height:** our printer can print smaller (0.05 mm) and bigger (0.3 mm) layer height. Smaller layers give outstanding quality prints, otherwise, they take too much time to print (more than 2 h) and higher layer height works the other way around. A compromise between printing time and quality was key and finally 0.1 mm layer height was always chosen.

- **Fill density (%):** in most printing scenarios, the fill density is commonly chosen between 20% and 50%, which give a good quality/time ratio. Nonetheless, in the world of microfluidics the best fill density is 100%. It makes the printing time longer, but the quality is perfect and spill problems are avoided.

- **Print speed:** although print speed can be easily tuned, each printer has a range that works properly. In our case, 100 mm/s.

- **Printing temperature:** the printing temperature is set depending on the material. As we have used the same commercial polylactic acid for fabrication of all devices the printing temperature was set to 220 ºC.

- **Bed temperature:** the bed temperature is set depending on the material. As we have used polylactic acid for fabrication of all devices the bed temperature was set to 45 ºC.

- **Platform adhesion type:** all printed devices were adhered using brim; the importance of brim will be explained in 3.4.6. troubleshooting.

- **Filament; diameter:** the printer works with ~2.9 mm filaments.

- **Nozzle size:** although nowadays there are a lot of nozzle size, we have used the traditional one always; 0.4 mm.

- **Retraction; speed:** an optimal retraction speed of 40 mm/s was chosen.

- **Retraction; distance:** in most printer 4.5 mm is the best retraction distance.

3.2.6. Printer considerations

A crucial point to consider is the specifications of the printer that is going to be used. Nowadays, there are hundreds of printers commercially available at different prices and each one presents different printing specifications. Understanding the limitations of the 3D printer is key to produce a microfluidic system. Although, 3D printing is a technique that presents high versatility in fabrication terms, some architectures cannot be achieved due to each printer specifications. During this PhD thesis, the 3D printer that has been used is BCN3D Sigma. This printer belongs to the fused deposition modeling style and is one of the top worldwide 3D printers.[2] This printer has independent dual extruder system that delivers high-resolution multi-material parts in a simple and effective way. The unique Independent Dual Extruder system allows to print 2 different materials whereas ensures the finest surface finish. The idle tool head remains parked, preventing the dripping of molten plastic onto the part. It presents a resolution of 12.5, 12.5 and 1 μm for x, y and z axis, respectively. It can work with several nozzle diameters (0.3, 0.4, 0.5, 0.6, 0.8 and 1 mm) and uses 2.85 mm filament. Several materials are available to be printed at temperature below 290 ºC (polylactic acid, acrylonitrile-butadiene-styrene, nylon, polyvinyl alcohol…).

3.2.7. Troubleshooting

As in every aspect of life, sometimes 3D printing also goes wrong. Experience gain by 3D printing failure through these years is depicted. The most common problems and the way of solving them are collected hereunder:[3]

- **Not extruding at start of print (Figure 3.11A):** this issue is a very common. We found two different causes for that issue. The first one is that the extruder was not primed before beginning the print. At high temperatures the filament oozes out of the nozzle and an empty place appears. The simplest solution is to use a brim or a skirt which will ensure the extruding at the point of printing the device. The other possibility is that the teeth of the gear responsible of pushing the filament to the nozzle has break the filament. Just get rid of the broken filament and fill it with a new one.

- **Print not sticking to the bed (Figure 3.11B):** it is very important that the first layer of your print is strongly connected to the printer's bed so that the remainder of your part can be built on this foundation. Otherwise, a printing failure is ensured. There are different causes that provoke this fact to happen. The most important one is that the printer calibration was not done properly. The bed must be well adjusted and the distance of the nozzle from the bed must me optimized. Some materials (*e.g.* acrylonitrile-butadiene-styrene) are hardly attach to the bed, therefore an adhesive should be used. There are some printers that have their own adhesive platforms. An alternative option is to use any hair lacquer (beware, some companies sell their own 3D printing adhesive spray at a high cost; it is composed with the same chemicals that hair lacquer).

- **Not extruding enough plastic (Figure 3.11C):** sometimes on top of the device will appear holes between the corners and the infill. In our case this has never happened. However, non-expert 3D printer users can face this problem and the solution is not obvious. This is caused by an incorrect filament diameter. All fused filament fabrication 3D printer uses either 1.75 mm or 2.85 mm filament. Filament can be purchased in a wide variety of online webs at different prices. There are some places that sell them at a lower cost compared to others. In those cases, the filament is commonly one that has not the correct diameter (*i.e.* the filament has a diameter of 2.80 mm) which will cause under-extrusion. Therefore, always buy filaments that the company of the 3D printer endorse.

- **Layer separation and splitting (Figure 3.11D):** 3D printing works by consecutive printing layers of plastic on top of the previous. To end up with a strong and reliable device, you need to make sure that each layer adequately bonds to the layer below it. If the layers do not bond together well enough, the final part may split or separate and fluid will spill of it. There are to possible ways to outcome that problem. The first one is to reduce the layer height. If the layer height is 0.1 mm and this problem persist, then increase 10-20 ºC the printing temperature. All filaments have a working temperature in the material datasheet. When building microfluidic devices always use the higher temperature that your filament can handle; this will increase cohesion between layers and avoid spills.

- **Layer shifting or misalignment (Figure 3.11E):** almost all 3D printers have an open-loop control system. This means that during the printing process there is no tracking of the position of the nozzle. Therefore, if something goes wrong, there is no way for the printer to reset and fix the issue. There are two possible explanation for that. First one is that the print head moves too fast; for most of the printers try to avoid travel speed higher than 100 mm/s. The other possibility is that the rubber belts that are attached to the motor have been damaged through time and must be replaced.

- **Vibrations and ringing (Figure 3.11F):** ringing is a wavy pattern that may appear on the surface of your print due to printer vibrations or wobbling. These can be caused by the same reason that layer shifting and can be solved alike. However, in some printer it is caused by the vibration of the printer during the printing process. In most of the cases is solved by moving the printer to a more stable table.

- **Warping (Figure 3.11G)**: as you start printing larger models, you may start to notice that even though the first few layers of your part successfully adhered to the bed, later the part begins to curl and deform. This fact can be such devastating that your 3D printed model can move completely making the printing process fail. This problem is very common when printing high planar surface objects such as the microfluidic systems. This problem is caused by the shrinkage of plastic while cooling. There are three combined ways that will ensure the print to be stick to the bed throughout the printing process. First, when designing the model, use fillet in every corner of the device; this will make plastic shrinkage less aggressive. Second, always use brim as platform adhesion. Finally, use hair lacquer.

- **Poor bridging (Figure 3.11H):** bridging is a term that refers to plastic that needs to be extruded between two points without any support from below. Some slicer allows you to determine the path that your printer does when drawing the structure. However, most slicers lack of this feature. If one of the microfluidic paths goes alongside the printing path it will be partially or totally clogged. The simplest way to avoid that is to twist the device 15º to avoid the coincidence of both paths.

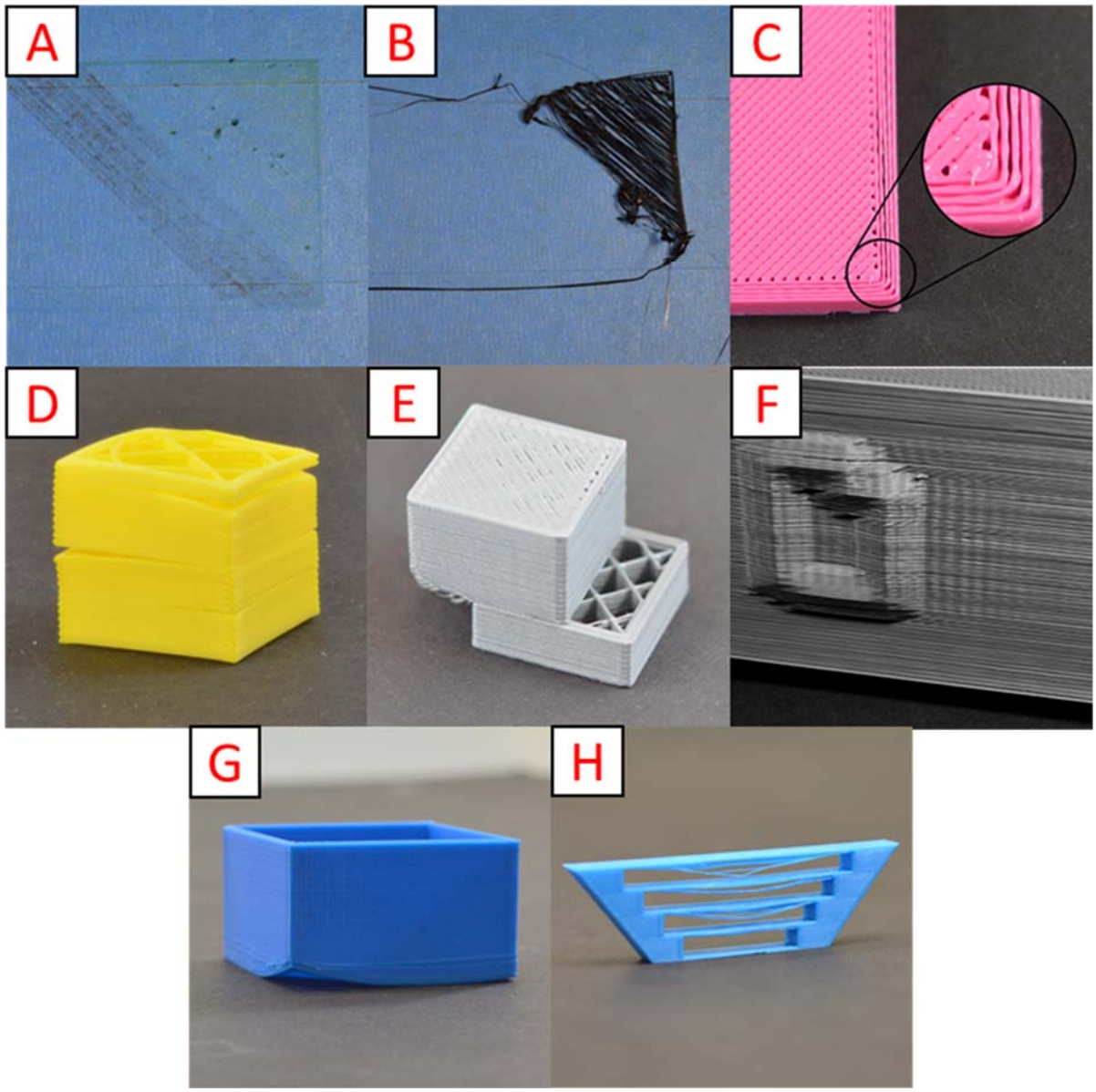

Figure 3.11. Troubleshooting examples: not extruding at the start (A), not sticking to the bed (B), under-extrusion (C), layer splitting (D), layer shifting (E), vibrations (F), warping (G) and poor bridging (H).

3.3. References

(1) Introduction to Fusion360 (2018): https://myhub.autodesk360.com/ue29c9141/g/shares/SH7f1edQT22b515c761ee5876890150905c9.

(2) BCN3D Sigma (2018): https://www.bcn3dtechnologies.com/en/3d-printer/bcn3d-sigma/.

(3) Troubleshooting (2018): https://www.simplify3d.com/support/print-quality-troubleshooting/#not-extruding-at-start-of-print.

CHAPTER 4

Microfluidic lab-on-a-chip platforms for environmental monitoring

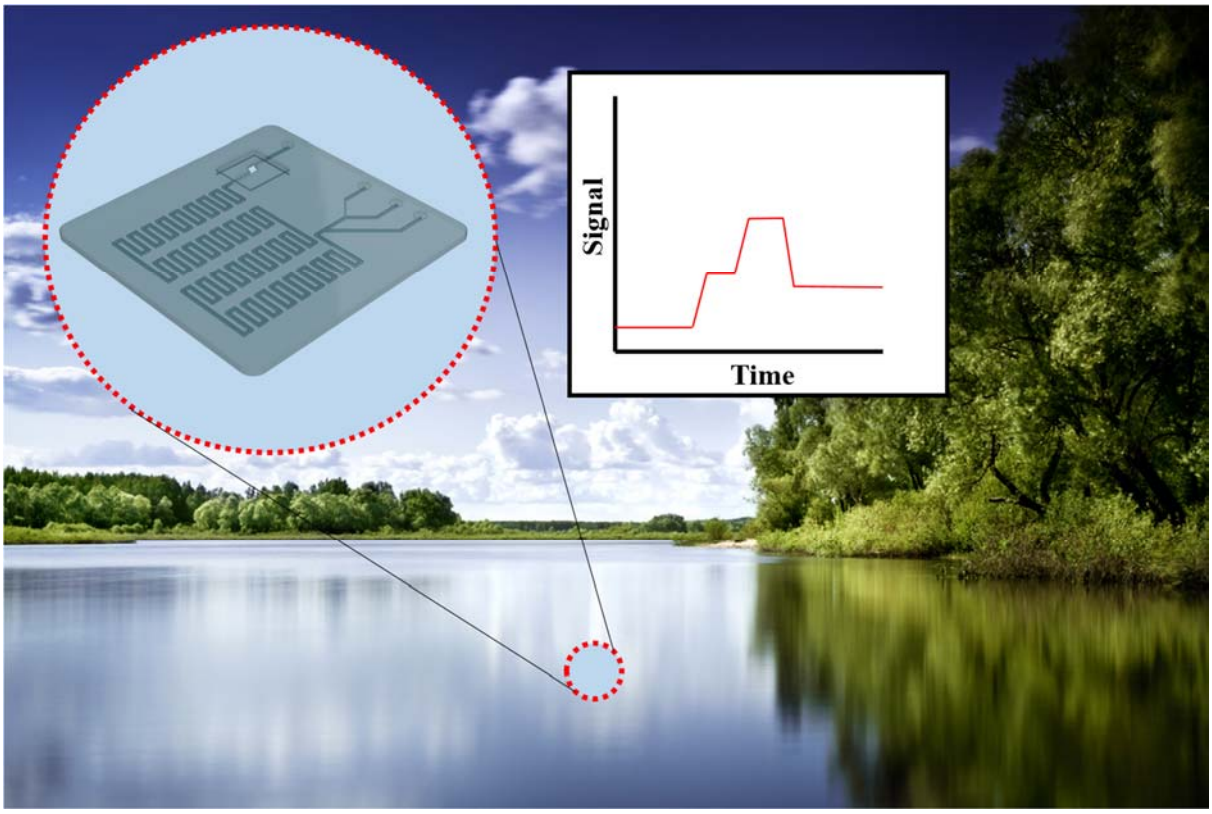

This chapter is a modification of:

Microfluidic lab-on-a-chip platforms for environmental monitoring
R Pol, F Céspedes, D Gabriel, M Baeza
Trends in analytical chemistry 95, 62-68 (2017)

4.1. Foreword

The first stage that everyone encounters when facing the beginning of a research project is the exploration of the so-called "state-of-the-art". Scientist need to review foregoing works regarding their targeted problem and try to find a better alternative or at least a gap that has not been covered yet. The aforementioned project (Chapter 2) already covered the sensors that were going to be used. For instance, sulfide was going to be measured by potentiometric means using a crystalline-membrane electrode. Furthermore, integration of the sensors in a microfluidic platform to enable online monitoring was also enclosed.

Although the development of sensors for the monitoring and control of the two most significant chemicals, the sulfide and sulfate ions involved in the biotechnological process, was well-covered, we decided to further explore what was being done in terms of the fabrication of microfluidic devices for environmental purposes (biotechnological and environmental sensing application are closely related). In this context, we tried to find a way to fulfill both statements:

i. Find a better alternative.
ii. Fill a gap that has not been covered yet.

4.2. Introduction

Microfluidic lab-on-a-chip (LOC) platforms have been extensively studied due to their possibility of replacing a fully equipped conventional laboratory.[1,2] Since traditional analysis methods consist of multiple steps (e.g. sampling, transport, pre-treatment…) and are rather costly and time consuming, the emphasis nowadays is shifted towards the use of remote automated systems in a miniaturized fashion. Well-known advantages of these LOC sensing systems include: compactness, low sample consumption, low-cost production, better overall process control, real-time analysis and a fast response.[3,4] These characteristics open the possibility of performing in situ, real-time measurements. Also, LOC operate in such a manner that sample pre-treatment as well as chemical assay can be performed therein. Their ergonomic and user-friendly design allows LOC to be easily adapted to perform a desired analysis just by simply modifying the pattern of the channels. This makes LOC of interest in processes that require multiple analyses at the same time. For instance, a LOC device could be able to continuously analyze pollutants from wastewater serving as an always-on environmental alarm.[5] When combining the aforementioned technology with wireless communication, it becomes a powerful tool with the possibility of remotely modify acquisition parameters as well as enable data transfer. Therefore, the ever-increasing demand of remote autonomous multiplexed analytical systems make LOC a suitable approach for chemical agents screening in different fields. That said, in the present review we expose the latest developments in environmental LOC monitoring devices (that could determine concentration of contaminants around the maximum level that is allowed in drinking water by the Environmental Protection Agency) and provide future perspective.

4.3. Electrochemical

Commonly, electrochemical LOC working principle is based on an electrical signal produced by an interaction between the analyte and the electrode surface. In this section, we will briefly discuss some of the latest electrochemical devices for environmental monitoring that have been proposed by the scientific community.

A smart approach for the detection of inorganic anions (Cl^-, NO_3^-, SO_4^{2-} and NO_2^-) in environmental samples using a microchip electrophoresis system with capacitive coupled contactless conductivity detection (Figure 4.1a) was reported by Freitas *et al*.[6] The device was composed by four electrodes; two of them were used as excitation or receiver and the other two were used as reference electrodes to minimize the stray capacitance. Inorganic anions were successfully separated within 60 s using a mixture of lactic acid (30 mM) and L-histidine (15 mM), and $Cr_2O_7^{2-}$ as internal standard (Figure 4.1b). Once selectivity and sensitivity were optimized, the device presented a linear behavior from 0 to 120 μM for Cl^-, NO_3^- and NO_2^- and from 0 to 60 μM for SO_4^{2-}. The authors explored the feasibility of the presented device in real environmental samples. First, an artificial spiked-environmental sample was used to check the spontaneous oxidation of ammonium to nitrite and a further oxidation to nitrate for twelve weeks. After the concept was proven to be suitable for the simulated environment, authors proceeded with the screening of nitrogen species in an aquarium containing *Danio rerio* fishes. For eight weeks, they were able to monitor an absence of nitrite, suggesting the direct oxidation of ammonium to nitrate. These results demonstrate the feasibility of the device for *in situ*, real-time inorganic anions analyses.

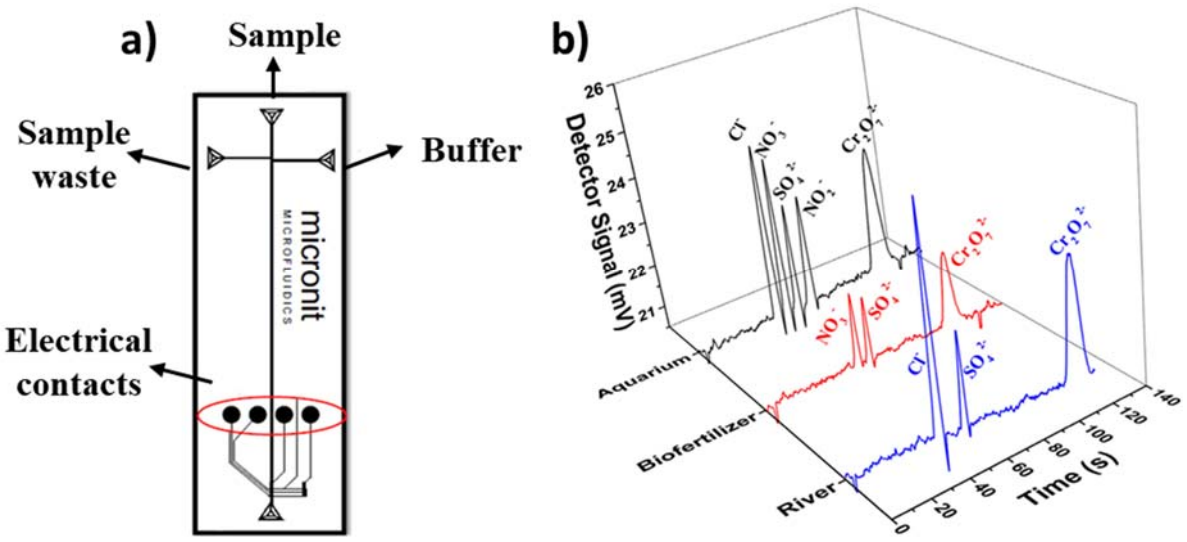

Figure 4.1. Scheme of the microchip electrophoresis device for inorganic anions quantification (a). Electropherograms showing both, separation and detection of diverse ions Cl^-, NO_3^-, SO_4^{2-} and NO_2^- in three kinds of real samples: aquarium (black), biofertilizer (red) and river (blue), using $Cr_2O_7^{2-}$ as internal standard (b).

An interesting environmental application for LOC platforms was reported by Calvo-López *et al*. [7] As the total charge of an aerospace ship is limited, recycling of resources like water is crucial, and thereby tracking the quality of water. The authors reported a bipotentiometric (NO_3^- and K^+) LOC system for water monitoring in manned space flights (Figure 4.2). The LOC system was constructed using low temperature co-fired ceramics with integrated potassium and nitrate ion-selective electrodes and a silver paste-based pseudo-reference electrode. Polyvinyl chloride-based membranes containing well-known ionophores for nitrate and potassium ions (tetraoctylammonium nitrate and valinomycin, respectively) were used as recognition elements. Authors studied the behavior of the response towards the most common interferences (Na^+, NH_4^+, Ca^{2+}, Mg^{2+}, HCO_3^- and Cl^-), demonstrating no significant interference at the expected concentrations on these particular ions at environmental conditions. Moreover, authors tested the performance of their device with recycling water provided by the Antarctic Concordia station and compared their results with the ones obtained by optical emission spectrometry (K^+) and ionic chromatography (NO_3^-). While potassium ion determination gave outstanding results, nitrate ion determination selectivity was outperformed by chloride ion at concentration surrounding the limit of detection. Moreover, authors demonstrated the feasibility of low temperature co-fired ceramics-based LOC for multiplexed ionic determination in recycling water with potential applicability in manned space flights.

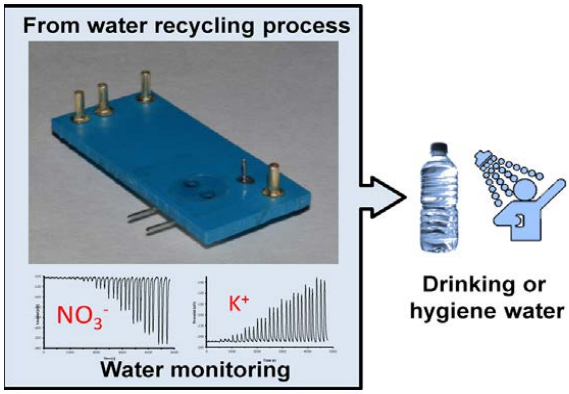

Figure 4.2. Concept representation of the presented bipotentiometric LOC (NO_3^- and K^+) constructed in low temperature co-fired ceramics for water monitoring in manned space flights.

The crucial point as far as toxicity is concerned is the understanding of the chemical changes of pollutants produced by external factors. A LOC electrochemical cell with boron-doped diamond (BDD) electrodes (Figure 4.3a) for metabolism studies of common environmental xenobiotics and their respective protein adduct formation was developed by Floris *et al*. [8] One

of the main features of microfluidics systems is the laminar flow behavior of the liquid which slow the final mixing purpose of the device. To overcome that feature, the authors developed a passive gradient rotation micromixer (Figure 4.3b) reducing the mixing time to milliseconds. To prove the potential of the device, 1-hydroxypyrene was chosen as a common polycyclic aromatic carbon produced by the non-complete combustion of organic matter. To produce the corresponding oxidized molecules of 1-hydroxypyrene, a 1.2 V potential was applied by the BDD electrode. Then the xenobiotics obtained were analyzed by a mass spectrometer directly coupled to the LOC system. The oxidized molecules were allowed to react with two different proteins, β-lactoglobulin A and hemoglobin showing the formation of adducts and therefore affecting their biological capabilities. To conclude, authors demonstrate the potential of LOC systems for understanding the toxicity of common environmental xenobiotics in a fast and cheap manner.

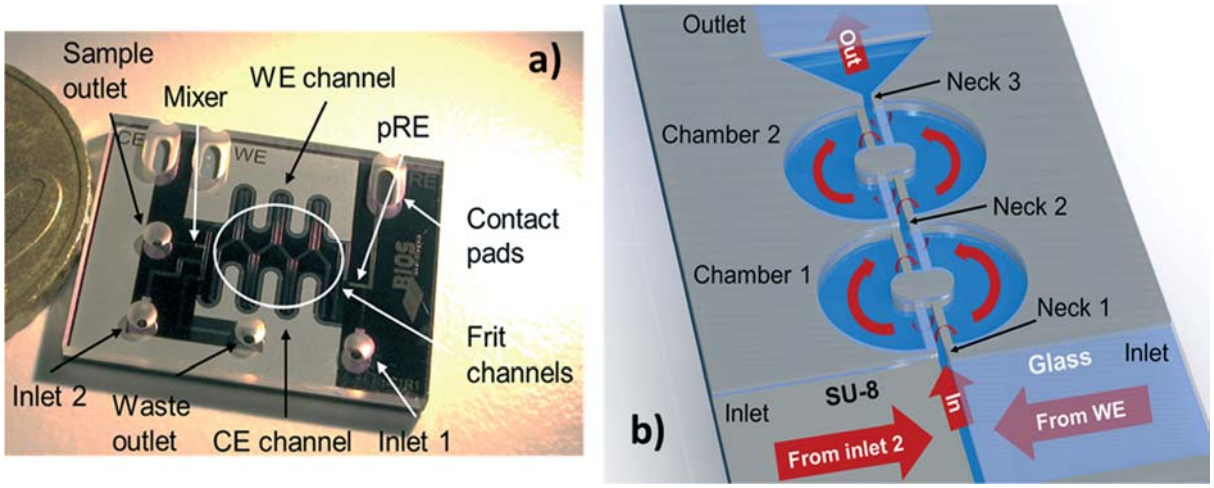

Figure 4.3. Image of the LOC device for xenobiotic metabolites monitoring (a). Proposed passive gradient rotation micromixer (b).

Along the present review chapter, electrochemical LOC devices have been presented as portable sensing platforms. However, Medina-Sánchez *et al.* [9] step forward designing a set of microfluidic platforms for atrazine sensing and degradation based on BDD electrodes (Figure 4.4). Smartly, selection of BDD electrodes was due to their low adsorption capacity towards organic pollutants, inert nature and higher O_2 overvoltage making them an appealing option for both, sensing and degradation in flow systems. On the one hand, the working principle of the sensor relied on a competitive assay between horseradish peroxidase-labelled atrazine and free atrazine for anti-atrazine antibody immobilized onto magnetic beads. On the other hand,

simultaneous degradation of atrazine takes place in a different microfluidic platform. The degradation is based on the production of superoxide radicals when a current is applied to the BDD electrode, being those radicals able to breakdown atrazine into cyanuric acid, which is a considerable less toxic molecule. Overall, authors presented a LOC which shows an impressive limit of detection of 1 nM of atrazine whilst degrading over a 97% of atrazine (30 nM).

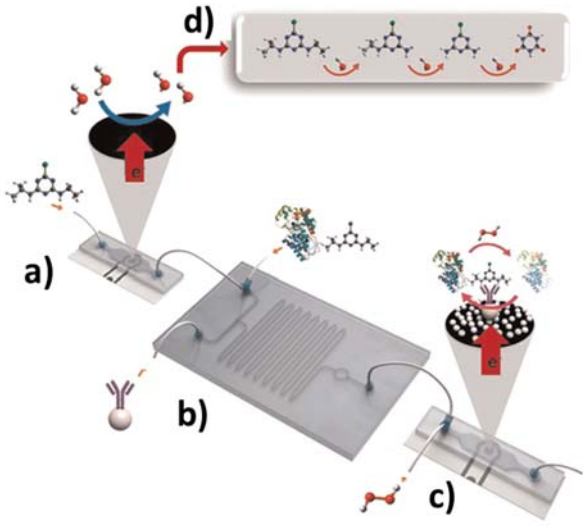

Figure 4.4. LOC platform scheme for detection and degradation of atrazine. Degradation microfluidic platform (a). Microfluidic mixer for magneto-enzyme immunoassay (b). Detection microfluidic platform with a platinum nanoparticles-modified BDD electrode as the detector (c). Mechanism proposed for the atrazine degradation via superoxide radicals; from atrazine (left) to cyanuric acid (right) (d).

Another approach that includes sensing and degradation was reported by the same research group. [10] The contaminants studied were polybrominated diphenyl ethers (PBDE), a family of flame retardants that has become a global threat. Once again, the working principle of the sensor relied on a competitive assay between free PBDE and horseradish peroxidase-labelled PBDE for anti-PBDE immobilized onto magnetic beads. The system consisted of three consecutive microfluidic platforms each one with a defined function (Figure 4.5). In the first platform, the immunoreaction takes place through a simple passive mixer. Then, detection happens in the second chip by measuring the reduction of 3-aminophenoxazone (produced by the oxidation of o-aminophenol) using square wave anodic stripping voltammetry. With the use of this electrochemical technique the authors were able to achieve an impressive limit of

detection of 0.018 ppb. Finally, in the third chip PBDE is adsorbed onto a composite containing reduced graphene oxide thanks to π-π stacking interactions. Furthermore, authors demonstrate the potential of their system for real measurement of spiked seawater samples.

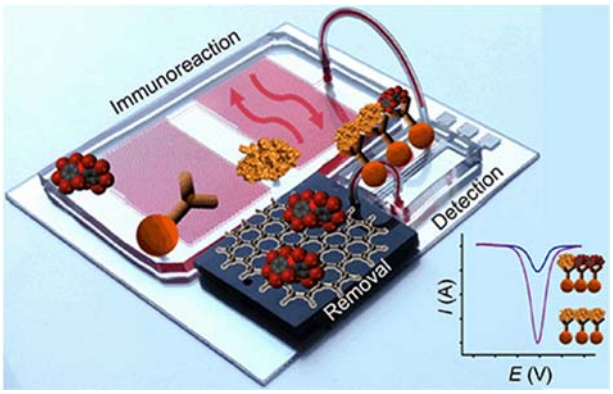

Figure 4.5. Assembled device containing three consecutive LOC for immunoreaction, detection and removal of PBDE.

Gonzalez-Rivera *et al*. [11] developed a flow-injection LOC platform for determination of phenolic compounds by amperometry (Figure 4.6). Authors extensively studied the grade of immobilization of lacasse by potential step chronoamperometry. To demonstrate the successful immobilization, electrochemical impedance and cyclic voltammetry were carried out before and after immobilization. The increase of the charge transfer resistance and the current decrease of oxidation and reduction peaks ensured a successful approach for electrochemical immobilization of enzymes. Once the presence of laccase in the working electrode was proved, authors studied several parameters (pH, temperature, potential applied and injection rate) that would affect the electrochemical performance of the LOC. To prove the performance of this device (2,2-azino-bis(3-ethylbenzothiazoline-6) sulphonic acid) and syringaldazine were chosen as phenolic compounds achieving a limit of detection of 0.149 and 10 μM, respectively. Furthermore, this LOC platform showed good stability up to 10 days. To conclude, this microfluidic biosensor showed its potential for monitoring of phenolic compounds.

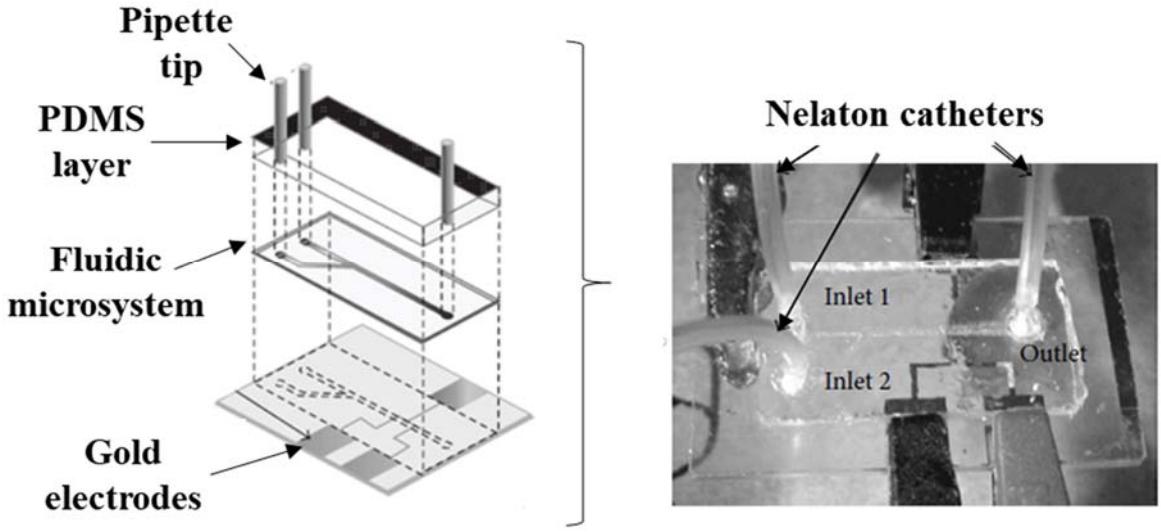

Figure 4.6. Diagram of the microfluidic biosensor system layer by layer and its set-up.

4.4. Optical

So far, several electrochemical strategies have been presented for environmental screening purposes. Otherwise, optical devices are well-known for their simplicity and low-cost. Commonly, optical LOC rely on a color change given by an interaction or reaction between the pollutant (analyte) and a chemical reagent. Although most of the microfluidic devices shown so far are made of polymeric materials, paper-based microfluidic systems will excel as platforms for simple colorimetric reactions.

Cardoso *et al.* [12] reported the use of disposable microfluidic paper-based device for colorimetric detection of nitrite ion in environmental samples. The change of color (from colorless to strong pink) in the presence of nitrite was based on the well-known Griess reaction. The device itself consists of eight star-like paths, in which three of them were used as controls (1-3) and five of them as detection areas (4-8) for standards or samples (Figure 4.7a). Although the presence of nitrite ion was easily discernible by naked eye, the use of a common office scanner and digital photo software for colorimetric calibration was explored. A linear response between 0 and 100 μM (Figure 4.7b) with a limit of detection of 11.3 μM. Authors determined the nitrite ion concentration in a river and compared it with the one quantified by spectrophotometry in batch, finding no significant difference at a confidence level of 95%.

Therefore, a cheap substrate was demonstrated to be a powerful tool for *in situ* colorimetric determination with environmental sensing purposes.

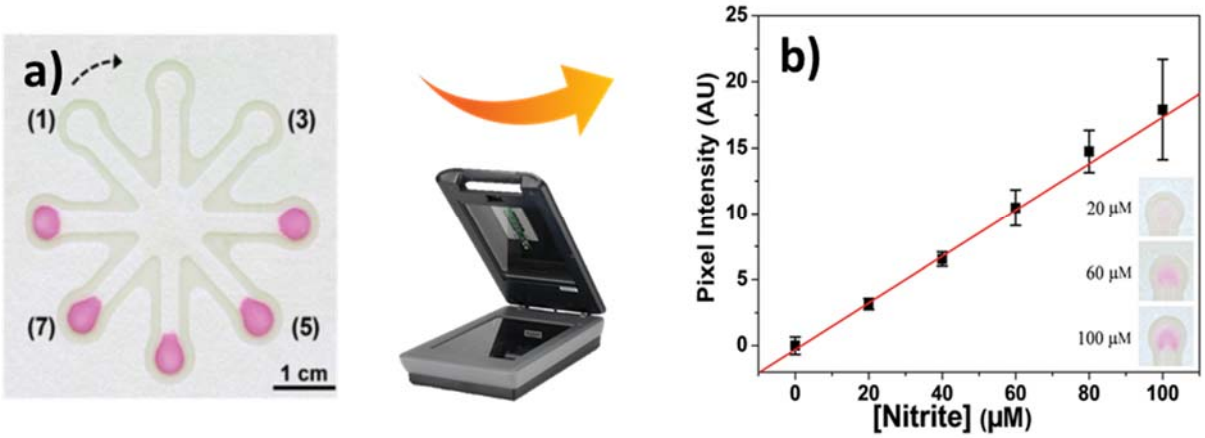

Figure 4.7. Microfluidic paper-based analytical device used for nitrite ion determination through the modified Griess reaction (a). (1-3) and (4-8) cavities correspond to control and detection areas for standards or samples, respectively. Calibration curve obtained for nitrite ion from 0 to 100 μM (b).

Another paper-based LOC system was developed by Kim *et al*. [13] The wax-printed LOC platform was designed for fast microorganism detection in environmental samples using *Escherichia coli (E. coli*) as a proof of concept. The sensor working principle relied on the combination of catalase and Fenton's reactions for an easy colorimetric detection. First, a solution containing *E. coli* is mixed with hydrogen peroxide. Then, the remaining hydrogen peroxide reacts with iron (II) compound at the paper-based LOC chambers and a change of color from pale yellow (higher *E. coli* concentration) to brown (lower *E. coli* concentration) occurs. Therefore, brightness increases as the microorganism concentration increases (Figure 4.8a). The authors also designed a simple 3D-printed holder for fully integration into a hand-held LOC device for field detection without the need of expensive equipment (Figure 4.8b). Finally, the device performance was tested on several real environmental samples (mineral water, drinking water, humidifier water…) showing good correlation with their calibration for an *E. coli*-simulated environment. As a result of the paper-based LOC performance, authors conclude that it could find uses in real environmental contexts for *in situ* measurements.

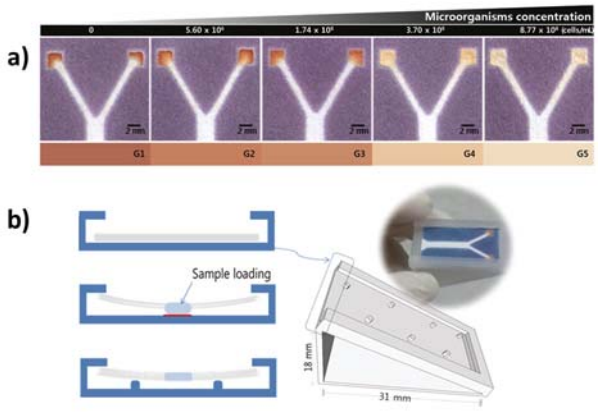

Figure 4.8. Colorimetric assay with paper-based LOC for five different E. coli concentrations (from 0 to 8.77x108 cells/mL) (a). 3D-printed paper LOC holder design to prevent sample adhesion to the surface (b).

Another interesting LOC platform for microorganism detection was studied by Huang *et al*.[14] The LOC platform is coupled with a multi-angle laser scattering system which could acquire scattering patterns of single molecules (Figure 4.9). The LOC itself is composed of one-channel with a stretching (called interrogation zone) at which analysis are performed. To process the complex data acquired, a pattern recognition method and support-vector-machine algorithm. Authors optimized the configuration of the LOC using polystyrene microparticles to accomplish high signal to noise ratio. Afterwards, authors tested the device using several waterborne microorganisms (*C. parvum, G. lamblia and E. coli*) over silt. The results agreed to count or identification using a standard optical microscope. Overall, this identification strategy constitutes a game changer in the label-free identification of microorganism in water.

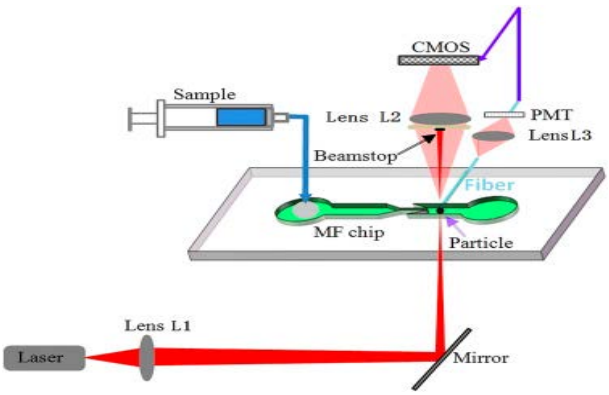

Figure 4.9. Schematic configuration of the LOC coupled with coupled with a multi-angle laser scattering.

Cate *et al*. [15] reported a different optical strategy for heavy metal ion detection, in which the quantification was made by travelled distance (same principle as mercury thermometers) instead of color intensity (Figure 4.10a). Authors produced a simple multiplexed paper-based LOC with the capability to determine Fe (20-1300 mg/L, Ni (100-1100 mg/L) and Cu (100-1300 mg/L) concentrations simultaneously in ~40 min (Figure 4.10b). The device itself was fully constructed by the use of printing techniques. The channels were delimited by wax printing while the reagents were inkjet-printed by a common modified office printer. When the sample is drop-casted onto the system, it flows through the channels reacting with the colorimetric reagents (4,7-diphenyl-1-1,10-phenanthroline, dimethylglyoxime and dithiooxamide for Fe, Ni and Cu, respectively) forming a colored precipitate. The efficiency of the device was tested with certified stainless-steel welding powder and further compared with the company quantification values, showing a significant good performance. Truly, the concentration ranges measured with this system heavily exceeds the concentrations establish by the legislation and therefore further development to decrease the linear range and the detection limit should be performed. Nonetheless, the fact that this new strategy could overcome the need for external readers as distance can be easily determined by naked-eye will represent an important advance for on-field applications.

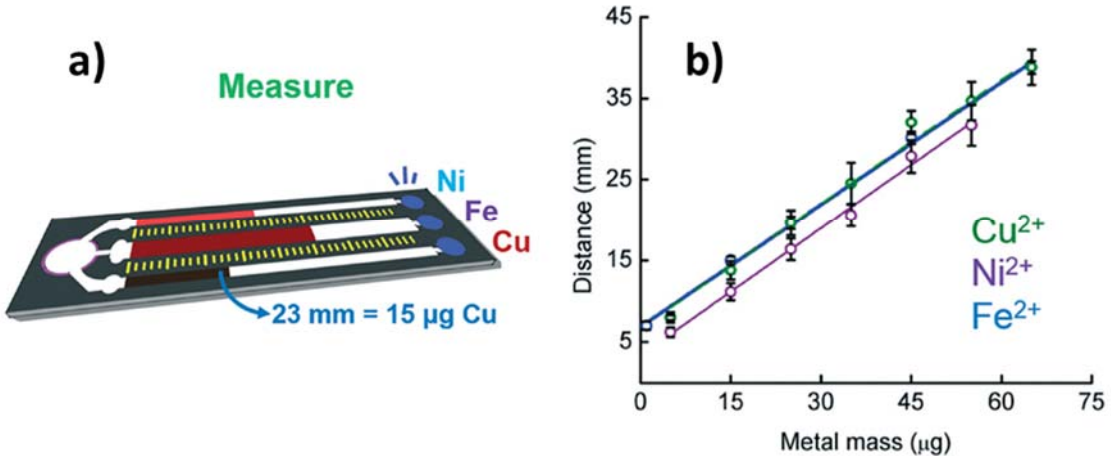

Figure 4.10. a) Distance-based multiplexed device for Ni, Fe and Cu detection (a). Calibration curves, for Ni, Fe and Cu, obtained using the multiplexed device (b).

Bell *et al*. [16] developed a LOC device that combines droplet-based microfluidic system with gated indicator for Hg^{2+} detection. The gated indicator principle is based on the release of a chemical embedded onto a scaffold that can be easily quantified. Authors designed a polyethylene glycosylated boron dipyrromethene (indicator)-loaded silica nanoparticles

(scaffold) with a squaraine acting as gate. Upon reaction of Hg^{2+} the gate is "opened" releasing the indicator, which is directly proportional to the heavy metal concentration (Figure 4.11). The use of droplet-based microfluidic system was chosen to take advantage of the microreactor-like behavior. Therefore, Hg^{2+} recognition and indicator release takes place in the water drop. Then, the dye is extracted into an organic phase (CH_2Cl_2, carrier) in order to avoid the readout interference coming from the indicator that remains in the nanoparticles. Overall, authors were able to detect Hg^{2+} ions in water with a limit of detection of 20 ppt, which is 50 times less than the maximum amount of Hg^{2+} allowed in drinking water.

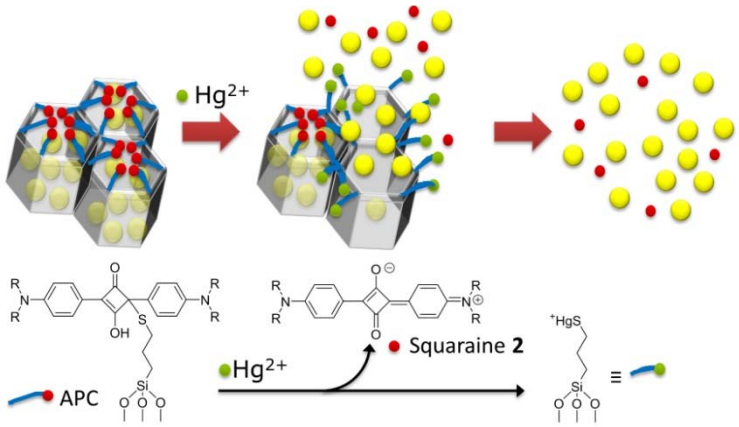

Figure 4.11. Schematic representation and reaction of 2,4-bis(4-dialkylaminophenyl)-3-hydroxy-4-alkylsulfanylcyclobut-2-enone (red sphere) with Hg^{2+} (green sphere) releasing polyethylene glycosylated boron dipyrromethene indicator (yellow sphere) showing the gated working principle of the device for Hg^{2+} ion determination.

A nanoceria-coated paper device for determination of organophosphate was reported by Nouanthavong. [17] The formation of H_2O_2 by two consecutive enzymatic reactions is used to oxidize Ce^{3+} to Ce^{4+} giving a change of color (colorless to yellow, Figure 4.12). The first enzymatic reaction (by acetylcholinesterase) uses acetylcholine as substrate to produce choline, while the second enzymatic reaction (by choline oxidase) produces H_2O_2 from choline. Generally, the sensor relied on an inhibition of acetylcholinesterase in the presence of organophosphate compounds, which in turns decrease the intensity of yellow. The sensor could achieve impressive limits of detections of 18 and 5.3 $ng{\cdot}mL^{-1}$ for methyl-paraoxon and chlorpyrifos-oxon, respectively. Furthermore, authors demonstrate the potential of the device in spiked cabbage and green mussel and compare the values obtain with chromatography couplet to a mass spectrometer showing no significant differences. Therefore, the potential of this system is for accurate and simple organophosphate detection is highlighted.

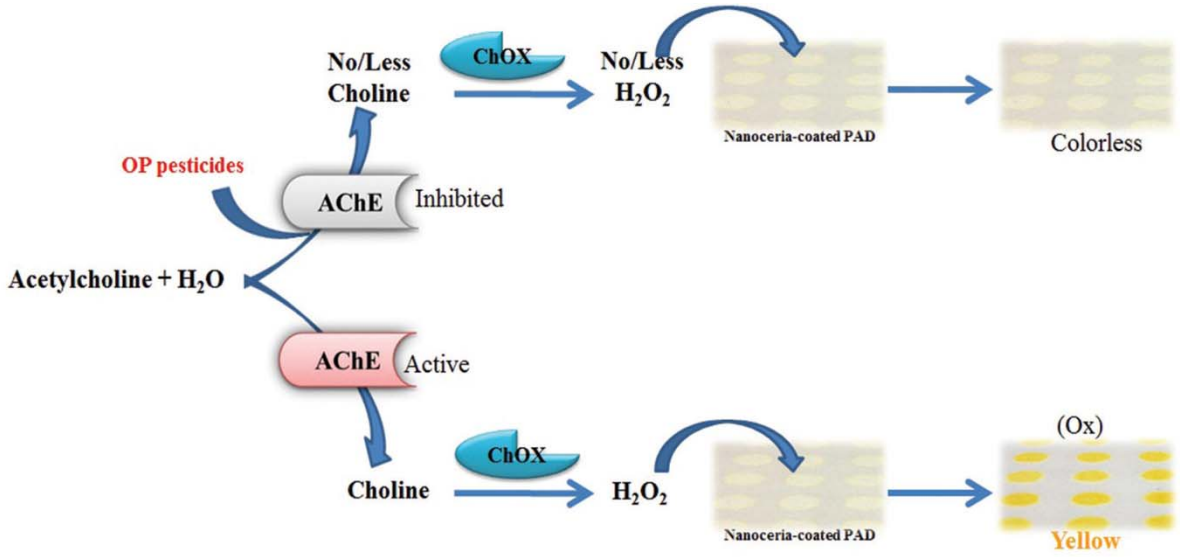

Figure 4.12. Conceptual scheme of the reactions involved in the determination of organophosphates by two stage enzymatic reactions.

4.5. Autonomous field deployable devices

Tracking of chemical compounds in the environment remains challenging due to the full integration of the sensing system in an autonomous way. It must be considered that a fully integrated device must provide storage containers, power supply and electronics for process control and data transfer.

That said, Perez de Vargas *et al*. [18] developed an autonomous colorimetric LOC prototype for pH sensing. The device consists of a battery, electronics, reagents and waste containers and pumps for microfluidic management (Figure 4.13). Authors explored the use of different combination of dyes in order to extend the pH detection range, in which a mixture of phenol red, chlorophenol red and bromophenol blue showed the broadest range (from 4 to 9). Repeatability tests were performed presenting an overall relative standard deviation of 2.82%, hence ensuring the capability of the system for analyses along time. Moreover, authors estimated the pH of effluent, drinking water, surface water and buffer (pH=6) and compared the values obtained with the ones analyzed by an external company showing an overall relative error of 5.96%. Lastly, reagents presented stability for 8 months confirming the feasibility for system deployment in the environment.

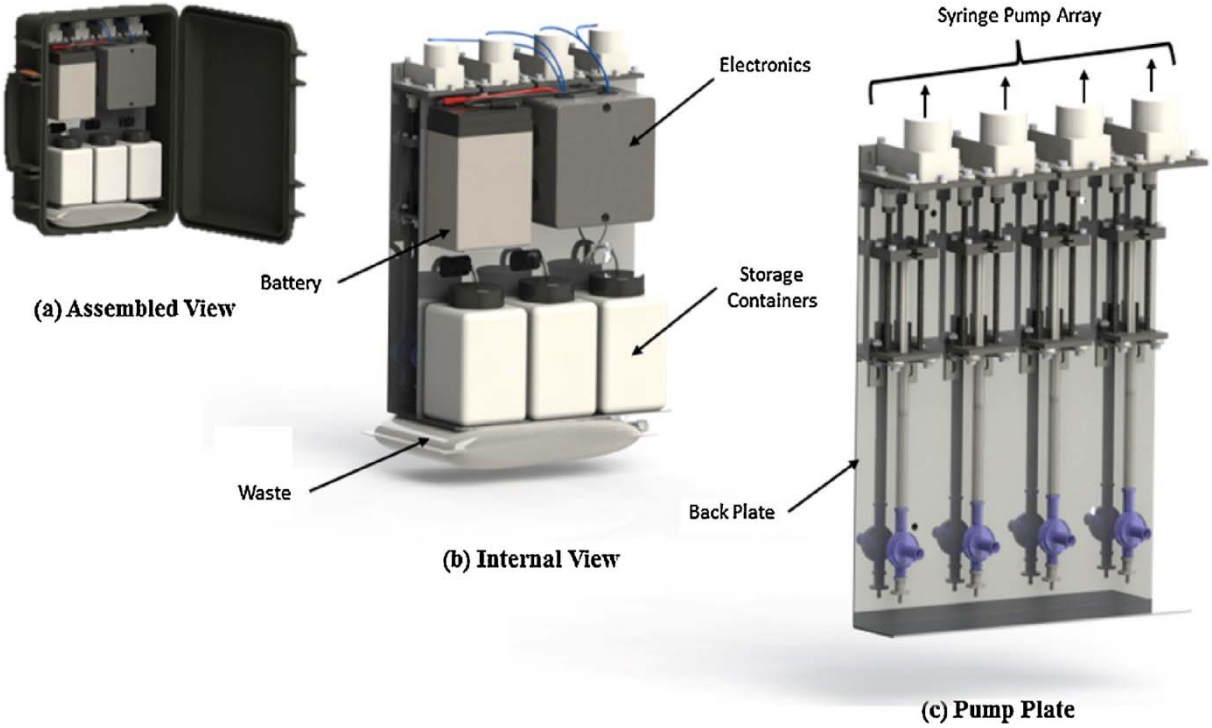

Figure 4.13. Schematic representation of the portable prototype for pH sensing; assembled view, internal view and pumps (from left to right).

One of the main problems in deployable devices is the use of batteries as power supplies, which are heavy, heat up affecting the measurements and do not last for long periods of time. To solve that problem, Höfflin *et al.* [19] reported a technical innovation; a wireless power transfer based on inductively coupled coils, to a spinning disk that could be easily integrated in a sensing rotating platform (Figure 4.14). The system itself is able to wireless supply 5V for both, Arduino microcontroller and sensors and actuators opening the possibility of designing more complex field deployable LOC devices. Authors strongly believe that this kind of power supply will find numerous applications in field deployable devices in the near future.

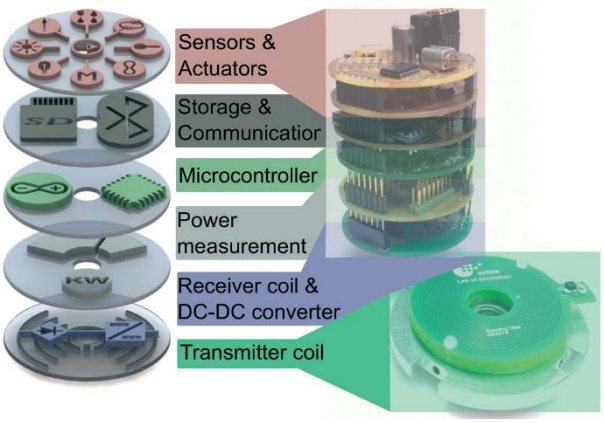

Figure 4.14. 3D representation of the full integrated lab-on-a-disk proposed device with the inductively coupled coil as power facility and all steps included on a measurement process.

4.6. Challenges

Finally, in this section we will describe the challenges that environmental monitoring still faces and discuss the feasibility of printing technologies to overcome them (Figure 4.15).

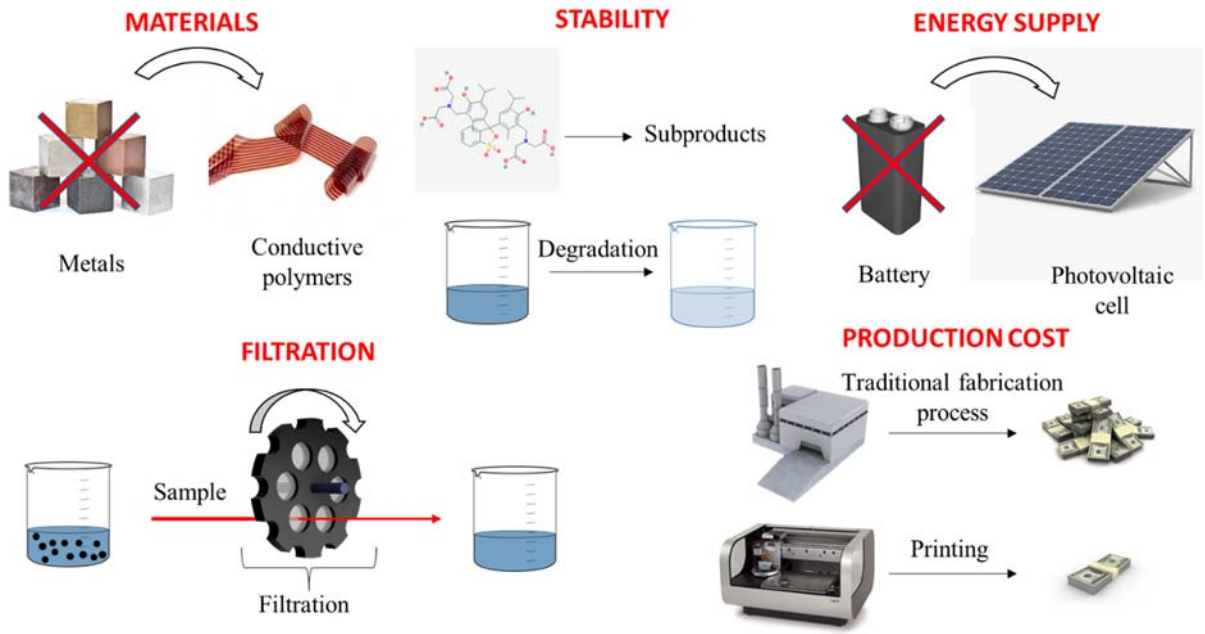

Figure 4.15. Scheme representing the possible solutions that we propose for the challenges environmental monitoring face.

One of the features that limits the lifetime of a system in the environment is the stability of the material that is it made of. Polymeric materials, which excel because of their chemical

stability have been exploited as the scaffold to contain the sensors and actuators. However, the metallic nature of the electronics involved is the critical point that delimits the performance of the device. Deployable systems undergo oxidant conditions as they are placed in water, which in turns means the analytical performance of the device will be affected after a period. Metallic materials could be easily replaced for conductive polymers like polyaniline or Poly(3,4-ethylenedioxythiophene) which can be directly printed on almost any desired surface o even 3D printing conductive filaments.[20,21]

Another important factor to consider is the stability of the reactants involved in the analyses. Typically, reactants used in optical assay contain aromatic rings. Upon severe oxidation conditions these rings may breakdown in to colorless chemicals decreasing the sensitivity of the assay. On the other hand, electrochemical assays commonly relied on the capability of a biomolecule to interact with an analyte. The use of biomolecules such as antibodies, aptamers or enzymes must be avoided as their bioactivity decreases drastically due to their low stability in environmental conditions.

As mentioned previously, an important problem to solve in deployable devices is the use of batteries as power supplies. Although in this review we have exposed a technology based on inductively coupled coils for wireless power transfer, this technology still requires an external power supply. A smart alternative could be the use of renewable energies in which energy harvested from external factors such as sunlight or hydrodynamics would supply the device. Scientists across the globe have made a lot of effort to develop affordable photovoltaic cells that would be able to provide the energy expenses of an autonomous system. Moreover, inkjet printing and 3D printing has been widely used as the main technology to produce low-cost fuel cells as they consist on multiple stacked layers.[22,23]

Another big challenge associated with any analytical assay is the treatment of interferences. In the case of environmental assays, highly complex matrices commonly lead to a wide variety of interferences, which could not only affect the read-out value, but also the lifetime of the system. Over the last years, different manners to discriminate one analyte upon the matrix with the use of highly selective molecules have been proposed. Although, some interferences in the read-out value could be solved using selective molecules there is still another problem in real environmental samples. Among others, environmental samples usually contain colloidal

particles, which could affect both, optical, and electrochemical-based analyses. On the one hand, particles provoke light scattering, which will slightly change the concentration value of the analyte. On the other hand, particles could scratch the external surface of the electrodes used for the assay. A simple and low-cost solution could be the use of a revolver-like filtration system enclosed within the device. This filtration system will be able to solve the problems that small particles in suspension cause. Furthermore, when the sieve clogged, the filtration system will spin, and a new sieve will be placed. This smart strategy could be easily implemented taking advantage of 3D printing and will increase the lifetime of the system. In addition, this system could eliminate interference in optical measurements.

Technology used so far to produce field deployable devices is complex and costly. Printing technologies have been overwhelmingly implemented to produce low-cost systems for analytical purposes. Although these printing technologies have been exploited to produce point-of-care devices and wearable electronics,[24] environmental application still need to be harnessed.

4.7. Conclusions and future prespectives

Throughout the present review chapter, the potential of LOC systems with different detection principles for environmental application has been discussed. The main advantage of these devices presented so far is the capability of integrating in a small space all processes involved in the analysis. This fact, allows the reduction of operational, production and reactants costs as long as offers the possibility to perform analyses in an autonomous way.

We strongly believe that unaddressed technological gaps could be filled in the near future with emerging technologies such as three-dimensional printing and inkjet printing. Printing technologies will not only solve the problems that environmental monitoring face, but also will become the standard technology to produce autonomous full deployable systems at a low cost. Moreover, wireless connectivity will be crucial to overcome the challenges autonomous deployable devices face. Overall, LOC sensing systems will excel as promising miniaturized platforms for in situ and real-time monitoring of pollutants. Despite in this review we

emphasized the LOC systems for environmental applications, they could also find uses in biomedical and biotechnological fields.

4.8. References

(1) Samiei, E.; Tabrizian, M.; Hoorfar, M. A Review of Digital Microfluidics as Portable Platforms for Lab-on a-Chip Applications. *Lab Chip* **2016**, *16*, 2376–2396.

(2) Li, H.; Lin, J. Applications of Microfluidic Systems in Environmental Analysis. **2009**, *393*, 555–567.

(3) Nge, P. N.; Rogers, C. I.; Woolley, A. T. Advances in Microfluidic Materials, Functions, Integration, and Applications. *Chem. Rev.* **2013**, *113* (4), 2550–2583.

(4) Stanley, C. E.; Grossmann, G.; Casadevall i Solvas, X.; DeMello, A. Soil-on-a-Chip: Microfluidic Platforms for Environmental Organismal Studies. *Lab Chip* **2015**, *16*, 228–241.

(5) Lin, Y.; Gritsenko, D.; Feng, S.; Teh, Y. C.; Lu, X.; Xu, J. Detection of Heavy Metal by Paper-Based Microfluidics. *Biosens. Bioelectron.* **2016**, *83*, 256–266.

(6) Freitas, C. B.; Moreira, R. C.; De Oliveira Tavares, M. G.; Coltro, W. K. T. Monitoring of Nitrite, Nitrate, Chloride and Sulfate in Environmental Samples Using Electrophoresis Microchips Coupled with Contactless Conductivity Detection. *Talanta* **2016**, *147*, 335–341.

(7) Calvo-López, A.; Arasa-Puig, E.; Puyol, M.; Casalta, J. M.; Alonso-Chamarro, J. Biparametric Potentiometric Analytical Microsystem for Nitrate and Potassium Monitoring in Water Recycling Processes for Manned Space Missions. *Anal. Chim. Acta* **2013**, *804*, 190–196.

(8) T G Van Den Brink, F.; Wigger, T.; Ma, L.; Odijk, M.; Olthuis, W.; Karst, U.; Berg, A. Van Den. Oxidation and Adduct Formation of Xenobiotics in a Microfluidic Electrochemical Cell with Boron Doped Diamond Electrodes and an Integrated. *Lab Chip* **2016**, *16*, 3990–4001.

(9) Medina-Sánchez, M.; Mayorga-Martinez, C. C.; Watanabe, T.; Ivandini, T. A.; Honda, Y.; Pino, F.; Nakata, A.; Fujishima, A.; Einaga, Y.; Merkoçi, A. Microfluidic Platform for Environmental Contaminants Sensing and Degradation Based on Boron-Doped Diamond Electrodes. *Biosens. Bioelectron.* **2016**, *75*, 365–374.

(10) Cha, A.; Merkoçi, A. Toward Integrated Detection and Graphene-Based Removal of

Contaminants in a Lab-on-a-Chip Platform. **2017**, *10* (7), 2296–2310.

(11) Gonzalez-rivera, J. C.; Osma, J. F. Fabrication of an Amperometric Flow-Injection Microfluidic Biosensor Based on Laccase for In Situ Determination of Phenolic Compounds. **2015**, *2015*, 1–9.

(12) Cardoso, T. M. G.; Garcia, P. T.; Coltro, W. K. T. Colorimetric Determination of Nitrite in Clinical, Food and Environmental Samples Using Microfluidic Devices Stamped in Paper Platforms. *Anal. Methods* **2015**, *7* (17), 7311–7317.

(13) Kim, J.-Y.; Yeo, M.-K. A Fabricated Microfluidic Paper-Based Analytical Device (MPAD) for in Situ Rapid Colorimetric Detection of Microorganisms in Environmental Water Samples. *Mol. Cell. Toxicol.* **2016**, *12* (1), 101–109.

(14) Huang, W.; Yang, L.; Lei, L.; Li, F. Label-Free Detection and Identification of Waterborne Parasites Using a Microfluidic Multi-Angle Laser Scattering System. *Opt. Commun.* **2017**, *400*, 25–29.

(15) Cate, D. M.; Noblitt, S. D.; Volckens, J.; Henry, C. S. Multiplexed Paper Analytical Device for Quantification of Metals Using Distance-Based Detection. *Lab Chip* **2015**, *15* (13), 2808–2818.

(16) Bell, J.; Climent, E.; Hecht, M.; Buurman, M.; Rurack, K. Combining a Droplet-Based Microfluidic Tubing System with Gated Indicator Releasing Nanoparticles for Mercury Trace Detection. *ACS Sensors* **2016**, *1*, 334–338.

(17) Nouanthavong, S.; Nacapricha, D.; Henry, C. S.; Sameenoi, Y. Pesticide Analysis Using Nanoceria-Coated Paper-Based Devices as a Detection Platform. *Analyst* **2016**, *141*, 1837–1846.

(18) Perez De Vargas Sansalvador, I. M.; Fay, C. D.; Cleary, J.; Nightingale, A. M.; Mowlem, M. C.; Diamond, D. Autonomous Reagent-Based Microfluidic PH Sensor Platform. *Sensors Actuators, B Chem.* **2016**, *225*, 369–376.

(19) Höfflin, J.; Torres Delgado, S. M.; Suárez Sandoval, F.; Korvink, J. G.; Mager, D. Electrifying the Disk: A Modular Rotating Platform for Wireless Power and Data Transmission for Lab on a Disk Application. *Lab Chip* **2015**, *15* (12), 2584–2587.

(20) Rohaizad, N.; Mayorga-Martinez, C. C.; Novotný, F.; Webster, R. D.; Pumera, M. 3D-Printed Ag/AgCl Pseudo-Reference Electrodes. *Electrochem. commun.* **2019**, *103* (April), 104–108.

(21) Browne, M. P.; Novotný, F.; Sofer, Z.; Pumera, M. 3D Printed Graphene Electrodes'

Electrochemical Activation. *ACS Appl. Mater. Interfaces* **2018**, *10* (46), 40294–40301.

(22) Feng, Z.; Liu, L.; Li, L.; Chen, J.; Liu, Y.; Li, Y.; Hao, L.; Wu, Y. 3D Printed Sm-Doped Ceria Composite Electrolyte Membrane for Low Temperature Solid Oxide Fuel Cells. *Int. J. Hydrogen Energy* **2019**, *44* (26), 13843–13851.

(23) Masciandaro, S.; Torrell, M.; Leone, P.; Tarancón, A. Three-Dimensional Printed Yttria-Stabilized Zirconia Self-Supported Electrolytes for Solid Oxide Fuel Cell Applications. *J. Eur. Ceram. Soc.* **2019**, *39* (1), 9–16.

(24) Pandey, C. M.; Augustine, S.; Kumar, S.; Kumar, S.; Nara, S.; Srivastava, S.; Malhotra, B. D. Microfluidics Based Point-of-Care Diagnostics. *Biotechnol. J.* **2018**, *13* (1), 1–11.

CHAPTER 5

Inkjet-Printed Sulfide-Selective Electrode

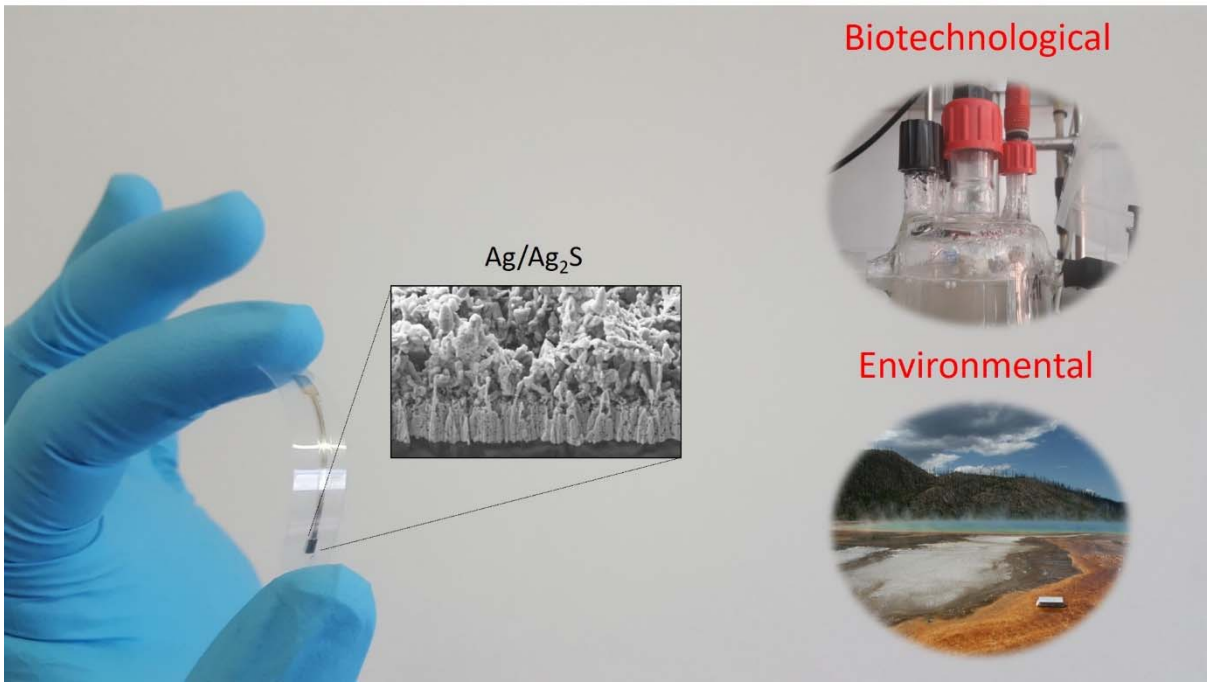

This chapter is a modification of:

Inkjet-Printed Sulfide-Selective Electrode
R Pol, A Moya, G Gabriel, D Gabriel, F Céspedes, M Baeza
Analytical chemistry 89 (22), 12231-12236 (2017)

5.1. Foreword

The best foreword for this chapter is to directly include the response to a comment of one of the referees involved in the revision of the publication.

The **referee comment** was "it would be nice if the Ag_2S sensing part could be developed as an ink and printed in one step, instead of electro-chemical deposition. This is already accomplished for AgCl and chloride sensing, so why not for Ag_2S and sulfide sensing?"

The **response was**, "we are grateful that reviewer opens the door to this discussion. On the early stage of the conception of the idea to use inkjet printing technology to produce a S^{2-} selective electrode, our first thoughts were to produce a Ag_2S nanoparticle-based inkjet printable ink. Then, the procedure we were thinking about was as simple as consecutive printing (Ag, Ag_2S and SU8) and sintering/curing. Then, we decided to look for previous publication in the literature in which a reproducible Ag_2S nanoparticles (size: <200 nm) solution (or even powder) was described. We found a few publications regarding the synthesis of these nanoparticles. With that information in mind, we met again and discuss the possible problems we would encounter following this path. Our experience in the formulation of other homemade printable inks was that first, there are many features (regarding particle size and rheological properties of the ink) that need to be controlled prior to optimization of the printing wave function. A lot of times, the particles require a change in the capping agent to be dispersible in a solvent with the required rheological properties. Also, this fact could change the size and shape of the particle making them big enough to clog the nozzle. Secondly, what bothered us the most was the stability of the ink. Other homemade inks we have tried to develop presented stability problems and only could be used (with high reproducibility) the day they were prepared. Finally, once the ink is suitable for printing then there could be problems with phase boundary cohesion and electron transfer. In this scenario and in a rush to provide a functional S^{2-} sensor for the biotechnological reactor samples, we decided to explore the electrodeposition alternative. Actually, if we put in a balance the overwhelming effort of producing the ink *vs*. the simplicity of preparing a solution for electrochemical deposition, the second option excel. Right now, alongside this study we are discussing the feasibility of

developing a Ag_2S nanoparticle-based inkjet printable ink, which in our opinion, only the formulation will warrant a publication".

Personally, it took me one week searching for Ag_2S nanoparticle synthesis that the resulting particles had the perfect size and capping agent to produce a printable ink and I was not sure if they would work properly. My ever-wise supervisor told me to change my mind and just electrodeposit the Ag_2S, alike Ag/AgCl reference electrode are done. After 2 years, these electrodes are still functional.

5.2. Introduction

Modern manufacturing processes have left wide-spread hazardous compounds across the globe. Sulfide, which is present in several waste waters, has gain significant attention within the scientific community due to its toxicity.[1] The over exposure of workers involved in decontamination processes in sewage treatment plants and the direct impact in surface waters, as rivers and streams, has triggered the alarms. Therefore, production of durable, fast and robust sensing platforms to track sulfide concentration across the environment and in treatment processes has become a global concern.

Manufacturing of electrochemical sensors has represented a hot topic during decades. [2,3] Traditionally, electrochemical sensors were home-made using metal wires for their subsequent use in the laboratory. Those hand-crafted sensors lack certain requirements (e.g. reproducibility, repeatability, robustness) regarding the performance of the analytical assays. Moreover, their operational configuration makes them a bad choice for on the field analyses. Nowadays, breakthrough technologies, such as microfabrication and printing techniques have led to more automated sensor fabrication procedures.[4,5] With these technologies, typical requirements, such as reproducibility and repeatability are met in a miniaturized fashion, which in turns allow them to be used in broader situations. Therefore, their potential is spotted, and the feasibility of its commercialization has increased exponentially.

Among others, inkjet printing technology has emerged as a standard method for production of low-cost electronics. Inkjet printing constitutes a contactless, additive process with the capability to deposit microdroplets of ink on a substrate following a digitalized predefined pattern.[6,7] Ink formulations are composed by materials that can be dispersed, suspended or dissolved in a liquid with defined properties (viscosity, surface tension and boiling point). In fact, electrical conductive paths can be inkjet-printed from a wide variety of materials, from metals to conductive polymers.[8,9,10] Moreover, different substrates can be used depending on the final application of the electronics. In this context, flexible substrates excel thanks to their adaptability to different situations and their cost-efficiency.[11,12] Overall, inkjet printing allows *in situ* digital modification of the complex printed patterns removing the need for mask, outstripping other techniques with that dependence. The use of mask-less deposition not only

helps with the capability of changing the motifs on demand during the prototyping process, but also leads to an efficient use of materials and waste elimination.[13] With this outstanding technology available, the challenges to control all the parameters that affect the reproducibility and durability of the sensors are addressed alongside with achieving a substantial fall in prices. Thanks to all those benefits inkjet printing technology give, some electrochemical techniques such as potentiometry are coming back to play an important role.

Traditionally, one of the most used sensors so far are ion-selective electrodes due to their operational simplicity and reliability.[14,15] Their capability to measure a defined ion in highly complex matrices with high selectivity makes them appealing for any required situation. This kind of electrodes measure potential differences associated with permselective mass transfer across a phase boundary.[16] Depending on the nature of this phase boundary, ion-selective sensors are classified in different groups (glass membrane, crystalline membrane and polymeric membrane).[17] Over the above phase boundaries, the one that has attracted more attention is the polymeric matrix. For instance, Sjöberg et al.[18] described the fabrication of a potassium-selective electrode by means of inkjet printing. Authors demonstrate the importance of the methodology used for deposition of a homogeneous solid contact (poly(3,4-ethylenedioxythiophene) polystyrene sulfonate) between the ion-selective polymeric membrane and the transducer (gold). Another daily used worldwide potentiometric sensor (pH) has also been extensively investigated. Qin et al.[19] successfully developed a Pd-based printable ink and described the fabrication of a Pd/PdO inkjet-printed electrode with excellent response against H^+. Another inkjet-printed electrode for pH sensing was developed by Zea et al.[20] which produced an iridium oxide-based electrode that presented sub-Nernstian response to H^+. Although many efforts have been done to produce polymeric and glass-based potentiometric sensors, there is a gap in the production of second and third kind ion-selective electrodes.

Traditionally, sulfide was measured using potentiometry. Nonetheless, the phase boundary used was a crystalline membrane. The typical procedure to produce that crystalline membrane was a precipitation of Ag_2S from their respective ionic salts and then a pellet is produced by applying high pressure to the resulting powder. [21] This kind of potentiometric electrodes can encounter some problems (electrical contact, Galvani potential difference, mechanical influences…) in their tedious production.[22] Moreover, they can be hardly miniaturized, limiting their practical applications. The trend nowadays, is to produce simple optical sensors for naked-

eye quantification. For instance, Kang et al.[23] developed a G-Quadruplex DNAzyme which contains hemin that in the present of sulfide is activity is inhibited. Another simple sensor was reported by Rosolina et al.[24] in which a paper containing bismuth hydroxide changes the color in the presence of sulfide due to Bi_2S_3 precipitation. It is worth noting that sensors that contain biomolecules undergo degradation (sometimes caused by the interaction with compounds of the samples) and require special storage conditions. Moreover, in most scenarios optical sensors encounter several problems with environmental samples that contain particles (or color) that disperse light.[25]

In this chapter, the two-step fabrication of the first second kind Ag/Ag_2S inkjet-printed sulfide-selective electrode (IPSSE) is described. Despite the challenges, the device was successfully fabricated by printing a silver electrode followed by an electrochemical deposition of sulfide. Interestingly, advantage of the nature of the conductive printed ink was taken. The morphology of the device was characterized by scanning electron microscopy (SEM) coupled with energy-dispersive X-ray analysis. Furthermore, the electrochemical performance of the sensor was evaluated with potentiometric measurements in standard solutions and in real environmental and biotechnological matrices.

5.3. Experimental section

5.3.1. Materials and chemicals

All chemicals were commercially available and were used without further purification. Sodium sulfide nonahydrate (98%, $Na_2S{\cdot}9H_2O$), sodium hydroxide (98%, NaOH), sodium thiosulfate (99%, $Na_2S_2O_3$) and starch were purchased from SigmaAldrich. L(+)-ascorbic acid (99%), potassium iodide (99%, KI) and potassium iodate (99%, IO_3K) were purchased from Panreac (Spain).

Silver nanoparticle ink (PE410) was purchased from DuPont, Korea, and an SU8 ink (2002) was purchased from MicroChem, USA. Teonex Polyethylene Naphthalate (PEN) films

(Q65HA) with a thickness of 125 μm and a surface pre-treatment for improved adhesion was purchased from DuPont Teijin Films.

5.3.2. Sulfide standard solutions and standardization

Aqueous solutions were prepared employing deionized Milli-Q water (180 MΩ·cm^{-1}). Stock solution of S^{2-} (1 M S^{2-}) was prepared by dissolving 24.5 g of $Na_2S{\cdot}9H_2O$ in 100 mL of a 1 M NaOH solution. Standard solutions of S^{2-} were daily prepared by dilution of the stock solution in sulfide antioxidant buffer (SAOB). The SAOB was prepared by mixing 40 g L^{-1} (1 M) of NaOH (increasing the pH up to 14 which ensures that the predominant specie present in solution of the acid-base equilibrium will be S^{2-}) and 10.1 g L^{-1} (0.05 M) of ascorbic acid (which act as an antioxidant to avoid the presence of other sulfur oxidized forms).

The determination of the real concentration of the stock solution of sulfide was performed applying an iodometric method according to the Standard methods.[26] Briefly, standardization of a $Na_2S_2O_3$ with I_3^- takes place. Then, $Na_2S_2O_3$ standardized solution is used to determine the iodine produced by the reaction of sulfide with iodide.

5.3.3. Electrode fabrication. Printing procedure and sulfide electrodeposition

The two-step fabrication is shown in Figure 5.1. The first IPSSE step consists of printing a silver electrode and an insulator followed by an electrochemical deposition of sulfide to produce a second kind electrode (Ag/Ag_2S).

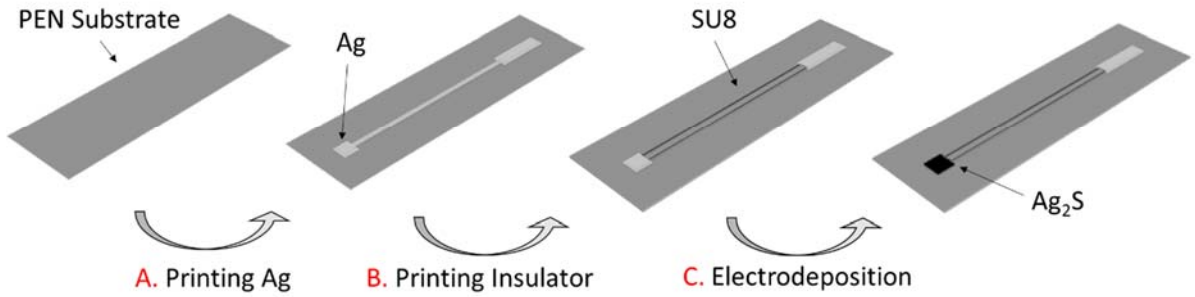

Figure 5.1. Scheme of the fabrication of the IPSSE: Inkjet printing of Ag paths (A), insulator printing (B) and electrodeposition step (C).

Silver electrodes were prepared by using a drop-on-demand inkjet printer (DMP-2831 Dimatix Fujifilm, Santa Clara, USA) and a disposable cartridge (DMC-xº11610) containing 16 individually addressable nozzles with nominal droplet volumes of 10 pL. The printing processes were carried out in a standard laboratory environment in ambient condition. The IPSSE were printed over a flexible and transparent PEN substrate using a commercially available Ag and SU8 inks. Printing parameters (cartridge temperature, piezoelectric nozzle voltage, frequency, etc.) were optimized for both employed inks. The active working electrode area delimited by the SU8 insulator is 2 mm per 1 mm (Figure 5.2).

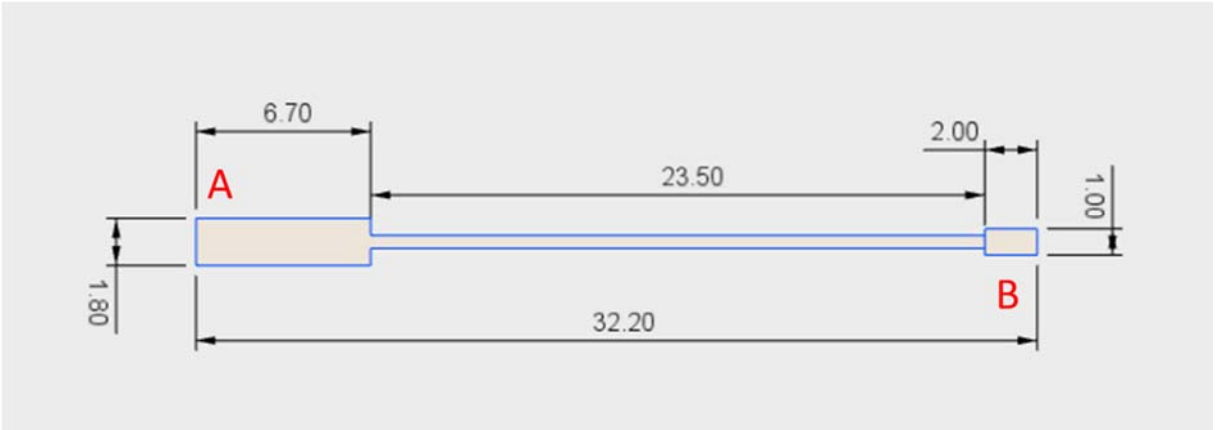

Figure 5.2. Geometry and dimensions of the Ag inkjet-printed electrode (in mm). Electrical contact (A) and Ag_2S tip (B).

Previously to begin the printing steps, silver and SU8 inks behavior was studied by printing a predefined line pattern over the PEN substrate. This test print pattern allows to know which is the drop spacing (DS) required to print a continuous line, and so the thickness and width of

lines. These parameters basically depend on the surface energy of each ink on the desired substrate, so it is mandatory to do it before each printing. In the first step of the printing (Figure 1A) the active working electrode area, track and pad were printed with Ag ink using a DS of 30 μm. During printing of the silver layer, the substrate temperature was set to 40 ºC in order to promote the beginning of evaporation of the ink carrier and thus to increase the pattern resolution. The completely evaporation was done outside the printer, at 100 ºC during 10 min using a hotplate. The inks contain different solvents, so, this drying step is necessary to achieve that all solvent molecules absorbed on the nanoparticles are completely removed. After the drying step, the patterns were sintered for 20 min at 140 ºC. This sintering step is considered necessary to lower the resistivity of the ink, and although high temperatures can achieve better conductivities, with the selected sintering conditions, it was achieved a resistivity down to 10 μΩ·cm. Afterwards, the insulator layer was printed over the silver tracks to precisely define the active area of the working electrode. The insulating SU8 UV curable ink, was printed using a DS of 15 μm. The SU8 achieves a high chemical resistance and a high thermal stability after a soft bake at 100 ºC for 5 min and a UV curing of 15 seconds where the layer polymerizes by cross-linking.

The electrochemical deposition (Figure 5.1C) was carried out by a potentiostat/galvanostat AUTOLAB (PGSTAT204, Eco Chemie, Utrech, The Netherlands) using chronoamperometry mode applying a potential of 0.7 V during 5 s under non-stirring conditions. A double junction reference electrode Ag/AgCl Orion 900200 (Thermo Electron Corporation, Beverly, MA, USA), a platinum–based electrode Crison (Crison Instruments, Alella, Barcelona, Spain) and the inkjet-printed silver electrode were used as reference, counter and working electrodes, respectively. Electrolytic solution used for electrodeposition was a 0.1 M S^{2-} solution with adjusted pH to 14 using NaOH.

5.3.4. Electrode characterization

Morphological changes produced by the electrodeposition were observed by SEM using a MerlinZeiss microscope operated at 5 kV. Samples for SEM were prepared by simply sticking the substrate onto the holder with carbon tape. The elemental composition was determined by Energy Dispersive X-ray Spectroscopy (EDX) at a voltage of 15 kV.

Evaluation of the electrochemical performance was done by a potentiostat/galvanostat AUTOLAB (PGSTAT204) using chronopotentiometry under constant stirring conditions. The IPSSE was used against a double junction reference electrode Ag/AgCl Orion 900200. All calibrations performed in this research are made in batch condition with subsequent addition (over 25 mL of SAOB) of standards S^{2-}solutions. The ionic strength remained constant in all calibrations.

5.3.5. Sampling, spiking and determination in real samples

River and sea water samples were collected following ISO 5667-6:2014 and ISO 5667-9:1992, respectively (details in Table 5.1). Subsequently, both samples were filtered through a Millex 0.45 μm filter and conditioned by dilution with twice concentrated SAOB (1:1) to increase the pH up to 14. Afterwards, both solutions were spiked with the same amount of S^{2-} from the stock solution to fit in the middle of the linear range. In addition, process samples were collected from the outlet sampling port of a 2L upflow anaerobic sludge blanket reactor (UASB) performing anaerobic sulfate reduction to sulfide using crude glycerol as electron donor. UASB performance at the time of sampling corresponded to almost complete conversion of a sulfate concentration of 0.25 kg S m^{-3}. Samples from the reactor were filtered through a Millex 0.45 μm filter and conditioned by dilution with twice concentrated SAOB (1:1).

Table 5.1. Further information regarding location point and sampling conditions.

Sample	Location	Coordinates	Day	Hour (24 h)	Depth (m)	Length (m)	Conditioning time (min)
River	Sant Hipòlit de Voltrega Vic Spain	42°01'47.9"N 2°15'10.2"E	25/02/2017	16:30	0.5	1	10
Sea	Castelldefels Barcelona Spain	41°15'49.9"N 1°58'55.4"E	09/02/2017	20:00	1	5	10

Measurements were done by simply immerse the IPSSE and the double junction reference electrode in the solutions (the ionic strength remained constant in all measurements). The results obtained were compared against a commercially available Orion 9616BNWP (Thermo

Electron Corporation, Beverly, MA, USA) sulfide-selective electrode using a SB90M5 potentiostat (SympHony™, VWR).

5.4. Results and discussion

Potential applied in the electrodeposition step constitute a key factor in the production of durable Ag_2S films. The first electrochemical deposition attempt was to use 1 V but the film was taken off after rinsing the electrode. This fact could be explained by the loss of cohesion between layers due to the overproduction of oxygen bubbles caused by the water oxidation reaction for potentials around 1 V. Then, different potentials were applied (0.9 and 0.8 V) until an optimal potential of 0.7 V was found (Figure 5.3A). Another factor that was crucial is the electrodeposition time. Long times (+30 s) causes the formation of Ag/Ag_2S until the interface of the polymeric support, decreasing the cohesion and falling off after the rinsing step. Therefore, 5 seconds was chosen as the electrodeposition time that gave a robust Ag/Ag_2S layer (Figure 5.3B).

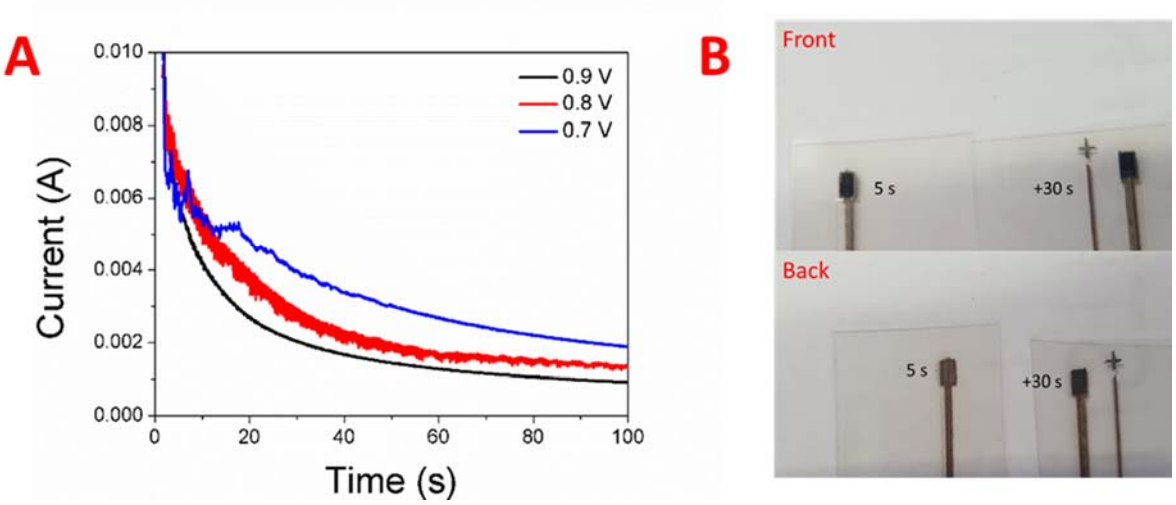

Figure 5.3. Electrodeposition chronoamperometries at different potentials (0.7, 0.8 and 0.9 V) (A). Front and backside of two electrodes after the electrodeposition step done with two different deposition time (B).

The successful electrochemical deposition of the as-fabricated IPSSE can be easily discerned by naked eye (Figure 5.4). A change from a pale grey (Figure 5.4A) to black (Figure 5.4B) is evidenced. Furthermore, SEM micrographs show a change in the morphology of the electrode. On the one hand, the inkjet-printed silver electrode (Figure 5.4A1 center) exhibits a granular

surface typical of an inkjet printing process of nanosized silver particles.[27] On the other hand, the IPSSE presents a transformation at the external surface to a coral-like shape after the electrochemical deposition (Figure 5.4B1 center).

EDX demonstrates the presence of S after the electrochemical deposition (Figure 5.4B2). The EDX data showed the appearance of two peaks at 2.3 and 2.7 KeV corresponding to S aside from the Ag peaks (3.1 and 3.3 KeV) once the deposition occurs (Figure 5.4A2).

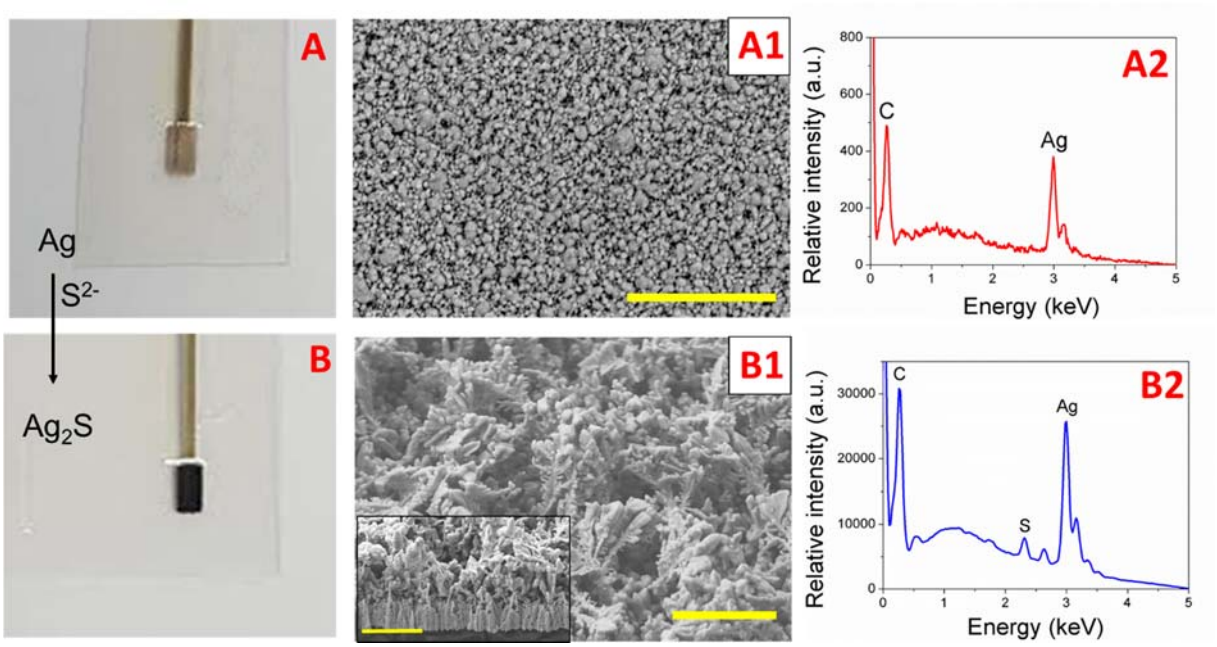

Figure 5.4. Ag inject printing electrode (A), SEM micrographs (A1) and EDX (A2). Ag/Ag_2S electrode (B), SEM micrographs (B1) and EDX for Ag/Ag_2S electrode (B2); scale bar = 2 μm.

The IPSSE must accomplish several statements prior to its use in real samples. A Ag_2S-rich surface for the ion-to-electron transduction based on the following redox reaction:

$$Ag_2S_{(s)} + 2e^- \leftrightarrow 2Ag_{(s)} + S^{2-}_{(aq)}$$

in which the redox potential is described by the Nernst equation:

$$E = E^0_{Ag_2S/Ag} - \frac{59.16}{n} log\{S^{2-}\} \qquad \text{(Equation 5.1)}$$

where E_0 is the standard potential for Ag_2S reduction to Ag, n is the number of electrons involved in the redox reaction and $\{S^{2-}\}$ is the activity of S^{2-} ions in solution. Therefore, the theoretical sensitivity of the sensor should be -29.58 mV·decade^{-1}.

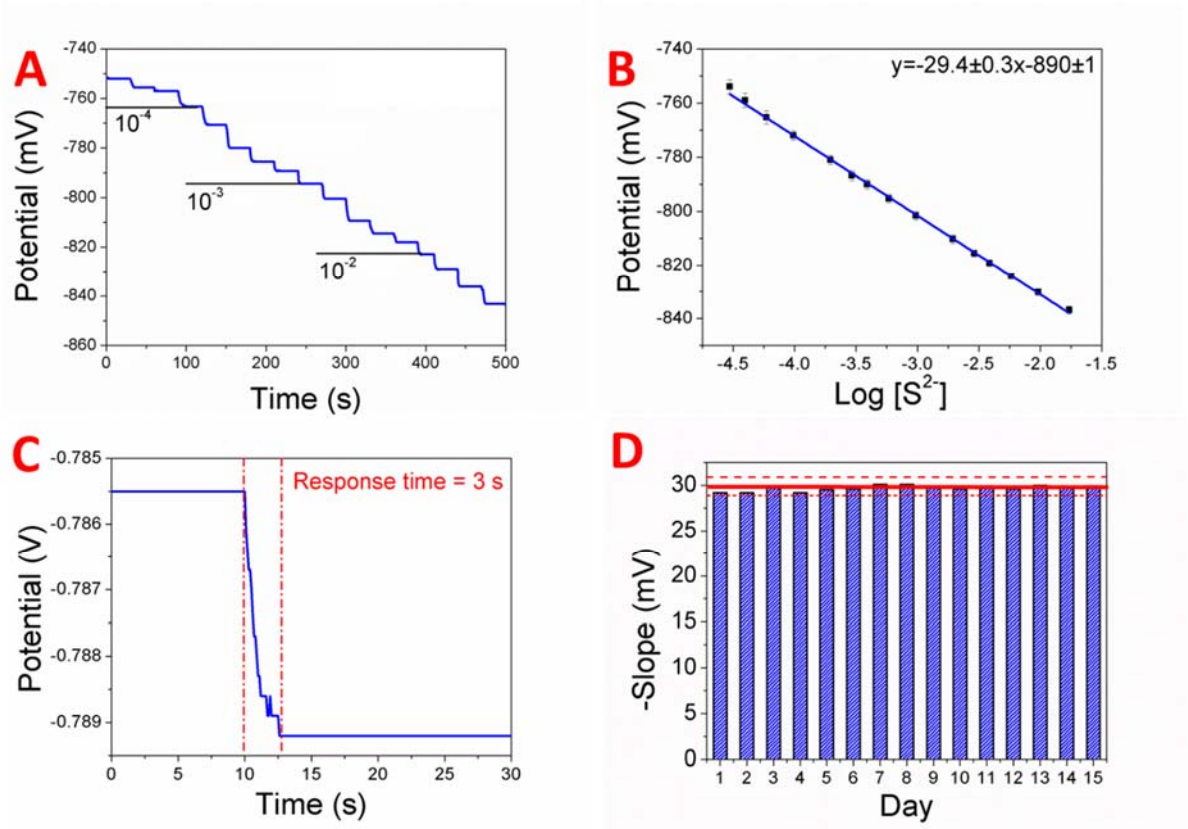

Figure 5.5. Response of the Ag/Ag_2S electrode for S^{2-} determination. Experimental data for consecutive additions of S^{2-} over SAOB medium (A), calibration plot for experimental data obtained (r^2= 0.998,B), time lapse between a consecutive addition in the middle of the calibration curve of the IPSSE (C) and durability study for n=15 sensitivities and k=3 replicates for each day obtained on different days. Mean slope value of all measurements (red line) and 3-folds the standard deviation (dashed red line) (D).

Thus, the electroanalytical performance of the as-fabricated IPSSE was extensively studied. Figure 5.5A shows an example of the time trace of the potentiometric response during consecutive additions (every 30 s) of sulfide. The corresponding calibration curve obtained for three subsequent calibrations (as the ionic strength is maintained constant, the concentration can be represented instead of the activity) is shown in Figure 5.5B. The calibration curve exhibit a Nernstian response of -29.4±0.3 mV/decade (±confidence interval at 95%) between 0.03-100 mM with a detection limit of 0.01 mM (calculated by intersection of the linear range of response and the asymptote)[28] in concordance with the expected value for these kind of electrodes.[29] Through all calibration curve data, the confidence interval (y error) cannot be

discerned thanks to its high repeatability. Is it worth noting that the IPSSE also shows a prompt response of 3 s (Figure 5.5C).

Generally, inkjet-printed electrodes are designed and produced to be disposable due to their poor mechanical properties as they detach from the surface and heavily suffer surface scratching affecting their performance. With this fact in mind, the durability of the IPSSE was tested over days (Figure 5.5D). Systematically, durability experiments were carried with daily triplicate calibrations. Surprisingly, the IPSSE was able to be reused for at least 15 days with no extent of the slope greater than 3-folds the standard deviation (of each daily calibration, both dashed red line) of the theoretical value (-29.58 mV/decade, red line) in the same linear response concentration range.

Although second kind electrodes are well-known for their specificity towards the ions that compose the electrode, a simple experiment to ensure the selectivity towards S^{2-} over a cocktail of ions (K^+, Na^+, Cl^- and SO_4^{2-}) was performed. Essentially, second kind electrodes only respond to their ionic counterparts, to ions that can exchange the lattice or species that can reduce the Ag^+ (Ag_2S) to Ag. In this particular case, there are no lower K_{ps} silver salts and no evidences of relevant reductant species on real samples were found. Three calibration curves with S^{2-} in highly concentrated background of common ions (10 mM) were done (Figure 5.6). Although slight differences in the slope existed, no remarkable difference in the limit of detection (from 0.01 mM, without interfering ions; to 0.02 mM, with interfering ions) was found whatsoever.

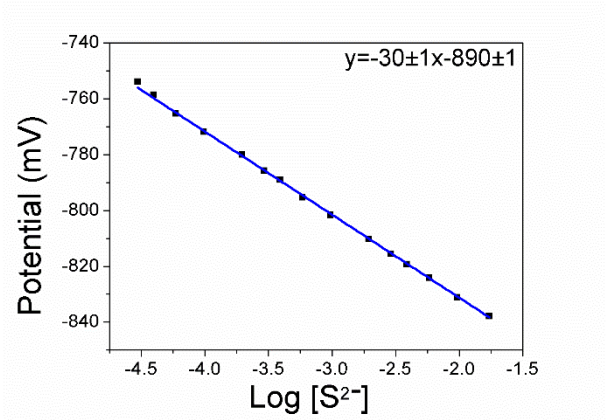

Figure 5.6. Calibration plot (r^2= 0.998) obtained by consecutive addition of standards over a cocktail of ions (K^+, Na^+, Cl^- and SO_4^{2-}) in SAOB using IPSSE.

Other factors that have to be studied to guarantee the validation of a method are repeatability and reproducibility. Repeatability was tested by the same analyst in a short period of time. The measurements were done preparing 10 beakers containing the same ions concentration (at three concentration level of sulfide ion corresponding to the linear response range) and then the electrodes (working and double junction reference) were systematically immerse and rinsed with copious amounts of water between every measurement. Results of this procedure are summarized in Table 5.2. Confidence intervals (95%) for each point were below 1 mV, which is in agreement with precision measured with other ion-selective electrodes.[29] In this particular case, the reproducibility was studied in terms of the fabrication process. Three different full fabrication processes separated in days were done. Results of the calibration curves by triplicate (of each one) gave a mean Nernstian response of 30±2 mV/decade (±confidence interval at 95%). Summarizing, the fabrication process successfully provided reliable sulfide-selective electrodes with potential to be used in real matrices.

Table 5.2. Repeatability study. Results obtained for analysis of different concentration of standards inside the linear response range of the IPSSE.

Concentration of S^{2-} (M)	**Mean signal of 10 measurements (mV)**	**RSD (%)**	**Confidence interval at 95% (mV)**
$\mathbf{10^{-4}}$	-771.1	0.08	0.4
$\mathbf{10^{-3}}$	-801.2	0.05	0.3
$\mathbf{10^{-2}}$	-827.4	0.10	0.6

The performance of the new IPSSE was tested towards real samples. Really different samples were chosen to showcase the performance of the sensor in different domains. Common river and sea water samples were chosen as environmental matrices, while samples from the outlet of the UASB reactor were selected as industrial matrices. Table 5.3 show the comparison between the S^{2-} concentrations obtained with the IPSSE and the obtained with a commercially available sensor. Results show that the concentrations of each sample found with both sensors do not differ significantly at a confidence level of 95% (details in Statistics section). In the case of environmental-spiked samples (diluted in the same manner), they were also measured without the presence of spiked sulfide by both sensors, giving concentrations below the detection limits. Furthermore, the recovery rates were calculated, 95-96% and 86-88% rates were achieved by the IPSSE and the commercial, respectively (Table 5.3). Overall, the

described fabrication methodology demonstrated to be capable to produce sulfide-selective electrodes (for S^{2-} sensing purposes) which can compete alongside a commercially available one.

Table 5.3. Real samples analysis. Comparison between the S^{2-} concentrations obtained with the IPSSE and with a commercial sulfide ion sensor.

Samples	IPSSE			Commercial sulfide sensor		
	Mean concentration of 3 measures (mM)	Standard deviation (mM)	Recovery rate (%)	Mean concentration of 3 measures (mM)	Standard deviation (mM)	Recovery rate (%)
Reactor 1	4.44	0.55	-	5.0	0.61	-
Reactor 2	4.50	0.15	-	4.40	0.10	-
River	1.57	0.50	95	1.46	0.35	88
Sea	1.60	0.62	96	1.42	0.37	86

Therefore, the fabrication methodology proposed in this experimental study excels providing functional sulfide sensors in a miniaturized fashion that have demonstrated to be useful in a wide variety of situations. It represents a complementary alternative to this kind of electrodes and sulfide analytical methods described in the introduction of the chapter.

Apart from this breakthrough fabrication process, a less sophisticated and more hand-crafted process was briefly tested. The inkjet printer was replaced by a nail brusher and the electrochemical oxidation by long term spontaneous deposition. A silver electrode was manually drawn and sintered. Then, milling conditions (Ag is oxidized in basic media) of the electrolytic solution allow the deposition of Ag/Ag_2S in 1 day. Surprisingly, the electrode gave a Nernstian response. This non-controlled test could constitute a game changer in the self-production home-made of electrodes.

5.5. Statistics

Comparison of the performance of IPSSE against the commercial one (Orion 9616BNWP; Thermo Electron Corporation, Beverly, MA, USA) was done comparing replicate measurements. This comparison experiment was done measuring S^{2-} in multiple samples multiple times by both methods giving two different values, each with its own standard deviation.

First, F test tells whether two standard deviations significantly different from each other.

$$F_{calculated} = \frac{s_1^2}{s_2^2}, \quad s_1 > s_2 \qquad \text{(Equation 5.2)}$$

If the $F_{calculated}$ is lower than the $F_{tabulated}$ (39 for n_1=3 and n_2=3 at a confidence level of 95%) both standard deviations obtained do not present significant differences (Table 5.4).

Table 5.4. F values calculated for each one of the samples measured.

Sample	$F_{calculated}$
Reactor 1	1.23
Reactor 2	2.25
River	2.04
Sea	2.08

In all cases, it is demonstrated that there are no significantly differences in terms of standard deviations.

Second, for two sets of data consisting of n_1 and n_2 measurements (with averages $\bar{x}_1 - \bar{x}_2$) we calculate a value of t with the following formula:

$$t_{calculated} = \frac{|\bar{x}_1 - \bar{x}_2|}{S_{spooled}} \sqrt{\frac{n_1 n_2}{n_1 + n_2}} \qquad \text{(Equation 5.3)}$$

Where $|\bar{x}_1 - \bar{x}_2|$ is the absolute value of the difference and S pooled is a spooled standard deviation making use of both sets of data:

$$S_{spooled} = \sqrt{\frac{s_1^2(n_1-1)+s_2^2(n_2-1)}{n_1+n_2-2}} \quad \text{(Equation 5.4)}$$

If the $t_{calculated}$ is lower than the $t_{tabulated}$ (2.77) both results obtained do not present significant differences (Table 5.5).

Table 5.5. t values calculated for each one of the samples measured.

Sample	$t_{calculated}$
Reactor 1	1.26
Reactor 2	0.96
River	0.31
Sea	0.43

In all cases, it is demonstrated that there are no significantly differences in the S^{2-} concentration obtained by both methods.

5.6. Conclusions

The fabrication and the electrochemical performance of the first IPSSE is described. The IPPSE was successfully fabricated by printing a silver electrode followed by an electrochemical deposition of sulfide. Although this fabrication procedure was composed by two consecutive completely different techniques, further efforts could be done to try to produce an inkjet printable Ag_2S ink which will reduce the required equipment. Nonetheless, the fabrication process demonstrates high reproducibility and reliability. An expected Nernstian response of -29.4±0.3 mV/decade was obtained within concentrations of 0.03-100 mM with a short response time (3 s). Furthermore, the IPSSE was tested with real samples and gave results in agreement with a commercially available one. Considering the challenges inkjet-printed ion-selective face, this different fabrication approach could open new ways of mass production of all-solid-state ion-selective sensors.

Although, in this chapter is showcased the fabrication methodology of a single type of ion-selective electrode, the potential of inkjet printing to produce not only other potentiometric electrodes but also other kind of functional miniaturized electronics in a simple way should be highlighted.

5.7. References

(1) Nooredeen Abbas, M.; Radwan, A.-L. a.; Nawwar, G. a.; Zine, N.; Errachid, a. A Durable Solid Contact Sulfide Sensor Based on a Ceric Acrylohydrazide Ionophore Attached to Polyacrylamide with a Nanomolar Detection Limit. *Anal. Methods* **2015**, *7* (3), 930–942.

(2) Privett, B. J.; Shin, J. H.; Schoenfisch, M. H. Electrochemical Sensors. *Anal. Electrochem.* **2010**, *82*, 4723–4741.

(3) Kimmel, D. W.; Leblanc, G.; Meschievitz, M. E.; Cliffel, D. E. Electrochemical Sensors and Biosensors. *Anal. Chem.* **2012**, *84* (2), 685–707.

(4) Hughes, G.; Westmacott, K.; Honeychurch, K. C.; Crew, A.; Pemberton, R. M.; Hart, J. P. Recent Advances in the Fabrication and Application of Screen-Printed Electrochemical (Bio)Sensors Based on Carbon Materials for Biomedical, Agri-Food and Environmental Analyses. *Biosensors* **2016**, *6*, 50.

(5) Abdulbari, H. A.; Basheer, E. A. M. Electrochemical Biosensors: Electrode Development, Materials, Design, and Fabrication. *ChemBioEng Rev.* **2017**, *4* (2), 92–105.

(6) Gao, M.; Li, L.; Song, Y. Inkjet Printing Wearable Electronic Devices. *J. Mater. Chem. C* **2017**, *5*, 2971–2993.

(7) Guo, Y.; Patanwala, H. S.; Bognet, B.; Ma, A. W. K. Inkjet and Inkjet-Based 3D Printing: Connecting Fluid Properties and Printing Performance. *Rapid Prototyp. J.* **2017**, *23* (3), 562–576.

(8) Kell, A. J.; Paquet, C.; Mozenson, O.; Djavani-Tabrizi, I.; Deore, B.; Liu, X.; Lopinski, G. P.; James, R.; Hettak, K.; Shaker, J.; et al. Versatile Molecular Silver Ink Platform for Printed Flexible Electronics. *ACS Appl. Mater. Interfaces* **2017**, *9*, 17226–17237.

(9) Torrisi, F.; Hasan, T.; Wu, W.; Sun, Z.; Lombardo, A.; Kulmala, T. S.; Hsieh, G. W.; Jung, S.; Bonaccorso, F.; Paul, P. J.; et al. Inkjet-Printed Graphene Electronics. *ACS Nano* **2012**, *6* (4), 2992–3006.

(10) Ngamna, O.; Morrin, A.; Killard, A. J.; Moulton, S. E.; Smyth, M. R.; Wallace, G. G. Inkjet Printable Polyaniline Nanoformulations. *Langmuir* **2007**, *23* (16), 8569–8574.

(11) Zhang, G.; Hui, H. Y.; Chu, P. H.; Yuan, Z.; Chang, R.; Risteen, B.; Yang, H.; Reichmanis, E. From Staple Food to Flexible Substrate to Electronics: Rice as a Biocompatible Precursor for Flexible Electronic Components. *Chem. Mater.* **2016**, *28* (23), 8475–8479.

(12) Root, S. E.; Savagatrup, S.; Printz, A. D.; Rodriquez, D.; Lipomi, D. J. Mechanical Properties of Organic Semiconductors for Stretchable, Highly Flexible, and Mechanically Robust Electronics. *Chem. Rev.* **2017**, acs.chemrev.7b00003.

(13) Moya, A.; Gabriel, G.; Villa, R.; Javier, F. Inkjet-Printed Electrochemical Sensors. *Curr. Opin. Electrochem.* **2017**, (In press).

(14) Hu, J.; Stein, A.; B??hlmann, P. Rational Design of All-Solid-State Ion-Selective Electrodes and Reference Electrodes. *TrAC - Trends Anal. Chem.* **2016**, *76*, 102–114.

(15) Zuliani, C.; Diamond, D. Opportunities and Challenges of Using Ion-Selective Electrodes in Environmental Monitoring and Wearable Sensors. *Electrochim. Acta* **2012**, *84*, 29–34.

(16) Bu, P. Carrier-Based Ion-Selective Electrodes and Bulk Optodes . 2 . Ionophores for Potentiometric and Optical Sensors. **1998**, *2665* (97).

(17) Bakker, E.; Bühlmann, P.; Pretsch, E. Polymer Membrane Ion ˜ Selective Electrodes – What Are the Limits ? *Electroanalysis* **1999**, *11* (13), 915–933.

(18) Sjöberg, P.; Määttänen, A.; Vanamo, U.; Novell, M.; Ihalainen, P.; Andrade, F. J.; Bobacka, J.; Peltonen, J. Paper-Based Potentiometric Ion Sensors Constructed on Ink-Jet Printed Gold Electrodes. *Sensors Actuators, B Chem.* **2016**, *224*, 325–332.

(19) Qin, Y.; Alam, A. U.; Howlader, M. M. R.; Hu, N.; Deen, M. J. Inkjet Printing of a Highly Loaded Palladium Ink for Integrated , Low-Cost PH Sensors. **2016**, *26*, 4923–4933.

(20) Zea, M.; Moya, A.; Fritsch, M.; Ramon, E.; Villa, R.; Gabriel, G. Enhanced Performance Stability of Iridium Oxide-Based PH Sensors Fabricated on Rough Inkjet-Printed Platinum. *ACS Appl. Mater. Interfaces* **2019**, *11* (16), 15160–15169.

(21) Redondo, R.; Machado, V. C.; Baeza, M.; Lafuente, J.; Gabriel, D. On-Line Monitoring of Gas-Phase Bioreactors for Biogas Treatment : Hydrogen Sulfide and Sulfide Analysis by Automated Flow Systems. *Anal. Bioanal. Chem.* **2008**, *391*, 789–798.

(22) Gründler, P. *Chemical Sensors*; Springer: Berlin, 2006.

(23) Kang, S.; Oh, J.; Han, M. S. A Colorimetric Sensor for Hydrogen Sulfide Detection Using Direct Inhibition of Active Site in G-Quadruplex DNAzyme. *Dye. Pigment.* **2017**, *139*, 187–192.

(24) Rosolina, S. M.; Thomas, S.; Xue, Z. Bismuth-Based , Disposable Sensor for the Detection of Hydrogen Sulfide Gas. *Anal. Chem.* **2016**, *88*, 1553–1558.

(25) Pol, R.; Céspedes, F.; Gabriel, D.; Baeza, M. Microfluidic Lab-on-a-Chip Platforms for Environmental Monitoring. *TrAC - Trends Anal. Chem.* **2017**, *95*, 62–68.

(26) American Public Health Associetion. *Standard Methods: For the Examination of Water and Wastewater*, 22nd ed.; Washington, DC, 2012.

(27) da Silva, E. T. S. G.; Miserere, S.; Kubota, L. T.; Merkoçi, A. A Simple On-Plastic/Paper Inkjet-Printed Solid-State Ag/AgCl Pseudo-Reference Electrode. *Anal. Chem.* **2014**, *86*, 10531–10534.

(28) Bakker, E.; Bühlmann, P.; Pretsch, E. Carrier-Based Ion-Selective Electrodes and Bulk Optodes. 1. General Characteristics. *Chem. Rev.* **1997**, *97* (8), 3083–3132.

(29) Novell, M.; Parrilla, M.; Crespo, A.; Rius, F. X.; Andrade, F. J. Paper-Based Ion-Selective Potentiometric Sensors. *Anal. Chem.* **2012**, *84*, 4695–4702.

CHAPTER 6

3D-printed sulfide-selective microfluidic platform with fully integrated screen-printed electrodes

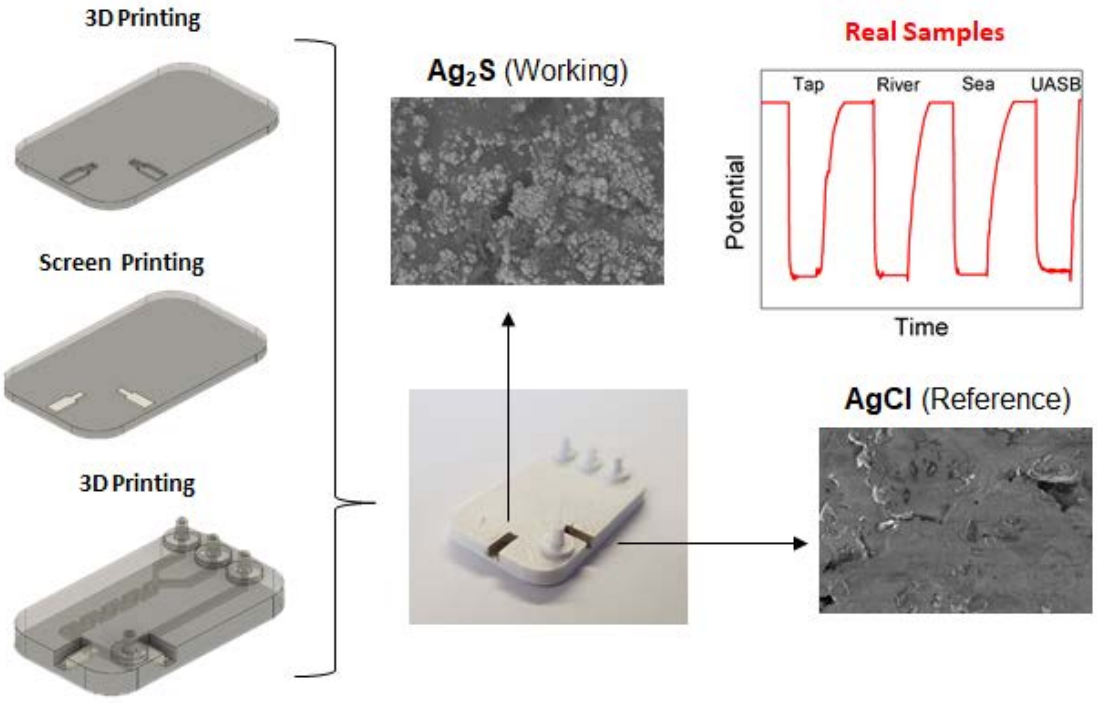

This chapter is a modification of:

Fully integrated screen-printed sulfide-selective sensor on a 3D-printed potentiometric microfluidic platform

R Pol, F Céspedes, D Gabriel, M Baeza

Sensors and Actuators B: Chemical 290, 364-370 (2019)

6.1. Foreword

The next step to measure sulfide on-line was to integrate the sample pretreatment in an autonomous manner. Previous PhD student of the research GENOVOV group (Dr. Andrea Monzón) already developed tubular electrodes with a crystalline Ag_2S membrane to determine sulfide ion in a biotrickling filter (Figure 6.1).

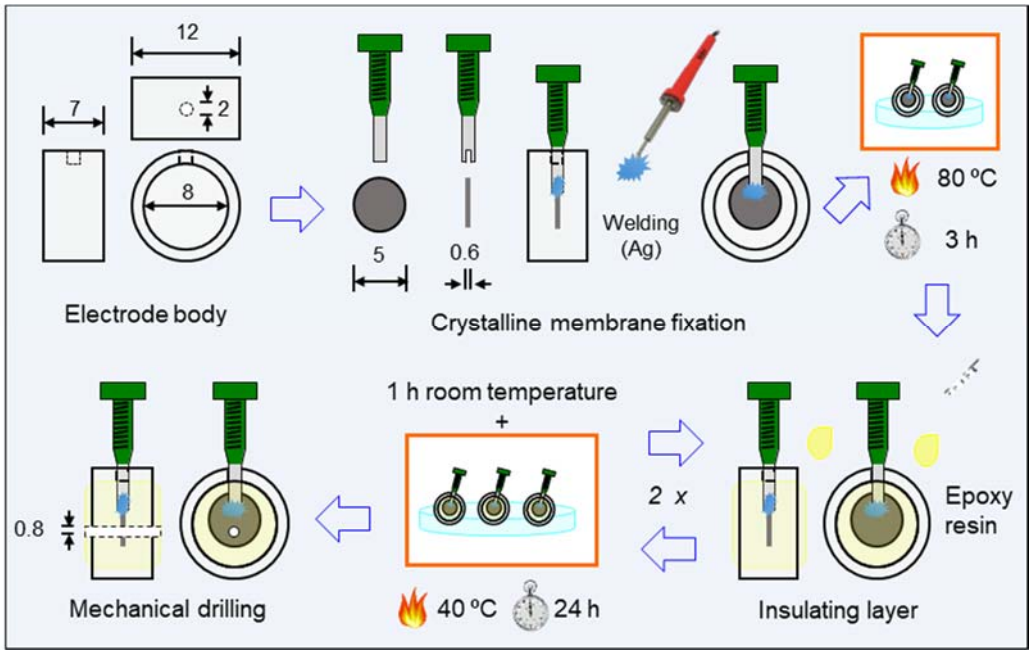

Figure 6.1. Scheme of the fabrication of tubular electrodes based on crystalline Ag_2S membranes; PhD thesis: Aerobic biotrickling filtration for biogas desulfurization. Monzón A.

Our first thoughts were to produce a 3D-printed platform that could contain these kind of disk-shaped crystalline-based membrane electrodes and include an external double junction reference. The production of the membrane required a pressing machine which was not available at that moment. Therefore, following the same idea than in the previous chapter, as a first approximation the electrodes were fabricated by electrodeposition of silver sulfide in this case onto a silver wire and then were stacked inside a 3D-printed microfluidic scaffold (Figure 6.2A-B). Finally, the electrodes were thoroughly characterized morphologically (Figure 6.2C-D) and in terms of their analytical performance giving promising results for the required situation (Figure 6.2E). A part of these results were obtained by our undergraduate student Yasmine Alonso. However, we decided to go for a higher automated fabrication methodology (dual consecutive printing) which will be presented in the core body of this chapter.

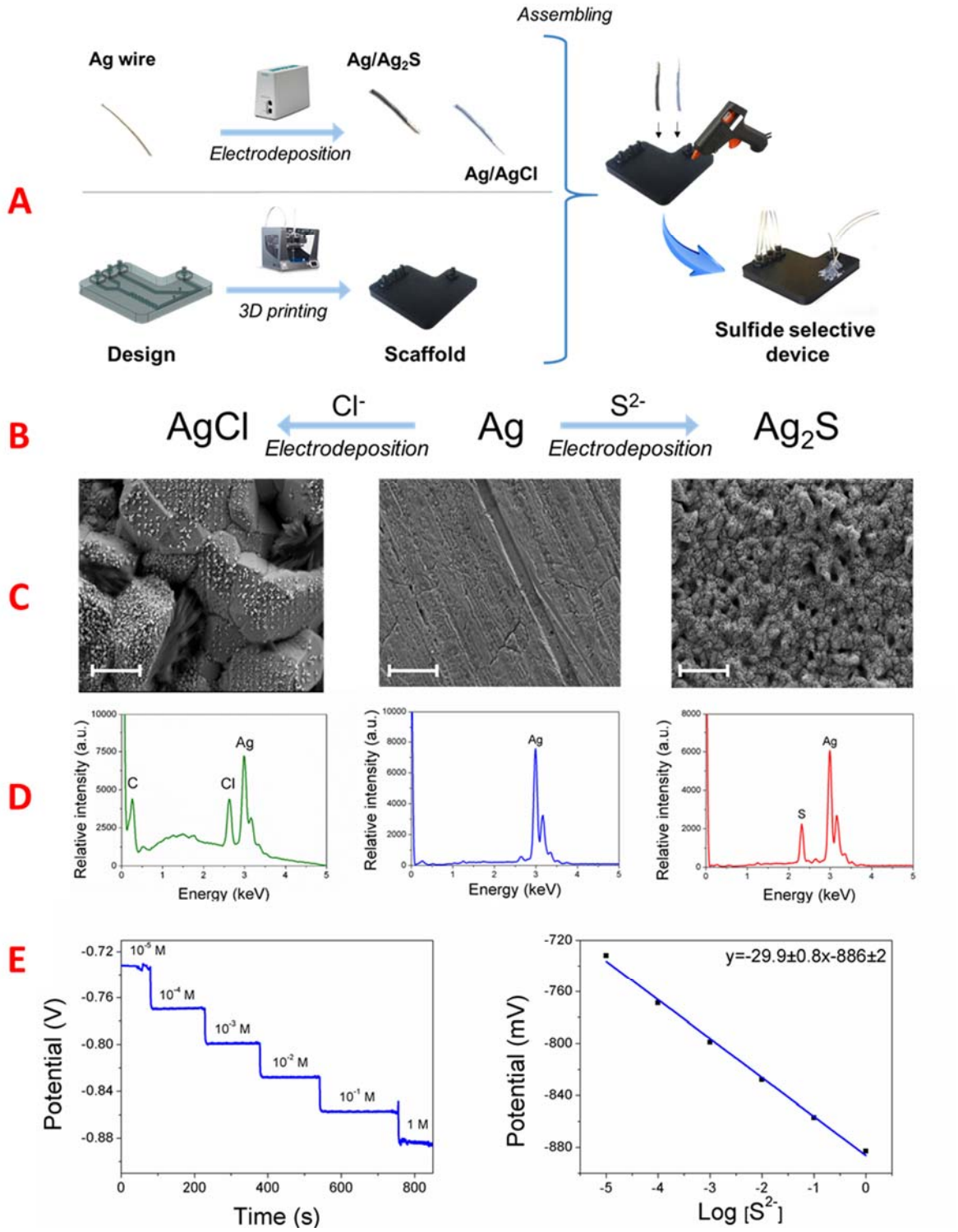

Figure 6.2. Fabrication methodology followed (A), electrodeposition reactions (B), morphological characterization by SEM; scale bar 10 μm (C), elemental characterization by XDS (D) and electroanalytical performance by potentiometry (E).

6.2. Introduction

World is constantly evolving. Every day, new manufacturing companies appear and so, new environmental problems. Among others, water pollution (i.e., the presence of substances in the water, resulting either from human activity or natural processes which affect welfare of persons or the environment) can be considered the most troublesome worldwide problem affecting millions of people.[1,2] Therefore, methodologies for monitoring and control of environmental relevant substances has pushed analytical chemists to produce new reliable analytical systems to track hazardous chemicals in a cheaper and environmental friendly manner.

Through many years, flow-based analyses have been used to obtain online analytical information of different complex matrices of real samples.[3] The main advantage of flow analyses compared to traditional methodologies is the capability to integrate the different analytical steps in a simple analytical instrument/device reducing the need of a specialized operator. Therefore, sample acquisition, pretreatment and assay can be performed subsequently. In addition, with the technological revolution, flow analyses techniques can now be performed in a miniaturized fashion, reducing sample consumption and response time.[4,5] Several microfabrication techniques (e.g., micromachining, hot embossing, injection molding, laser ablation, micromilling and soft lithography) and materials (e.g., silicon, polymers, metals, ceramics, etc.) have been used for the production of miniaturized analytical systems.[6,7,8,9] Nonetheless, all these methods require trained personnel and are expensive and time consuming. Moreover, they require further processing steps (e.g., etching, sealing, etc.) after the fabrication. Nowadays, scientists have been exploring new methodologies to produce such analytical systems in a more feasible and cheaper manner.

Among others, three-dimensional (3D) printing has emerged as an alternative to other fabrication methodologies thanks to its low-cost, simplicity, throughput and affordability.[10,11] 3D printing is an additive manufacturing technology based on the consecutive superposition of layers of a given material.[12] This technology allows to produce parts of a wide variety of materials; from metals to polymers reaching a broad spectrum of applications.[13] Also, 3D printing makes possible to manufacture practically any imaginable geometry at a high resolution, thus demonstrating an amazing potential for the production of both, prototypes and

fully functional structures. Moreover, the fact that motifs can be easily changed on demand makes it more versatile than other fabrication techniques. Although this technology emerged in 1980,[14] it is not until now that it has received a great interest in the scientific-technical field. Nowadays, a lot of effort is invested on the development of different kind of microfluidic platforms using this innovative technology. Therefore, thanks to all the features in which 3D printing excels, many functional optical/electrochemical detection-based microfluidic devices with interest in the analytical chemistry area have been reported.[15] On the other hand, screen printing technique constitutes an easy-to-use methodology for fabrication of electrodes.[16,17] This technique relies on applying pressure with a squeegee to define a motif (of a desired material) into a surface using a mask. In other words, the ability to modify the mask allows screen-printed electrodes to be easily adapted to a require situation. Hence, the combination of both technologies; 3D printing and screen printing will surely open new ways to fabricate analytical devices.

Commonly, 3D-printed microfluidic platforms with electrochemical detection are fabricated by 3D printing the scaffold and inserting the electrodes in it. Generally, there are two ways to couple the electrodes inside. In the first one, wires are just inserted inside the channels and are glued or covered. Gowers et al.[18] reported the fabrication of a 3D-printed microfluidic device with needle-like electrodes that were sealed with a flexible printable polymer. In the second one, the electrodes are placed inside a screw which is screwed on top of the fluidic channels. For instance, Erkal et al.[19] fabricated a one-channel 3D-printed microfluidic platform with threaded inlets for electrodes and tested sets of different material-based electrodes. Another device with screwed electrodes was developed by Bishop et al.[20] in which Prussian blue nanoparticles were synthesized inside the channels and subsequently used for hydrogen peroxide determination. Another approach for the production of 3D-printed microfluidic platforms with electrochemical detections is printing more than one part and stacked them with the electrodes. Nonetheless, all these methodologies lack of compactness and can present severe spills issues affecting the assay.

Herein, the fabrication and performance of a 3D-printed microfluidic platform with integrated potentiometric detection is described. The device contains completely integrated therein a second kind sulfide-selective electrode (Ag/Ag_2S) and a pseudo-reference electrode (Ag/AgCl). The fabrication was divided in two main 3D-printing stages with a screen printing

process interleaved. The first 3D-printing stage is allowed until the screen-printed holes are exposed and filled. Then, the second 3D-printing stage takes place. Furthermore, the analytical performance of the device was tested towards real samples in batch-like and flow condition giving no significant differences *vs*. a standard commercial sensor.

6.3. Experimental section

6.3.1. Materials and chemicals

All chemicals were commercially available and were used without further purification. Sodium sulfide nonahydrate (98%, $Na_2S{\cdot}9H_2O$), sodium hydroxide (98%, NaOH), sodium thiosulfate (99%, $Na_2S_2O_3$), potassium chloride (99%, KCl) and starch were purchased from SigmaAldrich. L(+)-ascorbic acid (99%), potassium iodide (99%, KI) and potassium iodate (99%, KIO_3) were purchased from Panreac (Spain). Polylactic acid (PLA) filament (2.98 mm) was purchased from Fundació DCIM (Spain). Finally, silver paste (H20E-PFC part A and B) was purchased from EPO-TEK (USA).

6.3.2. Sulfide standard solutions and standardization

Aqueous solutions were prepared employing deionized Milli-Q water (18.0 $M\Omega{\cdot}cm^{-1}$). Stock solution of S^{2-} (1 M S^{2-}) was prepared by dissolving 24.5 g of $Na_2S{\cdot}9H_2O$ in 100 mL of a 1 M NaOH solution. Standard solutions of S^{2-} were daily prepared by dilution of the stock solution in sulfide antioxidant buffer (SAOB). The SAOB was prepared by mixing 40 g L^{-1} (1 M) of NaOH (increasing the pH up to 14 which ensures that the predominant specie present in solution of the acid-base equilibrium is S^{2-}) and 10.1 g L^{-1} (0.05 M) of ascorbic acid (which act as an antioxidant to avoid sulfide oxidation).

The determination of the concentration of the stock solution of sulfide ion was performed applying an iodometric method according to the Standard methods.[21] Briefly, standardization of a $Na_2S_2O_3$ with I_3^- takes place. Then, $Na_2S_2O_3$ standardized solution is used to determine the iodine produced by the reaction of sulfide ion with iodide.

6.3.3. Screen-printed electrodes fabrication

Screen-printed sulfide-selective electrode (SPSSE) scaffold and 3D- screen-printed sulfide-selective electrode (3D-SSMP) were designed with the 3D modeling software Fusion360. 3D models were then transformed into a printable file using slicer Cura (parameters details in Table 6.1) and printed by a BCN3D Sigma printer using PLA.

Table 6.1. Slicer parameters used for the fabrication of the SPSSE and 3D-SSMP.

Parameter	SPSSE	3D-SSMP
Layer height	0.2 mm	0.1 mm
Shell thickness	0.4 mm	0.4 mm
Print speed	150 mm/s	100 mm/s
Printing temperature	220 ºC	220 ºC
Bed temperature	45 ºC	45 ºC
% Infill	100%	100%
Nozzle size	0.4 mm	0.4 mm
Initial layer thickness	0.1	0.08 mm
Travel speed	250 mm/s	200 mm/s
Bottom layer speed	100 mm/s	50 mm/s
Infill speed	100 mm/s	50 mm/s

The screen-printed electrodes were homemade by mixing part A and part B (1:1) of the commercial Ag paste and homogenizing it during 10 min. Then, the mixture was manually placed (using a squeegee) in the corresponding cavities and the electrodes were allowed to harden at 60 ºC for 48 h. To delimitate the exposed electrode area a transparent nail polish was used as insulator. Finally, the SPSSE was fabricated by long-term spontaneous deposition. Simply, immersing the tip of the electrode in a 0.1 M S^{2-} (in 1 M NaOH) for 24 h.

6.3.4. Screen-printed electrodes characterization

Morphological changes produced by the Ag_2S deposition over Ag paste were observed by scanning electron microscopy (SEM) using a MerlinZeiss microscope operated at 5 kV. Samples for SEM were prepared by simply sticking the screen-printed electrodes onto the

holder with carbon tape. The elemental composition was determined by Energy Dispersive X-ray Spectroscopy (EDX) at a voltage of 15 kV.

Evaluation of the electrochemical performance was done by a potentiostat/galvanostat AUTOLAB (PGSTAT204) using chronopotentiometry under constant stirring conditions. The SPSSE was used against a double junction reference electrode Ag/AgCl Orion 900200. Calibrations performed for the SPSSE were made in batch condition with subsequent additions (over 25 mL of SAOB) of standards S^{2-}solutions at constant ionic strength.

6.3.5. 3D-printed sulfide-selective microfluidic platform fabrication

Microfluidic scaffold was designed with the 3D modeling software Fusion360. 3D model was then transformed into a printable file using slicer Cura (orientation used in Figure 6.3) and printed by BCN3D Sigma printer using PLA.

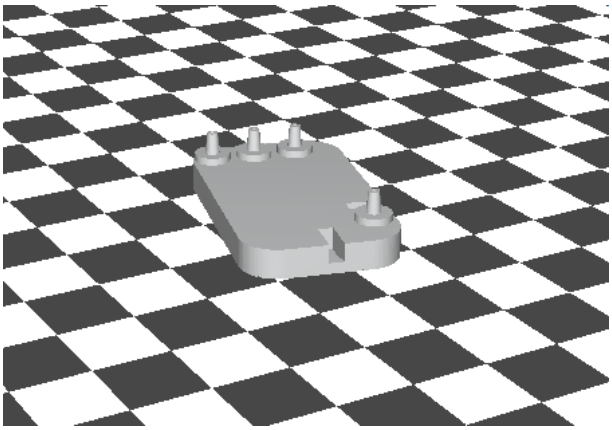

Figure 6.3. Printing orientation used.

The fabrication was divided in two main 3D-printing stages with a screen printing process interleaved (Figure 6.4A). The first 3D-printing stage is allowed until the screen-printed holes are exposed (printing process can be selectively paused by changing a parameter in the slicer software). Screen-printed electrodes were made by mixing part A and part B (1:1) of the commercial Ag paste. Ag paste was homogenized during 10 min and placed it in the corresponding cavities. Then, the second part of the 3D-printing process is performed and the 3D-printed platform with fully integrated electrodes is obtained. Once the printing process is finished, the whole system is set at 60 ºC for 48 h to harden the Ag electrodes. The setup used

for the production of the sulfide-selective electrode is shown in Figure 6.4B. A 0.1 M S^{2-} solution (in 1 M NaOH) was constantly pumped in (a) and (b) channels for 24 h to produce the deposition of Ag_2S and air (c) to be able to recirculate the deposition solution. The dimensions of the 3D-SSMP are shown in Figure 6.4C.

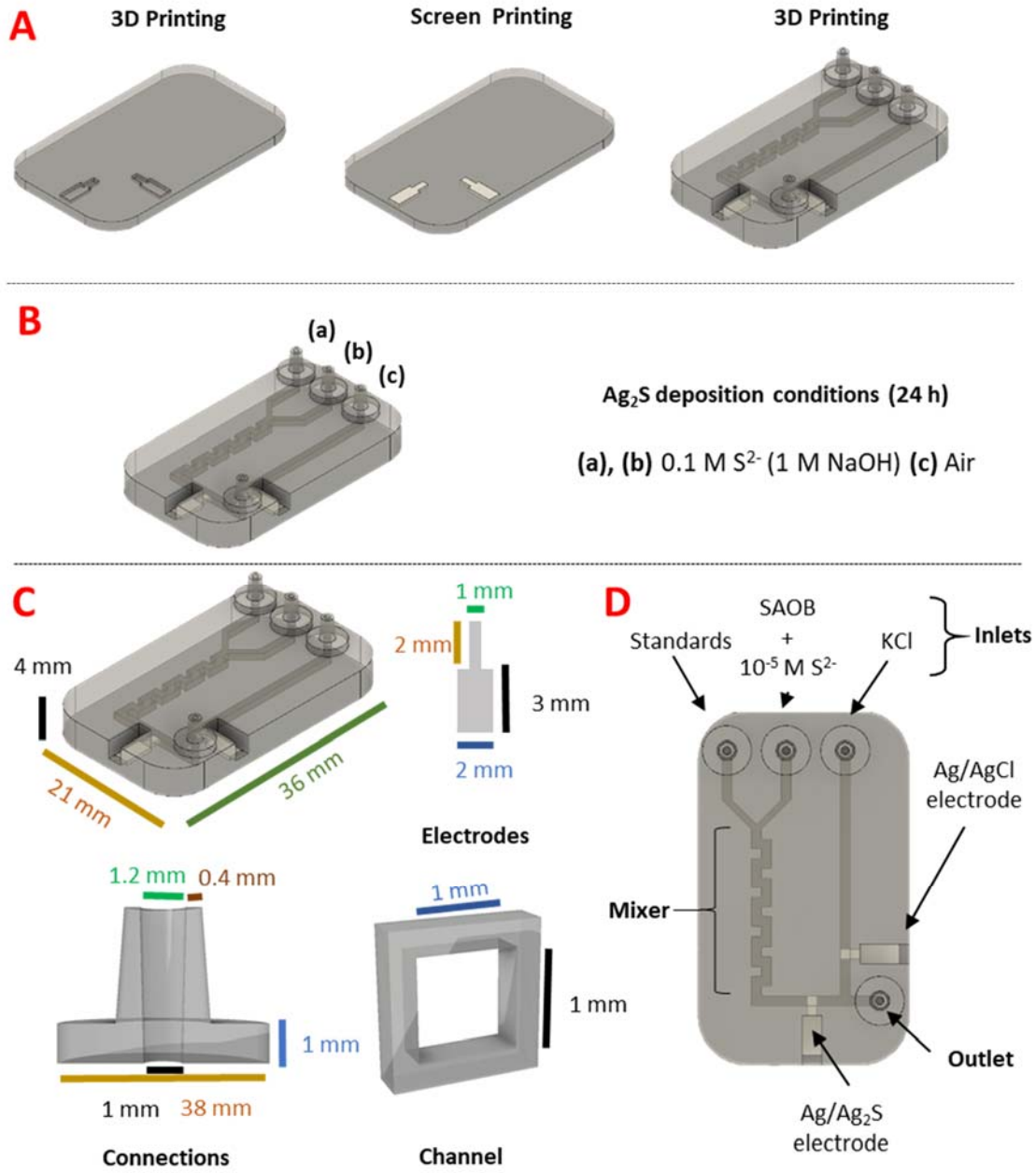

Figure 6.4. Scheme of the fabrication and functioning of the 3D-SSMP: Consecutive printing processes (A), Ag_2S deposition step (B), dimensions (C) and location of the electrodes and solutions used (D).

6.3.6. Experimental setup

The liquid management setup consists of an external peristaltic pump (Minipuls 2, Gilson) equipped with 1.14 mm internal diameter Tygon®tubing (Ismatec). The 3D-SSMP is composed by three inlets (Figure 6.4D). On the one hand, standards or sample inlet (inlet (a) Figure 6.4B) is connected by a internal Y-shaped to a constant carrier containing SAOB spiked with S^{2-} (inlet (b) Figure 6.2B), which after a short mixer chamber goes over the SPSSE. On the other hand, the channel which contains the pseudo-reference electrode is constantly fed with a KCl 0.1 M solution (inlet (c) Figure 6.2B) to maintain its potential constant.

Evaluation of the electrochemical response of the 3D-SSMP was done by a potentiostat/galvanostat AUTOLAB (PGSTAT204) using chronopotentiometry mode. The working electrode used was the second kind sulfide-selective electrode (Ag/Ag_2S) while a pseudo-reference (Ag/AgCl) was used as reference electrode, both contained inside the microfluidic platform.

6.3.7. Sampling, spiking and determination in real samples

River and sea water samples were collected following ISO 5667-6:2014 and ISO 5667-9:1992, respectively. Subsequently, both solutions were spiked with the same amount of S^{2-} from the stock solution to fit in the middle of linear concentration range (1 mM S^{2-}). In addition, process samples were collected from the outlet sampling port of a 2 L upflow anaerobic sludge blanket reactor (UASB) performing anaerobic sulfate reduction to sulfide using crude glicerol as electron donor. UASB performance at the time of sampling corresponded to almost complete conversion of a sulfate concentration of 0.25 kg S m^{-3}. Samples from the reactor were filtered through a Millex 0.45 μm filter and conditioned by dilution with twice concentrated SAOB (1:1).

The results obtained were compared against a commercial available Orion 9616BNWP (Thermo Electron Corporation, Beverly, MA, USA) sulfide-selective electrode using a SB90M5 potentiostat (SympHony™, VWR).

6.4. Results and discussion

The challenge faced in this project was the production of a fully integrated (all-in-one piece) electrochemical-based detection system taking advantage of the combination of 3D printing and screen printing technologies. To showcase the potential applications of devices fabricated by this combination of technologies, a potentiometric microanalyzer for determination of sulfide ion in different complex samples was developed. Nonetheless, prior to the production of the final device as a proof of concept, a SPSSE was produced and characterized morphologically and electroanalytically in batch conditions to ensure its functionality.

The successful long-term Ag_2S deposition can be easily discerned by naked eye due to a change of color; from grey to black (Figure 6.5A and 6.5B). Moreover, SEM micrographs demonstrate a change at the outer surface of the electrode. On the one hand, Ag electrode shows a typical morphology of a conductive epoxy composite (Figure 6.5A1).[22] On the other hand, an increase of roughness caused by the formation of Ag_2S microcrystals after the long-term deposition is evidenced (Figure 6.5B1).[23]

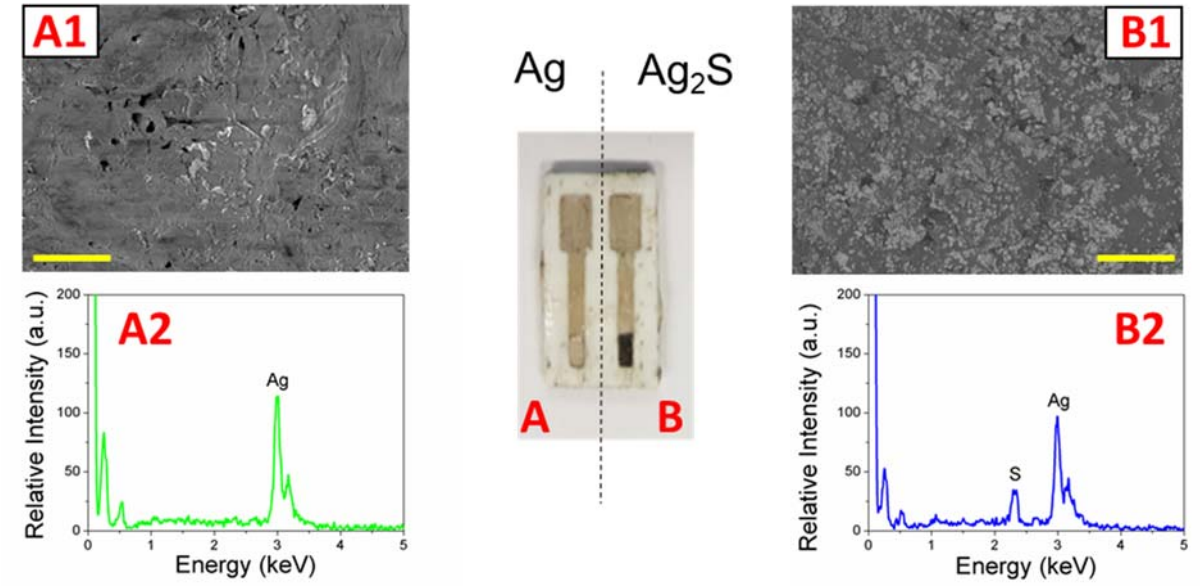

Figure 6.5. Screen-printed silver electrode (A), SEM micrograph; scale bar = 10 μm (A1) and EDX (A2). Sulfide-selective electrode (B), SEM micrograph; scale bar = 10 μm (B1) and EDX (B2).

Apart from SEM micrographs, elemental analyses were also carried out. EDX was performed to demonstrate the presence of S after the formation of Ag_2S. The EDX data showed the

appearance of two peaks at 2.3 and 2.7 keV corresponding to the presence of S (Figure 6.5B2) aside from the Ag (3.1 and 3.3 keV) peaks. Moreover, less relevant peaks appear, corresponding to the presence of C (0.26 keV) and O (0.50 keV) from the epoxy nature of the pastes in both cases.

Once characterized morphologically, the SPSSE must accomplish several statements to demonstrate its functionality prior to the fabrication of the 3D-SSMP. A Ag_2S-rich surface for the ion-to-electron transduction based on the following redox reaction,

$$\boldsymbol{Ag_2S_{(s)} + 2e^- \leftrightarrow 2Ag_{(s)} + S^{2-}_{(aq)}}$$

in which the redox potential is described by the Nernst equation (Equation 6.1):

$$\boldsymbol{E = E^0 - \frac{59.16}{n} log\{S^{2-}\}} \qquad \text{(Equation 6.1)}$$

Where E^0 is the standard potential ($E^0_{Ag_2S/Ag}$), n is the number of electrons involved in the redox reaction and $\{S^{2-}\}$ is the activity of S^{2-} ions in solution. Therefore, the theoretical sensitivity of the sensor should be -29.58 mV·decade^{-1}.

Consequently, the electroanalytical response of the SPSSE was tested. The potential of the SPSSE was measured under batch conditions using a commercial double junction reference electrode. The main reason for using a commercial reference (and not the screen-printed pseudo-reference) is that the presence of sulfide in basic media exchanges the chloride anions (AgCl →Ag_2S) defeating the purpose of the reference. The corresponding calibration plot for the SPSSE obtained for three consecutive calibrations is shown in Figure 6.6. The calibration curve presents a super-Nernstian response of -31±1 mV·decade^{-1} (± confidence interval at 95%) from 0.06 to 60 mM as linear response range with a limit of detection of 0.02 mM S^{2-} (calculated by intersection of the linear range and the asymptote).[24] The super-Nernstian response observed could be explained by the presence of the polymeric matrix (silver-epoxy resin). Moieties coming from the polymer interact with sulfide ion slightly modifying the potential measured at the working electrode.[25,26,27] Is it worth noting that through all the calibration plot the individual point error bars cannot be discerned, which demonstrates the

high repeatability of the measurements done with this type of second kind electrodes. A big concern when working with electrochemical detection is the potential interferences that can be encountered. Nonetheless, as demonstrated previously at chapter 5, second kind sulfide-selective electrodes do not present remarkable interferences for the most common ions.[21]

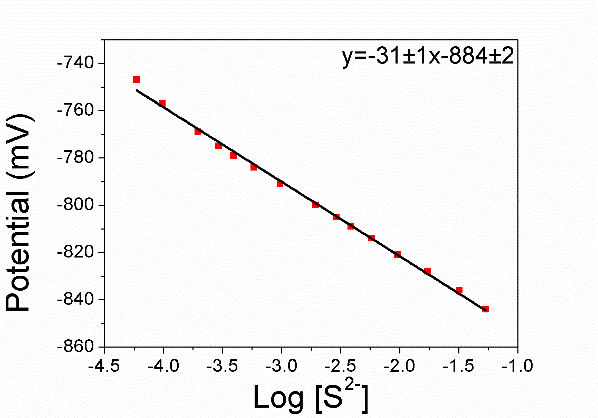

Figure 6.6. Calibration plot for the screen-printed sulfide-selective electrode (n=3).

Once the electrodes were tested and proved their practical application, the final 3D-SSMP was fabricated. Several factors were taken into account to produce the microanalyzer. First, there must be two main channels were the working and pseudo-reference electrodes are placed separately. Otherwise, the sulfide ion solutions will spoil the pseudo-reference electrode as aforementioned before. Moreover, these two channels must be connected to ensure ionic conductivity between the both solutions circulating in the microchannels. Another factor related was the distance between the electrodes. A short distance was kept between them, although in potentiometric measurements as far as there is conductivity and increase in resistance does not represent a drawback. The 3D-SSMP is composed by three inlets. In the pseudo-reference channel, a KCl (0.1 M) solution is constantly being pumped to ensure a constant and well-defined potential over the pseudo-reference electrode. In the other two inlets, standards or samples and SAOB spiked with sulfide ion to get a final concentration of 0.01 mM (carrier) are being pumped and mixed together. The chemical nature of the carrier was chosen for several reasons. First, the NaOH increases the pH up to 14 which ensures that the predominant specie present in solution of the acid-base equilibrium will be S^{2-} and helps to maintain a constant ionic strength. Second, the spiked sulfide (0.01 mM, chosen taking into account the SPSSE limit of detection) acts as a constant conditioning solution for the working electrode and helps to recover the baseline faster.[28] Finally, a constant flow rate of 0.9 mL·min-

[1] for the carrier and standards/samples was chosen for the assay in agreement with previous reports of ion-selective electrodes used in flow assays.[29] However, in this particular flow technique (continuous flow assay) modifications of the flow rate will only have a direct effect in the response time and only a minimum effect on sample dispersion because the maximum signal was obtained in all cases.

Finally, the electroanalytical performance of the as-fabricated 3D-SSMP was studied. Figure 6.7A shows an example of the time trace of the potentiometric response during consecutive increases of sulfide ion concentration. The corresponding calibration curve for three calibrations is shown in Figure 6.7B. The calibration plot exhibits a Nernstian response of -29±1 mV·decade^{-1} (± confidence interval at 95%) between 0.1 and 1000 mM with a detection limit of 0.03 mM and a response time of 8 s.

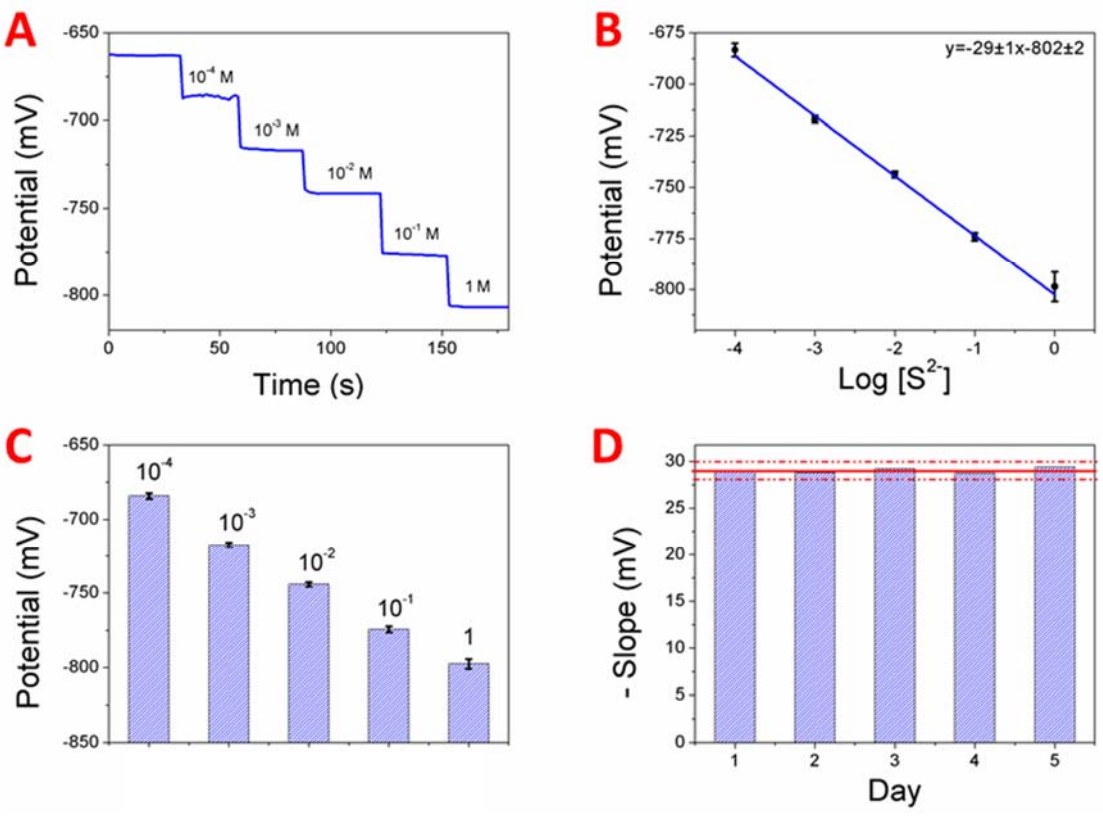

Figure 6.7. Response of the 3D-SSMP for S^{2-} determination. Experimental data for consecutive changes of S^{2-} concentration (A), calibration plot for experimental data obtained (n=3) (B), repeatability study of each standard solution used (n=5) (C) and reproducibility study for n = 5 measurements obtained different days; mean sensitivities of all calibration curve obtained using five different S^{2-} standards (red line) and 3-folds the standard deviation (dashed red line).

Other factors that have to be studied to guarantee the validation of a method are repeatability and reproducibility. Repeatability was tested by the same analyst in a short period of time. The measurements were done pumping each one of the standard solutions five times with the carrier interleaved (only carrier was pumped in both inlets). The device showed high repeatability over each one of the standard solution as expected with ion-selective electrodes (Figure 6.7C). Furthermore, reproducibility was also test. To test this important feature, different calibrations (done by simply using both endpoint solutions) were done in different days. Results of the calibration curve showed a mean Nernstian response with a sensitivity of -29±1 mV·decade^{-1} (± confidence interval at 95%) and were encompassed between 3-folds the standard deviation (of each daily calibration, red dashed lines) of the mean (red line) (Figure 6.7D). Moreover, the reproducibility of the fabrication methodology was also tested, two devices were fabricated in two consecutive weeks. Both were tested the same day and presented no relevant differences in the calibration curve. Finally, the life-time of the sensor was tested. The 3D-SSMP presented reliable calibration result for 6 months with no special storing conditions (inside a drawer dried).

To sum up, the device was successfully fabricated, and the analytical behavior provided relevant results. The performance of the 3D-SSMP was tested towards real samples. Different samples were chosen to demonstrate the potential of the microfluidic platform against a commercial sulfide-selective electrode. Two sets of experiments were carried out. In both cases, SAOB from carrier solution used was twice concentrated and samples measured with the commercial sensor were conditioned prior to the assay. The first case was composed by measuring triplicates of sulfide-spiked tap/river/seawater samples (Table 6.2). Table 6.2 shows the comparison between the sulfide ion concentrations obtained with the 3D-SSMP and the commercial sulfide-selective sensor. Results showed that the concentrations of each sample found with both methods did not differ significantly at a confidence level of 95% (details in statistics section). Moreover, outstanding recoveries rates (calculated by comparison between the concentration estimated and the nominal spiked concentration) of 90-98% and 98-105% by the 3D-SSMP and commercial sensor, respectively were achieved. Meanwhile, samples were also measured without the presence of spiked sulfide resulting in concentrations below the detection limits for both methods (0.1 μM for commercial sensor). In the second case, several samples (spaced in time) from the outlet of an UASB reactor were measured and compared

with the commercial sensor with no replicates. Table 6.3 summarizes the comparison between both methods showing no significant differences at a confidence level of 95%.

Table 6.2. Real spiked samples (tap, river and seawater) analysis. Comparison between the S^{2-} concentrations obtained with the 3D-SSMP and with a commercial sulfide ion sensor.

	3D-SSMP			**Commercial electrode**		
Sample	**Mean concentration of 3 measures [S^{2-}] (mM)**	**Standard deviation (mM)**	**Recovery rate (%)**	**Mean concentration of 3 measures [S^{2-}] (mM)**	**Standard deviation (mM)**	**Recovery rate (%)**
Tap	1.1	±0.1	98%	1.1	±0.1	98%
River	1.1	±0.2	94%	1.2	±0.1	105%
Sea	1.0	±0.2	90%	1.1	±0.3	100%

Table 6.3. UASB reactor samples. Comparison between the S^{2-} concentrations obtained with the 3D-SSMP and with a commercial sulfide ion sensor.

UASB sample	**3D-SSMP, [S^{2-}] (mM)**	**Commercial electrode, [S^{2-}] (mM)**
1	3.06	3.29
2	3.84	4.01
3	3.13	3.07
4	3.91	3.75
5	4.09	3.86
6	4.63	4.37
7	5.72	5.20
8	3.75	3.67

Overall, the dual printing fabrication process demonstrated its capability to produce reliable potentiometric detection-based microfluidic platform that can compete alongside a commercial potentiometric sensor.

6.5. Statistics

Comparison of the performance of the 3D-printed sulfide selective microfluidic platform against the commercial one (Orion 9616BNWP; Thermo Electron Corporation, Beverly, MA,

USA) for environmental samples was done comparing replicate measurements. This comparison experiment was done measuring S^{2-} in multiple samples multiple times by both methods giving two different values, each with its own standard deviation.

First, **F test** tells whether two standard deviations significantly different from each other (Equation 6.2).

$$F_{calculated} = \frac{s_1^2}{s_2^2}, \quad s_1 > s_2 \qquad \text{(Equation 6.2)}$$

If the $\boldsymbol{F_{calculated}}$ is lower than the $\boldsymbol{F_{tabulated}}$ (39 for n_1=3 and n_2=3 at a confidence level of 95%) both standard deviations obtained do not present significant differences (Table 6.4).

Table 6.4. F values calculated for each one of the samples measured.

Sample	$\boldsymbol{F_{calculated}}$
Tap	1
River	1.77
Sea	1.93

In all cases, it is demonstrated that there are no significantly differences in terms of standard deviations.

Second, for two sets of data consisting of n_1 and n_2 measurements (with averages $\bar{x}_1 - \bar{x}_2$) we calculate a value of ***t*** with the following equation (Equation 6.3):

$$t_{calculated} = \frac{|\bar{x}_1 - \bar{x}_2|}{S_{pooled}} \sqrt{\frac{n_1 n_2}{n_1 + n_2}} \qquad \text{(Equation 6.3)}$$

Where $|\bar{x}_1 - \bar{x}_2|$ is the absolute value of the difference and S_{pooled} is a pooled standard deviation making use of both sets of data (Equation 6.4):

$$S_{spooled} = \sqrt{\frac{s_1^2(n_1 - 1) + s_2^2(n_2 - 1)}{n_1 + n_2 - 2}} \qquad \text{(Equation 6.4)}$$

If the $t_{calculated}$ is lower than the $t_{tabulated}$ (2.77) both results obtained do not present significant differences (Table 6.5).

Table 6.5. Values of $t_{calculated}$ for each one of the samples measured.

Sample	$t_{calculated}$
Tap	0
River	1.04
Sea	0.67

In all cases, it is demonstrated that there are no significantly differences in the sulfide ion concentration obtained by both methods.

Comparison of the performance of the 3D-printed sulfide selective microfluidic platform against the commercial one (Orion 9616BNWP; Thermo Electron Corporation, Beverly, MA, USA) for UASB reactor was done comparing individual differences. This comparison experiment was done measuring S^{2-} in multiple samples one time by both methods giving one concentration value for each method.

First, the difference between the two results for each sample is calculated (Table 6.6).

Table 6.6. Concentration values obtained by both methods and the difference between them.

UASB Sample	3D-SSMP [S^{2-}] (mM)	Commercial electrode [S^{2-}] (mM)	Difference
1	3.06	3.29	-0.23
2	3.84	4.01	-0.17
3	3.13	3.07	0.06
4	3.91	3.75	0.16
5	4.09	3.86	0.23
6	4.63	4.37	0.26
7	5.72	5.20	0.52
8	3.75	3.67	0.08

Second, the mean value (**0.11**) and the standard deviation (**0.24**) of the differences is calculated, then we calculate a value of ***t*** with the following equation (Equation 6.5):

$$t_{calculated} = \frac{|\bar{d}|}{S_d}\sqrt{n} \qquad \text{(Equation 6.5)}$$

Where $|\bar{d}|$ is the absolute value of the mean differences, S_d is the standard deviation of the differences and n is the number of samples measured.

If the $t_{calculated}$ (**1.30**) is lower than the $t_{tabulated}$ (**2.37**) the methods do not present significant differences. Therefore, in this case there are no significant differences between the proposed 3D-SSMP device and the conventional commercial electrode.

6.6. Conclusions

The fabrication and the electrochemical performance of the first 3D-SSMP is described. First, a SPSSE was fabricated and characterized to ensure its functionality prior to the embedment in the microfluidic platform. Then, the 3D-SSMP was successfully fabricated by dividing the 3D-printing in two main stages with a screen-printing process interleaved and a long-term deposition of Ag_2S. A Nernstian response of -29±1 mV/decade of sensitivity was obtained within linear range concentrations of 0.1-1000 mM with a short response time (8 s) and detection limit of 0.03 mM. Furthermore, the 3D-SSMP was tested with real samples and the results showed no significant differences respect to the commercial electrode. Considering all the current challenges in the fabrication of 3D-printed microfluidic platforms with electrochemical detection for biotechnological and environmental screening applications, this appealing approach could constitute a new paradigm in the production of functional monitoring devices.

Although many efforts have been done to produce a sulfide-selective microfluidic platform, the potential of this dual printing fabrication methodology should be further exploited for production of other potentiometric, amperometric and impedimetric detection-based platforms for on-demand production of screening devices.

6.7. References

(1) Ginn, J. R. B. and J. S. *Practical Handbook of Soil, Vadose Zone, and Ground-Water Contamination: Assessment, Prevention, and Remediation*, Second Edi.; New York, 2004.

(2) Whelton, A. J.; McMillan, L. K.; Connell, M.; Kelley, K. M.; Gill, J. P.; White, K. D.; Gupta, R.; Dey, R.; Novy, C. Residential Tap Water Contamination Following the Freedom Industries Chemical Spill: Perceptions, Water Quality, and Health Impacts. *Environ. Sci. Technol.* **2015**, *49* (2), 813–823.

(3) Rechberger, P. H. B. and H. *Practical Handbook of Material Flow Analysis*; Ecomed: Florida, 2004.

(4) Pol, R.; Céspedes, F.; Gabriel, D.; Baeza, M. Microfluidic Lab-on-a-Chip Platforms for Environmental Monitoring. *TrAC - Trends Anal. Chem.* **2017**, *95*, 62–68.

(5) Nge, P. N.; Rogers, C. I.; Woolley, A. T. Advances in Microfluidic Materials, Functions, Integration, and Applications. *Chem. Rev.* **2013**, *113* (4), 2550–2583.

(6) Koesdjojo, M. T.; Tennico, Y. H.; Remcho, V. T. Fabrication of a Microfluidic System for Capillary Electrophoresis Using a Two-Stage Embossing Technique and Solvent Welding on Poly(Methyl Methacrylate) with Water as a Sacrificial Layer. *Anal. Chem.* **2008**, *80* (7), 2311–2318.

(7) Geissler, M.; Roy, E.; Diaz-Quijada, G. A.; Galas, J. C.; Veres, T. Microfluidic Patterning of Miniaturized DNA Arrays on Plastic Substrates. *ACS Appl. Mater. Interfaces* **2009**, *1* (7), 1387–1395.

(8) Baeza, M.; López, C.; Alonso, J.; López-Santín, J.; Álvaro, G. Ceramic Microsystem Incorporating a Microreactor with Immobilized Biocatalyst for Enzymatic Spectrophotometric Assays. *Anal. Chem.* **2010**, *82* (3), 1006–1011.

(9) Yap, Y. C.; Guijt, R. M.; Dickson, T. C.; King, A. E.; Breadmore, M. C. Stainless Steel Pinholes for Fast Fabrication of High-Performance Microchip Electrophoresis Devices by CO2 Laser Ablation. *Anal. Chem.* **2013**, *85* (21), 10051–10056.

(10) Gross, B.; Lockwood, S. Y.; Spence, D. M. Recent Advances in Analytical Chemistry by 3D Printing. *Anal. Chem.* **2017**, *89* (1), 57–70.

(11) Au, A. K.; Huynh, W.; Horowitz, L. F.; Folch, A. 3D-Printed Microfluidics. *Angew. Chemie - Int. Ed.* **2016**, *55* (12), 3862–3881.

(12) Bhattacharjee, N.; Urrios, A.; Kang, S.; Folch, A. The Upcoming 3D-Printing Revolution in Microfluidics. *Lab Chip* **2016**, *16* (10), 1720–1742.

(13) He, Y.; Wu, Y.; Fu, J. Z.; Gao, Q.; Qiu, J. J. Developments of 3D Printing Microfluidics and Applications in Chemistry and Biology: A Review. *Electroanalysis* **2016**, *28* (8), 1658–1678.

(14) Bártolo, P. J. *Stereolithography*; Springer US, 2011.

(15) Snowden, M. E.; King, P. H.; Covington, J. A.; MacPherson, J. V.; Unwin, P. R. Fabrication of Versatile Channel Flow Cells for Quantitative Electroanalysis Using Prototyping. *Anal. Chem.* **2010**, *82* (8), 3124–3131.

(16) Li, M.; Li, Y. T.; Li, D. W.; Long, Y. T. Recent Developments and Applications of Screen-Printed Electrodes in Environmental Assays-A Review. *Anal. Chim. Acta* **2012**, *734*, 31–44.

(17) Li, D. W.; Li, Y. T.; Song, W.; Long, Y. T. Simultaneous Determination of Dihydroxybenzene Isomers Using Disposable Screen-Printed Electrode Modified by Multiwalled Carbon Nanotubes and Gold Nanoparticles. *Anal. Methods* **2010**, *2* (7), 837–843.

(18) Gowers, S. A. N.; Curto, V. F.; Seneci, C. A.; Wang, C.; Anastasova, S.; Vadgama, P.; Yang, G. Z.; Boutelle, M. G. 3D Printed Microfluidic Device with Integrated Biosensors for Online Analysis of Subcutaneous Human Microdialysate. *Anal. Chem.* **2015**, *87* (15), 7763–7770.

(19) Erkal, J. L.; Selimovic, A.; Gross, B. C.; Lockwood, S. Y.; Walton, E. L.; McNamara, S.; Martin, R. S.; Spence, D. M. 3D Printed Microfluidic Devices with Integrated Versatile and Reusable Electrodes. *Lab Chip* **2014**, *14* (12), 2023–2032.

(20) Bishop, G. W.; Satterwhite, J. E.; Bhakta, S.; Kadimisetty, K.; Gillette, K. M.; Chen, E.; Rusling, J. F. 3D-Printed Fluidic Devices for Nanoparticle Preparation and Flow-Injection Amperometry Using Integrated Prussian Blue Nanoparticle-Modified Electrodes. *Anal. Chem.* **2015**, *87* (10), 5437–5443.

(21) American Public Health Associetion. *Standard Methods: For the Examination of Water and Wastewater*, 22nd ed.; Washington, DC, 2012.

(22) Montes, R.; Bartrolí, J.; Céspedes, F.; Baeza, M. Towards to the Improvement of the Analytical Response in Voltammetric Sensors Based on Rigid Composites. *J. Electroanal. Chem.* **2014**, *733*, 69–76.

(23) Pol, R.; Moya, A.; Gabriel, G.; Gabriel, D.; Céspedes, F.; Baeza, M. Inkjet-Printed

Sulfide-Selective Electrode. *Anal. Chem.* **2017**, *89* (22), 12231–12236.

(24) Bakker, E.; Bühlmann, P.; Pretsch, E. Carrier-Based Ion-Selective Electrodes and Bulk Optodes. 1. General Characteristics. *Chem. Rev.* **1997**, *97* (8), 3083–3132.

(25) Cai, J.; Sessler, J. L. Neutral CH and Cationic CH Donor Groups as Anion Receptors. *Chem. Soc. Rev.* **2014**, *43* (17), 6198–6213.

(26) Hartle, M. D.; Hansen, R. J.; Tresca, B. W.; Prakel, S. S.; Zakharov, L. N.; Haley, M. M.; Pluth, M. D.; Johnson, D. W. A Synthetic Supramolecular Receptor for the Hydrosulfide Anion. *Angew. Chemie - Int. Ed.* **2016**, *55* (38), 11480–11484.

(27) Atta, N. F.; Galal, A.; Mark, H. B.; Yu, T.; Bishop, P. L. Conducting Polymer Ion Sensor Electrodes-III. Potentiometric Sulfide Ion Selective Electrode. *Talanta* **1998**, *47* (4), 987–999.

(28) Ruzicka, J.; Marshall, G. D. Sequential Injection: A New Concept for Chemical Sensors, Process Analysis and Laboratory Assays. *Anal. Chim. Acta* **1990**, *237* (C), 329–343.

(29) Calvo-López, A.; Ymbern, O.; Puyol, M.; Casalta, J. M.; Alonso-Chamarro, J. Potentiometric Analytical Microsystem Based on the Integration of a Gas-Diffusion Step for on-Line Ammonium Determination in Water Recycling Processes in Manned Space Missions. *Anal. Chim. Acta* **2015**, *874*, 26–32.

CHAPTER 7

3D-printed microfluidic platforms for sulfate quantification

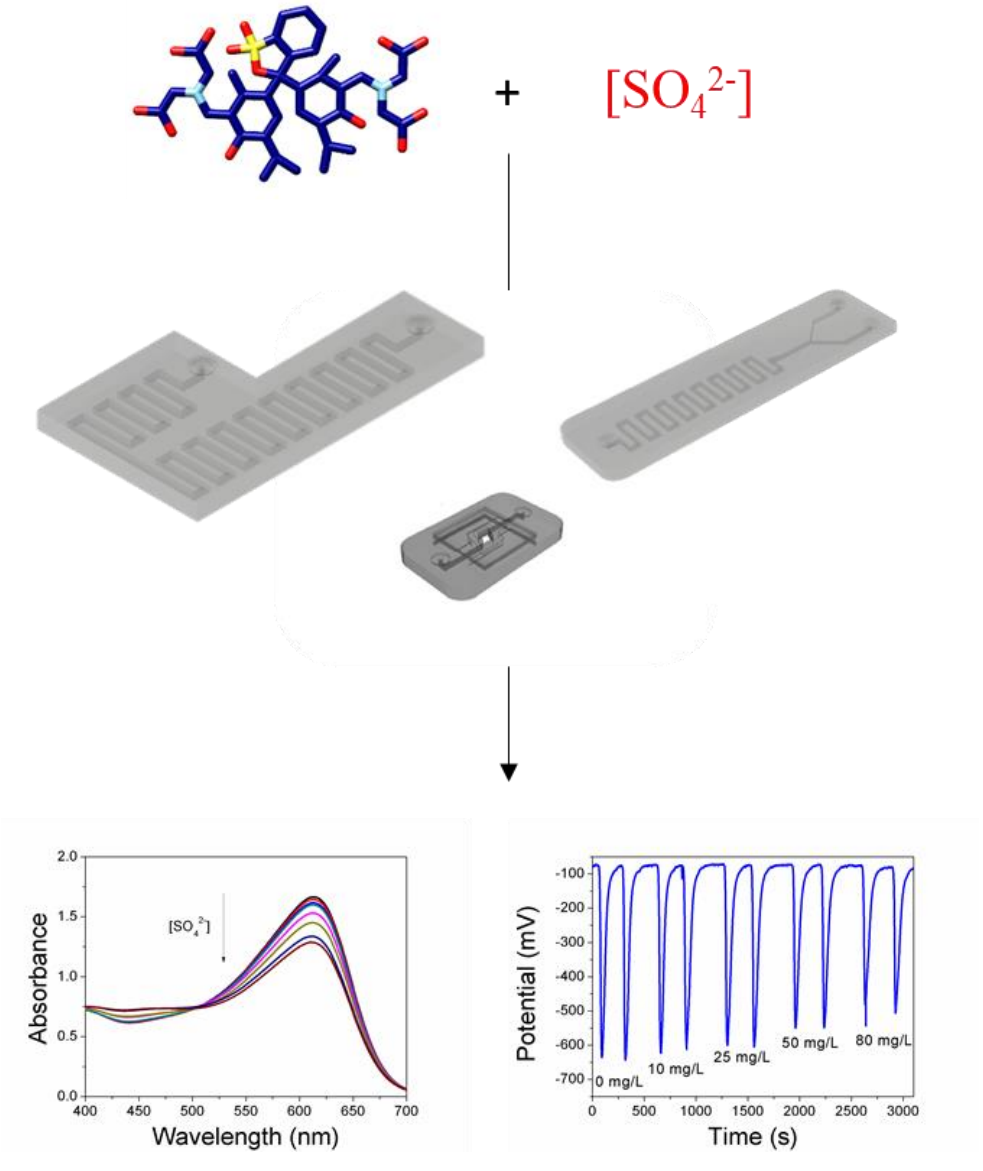

7.1. Foreword

This is by far the most challenging chapter in this PhD thesis. Two students have severely contributed to the results and almost all the experiments were performed by them (Marc Martín with his master and Ariadna Burgos with her final degree work). The chapter target analyte is sulfate ion and the analysis is performed by the old-fashion methyl thymol blue method. The analysis itself consist of a displacement of barium from a complex by its precipitation in the presence of sulfate. Although the theoretical bases of the method are apparently simple, there are too many factors in the whole analytical system to control. For instance, the position of the optical chamber in the light-emitting diode and photodetector path plays a crucial role in the potential measured and a small blow can completely change the established baseline shattering the assay.

7.2. Introduction

The presence of high sulfate ion concentrations in industrial wastewaters represents an important issue to consider as might be responsible of some environmental related problems. Sulfate-reducing microorganism are commonly used to treat high sulfate levels, producing sulfide, which is also treated to form elemental sulfur.[1,2,3] Hence, tracking the sulfate concentration before (present in the effluent of the SO_2 absorption process) and after the first biological stage gives an overall view of the conversion of part of the treatment process.

Traditionally, there have been proposed a wide variety of methodologies for sulfate ion determination such as, gravimetry, nephelometry and turbidimetry, among others.[4,5,6,7,8] Moreover, other alternative that present the best response, but present higher complexity is ionic chromatography.[9,10] However, all of them present high analysis time, high equip investment and require trained personnel. Furthermore, these methods have the disadvantage that they do not allow online monitoring. To overcome sulfate quantification challenges, the use of ion selective electrodes as user-friendly and cheaper alternative has been proposed. Many efforts have been invested to develop a liquid membrane-based sulfate-selective electrode.[11,12,13] Although the ionophores studied presented a well-defined Nernstian response, their lack of selectivity still represents a problem for sulfate ion quantification in real samples. Another methodology for sulfate determination is the methyl thymol blue method.[14,15,16] In this case, the sulfate quantification principle relied on a colorimetric change caused by the displacement of barium by its precipitation with sulfate in a barium ion-containing chromophore.[17]

Through the past decades, flow-based assays have been exploited to quantify relevant chemical in an online manner.[18] Flow-based analyses excel from their capability to integrate all the analytical stages (pretreatment, reaction and detection steps, among others) without requiring a trained personnel and its ability to automate analytical methods. Moreover, with innovative technologies the size of this analytical systems has been severely reduced decreasing response time and sample consumption. [19,20] Different materials (e.g., silicon, polymers, metals, ceramics, etc.) and fabrication techniques (e.g., micromachining, hot embossing, injection molding, laser ablation, micromilling and soft lithography) have been explored for the fabrication of miniaturized analytical systems.[21,22,23,24] However, the time and

personnel required as far as the high cost of all these methods makes them unsuitable for daily production routines. Furthermore, the fabrication process also contained several postprocessing steps (e.g., etching, sealing, etc.). Hence, the scientific community have been looking for new simple and affordable fabrication methods to produce such analytical devices with higher throughput in an automatic manner.

Three-dimensional (3D) printing has arisen as a low-cost and simple alternative to other fabrication methodologies.[25,26] 3D printing constitutes an additive manufacturing technology based on the consecutive stacking of layers.[27] The potential of producing parts of different materials makes it appealing to reach almost any required analytical application.[28] Furthermore, its versatility to modify any shape on demand makes them one of the best technologies to produce prototypes or final functional devices. Additionally, its high resolution in any axis allow 3D printing technology to fabricate extremely complex scaffolds unimaginable to be produced by other means.

Herein, the fabrication of a system of three 3D-printed microfluidic platforms for quantification of sulfate ion is described. The detection principle relies on a colorimetric change produced by the precipitation of barium sulfate due to the interaction of sulfate ion with a barium complex. A reverse flow injection analysis (rFIA) was chosen to automatize analytical method. Furthermore, common parameters involved in this kind of assay (injection volume, reaction chamber volume and flow rate) were optimized to find a suitable response to the requirements. Finally, the system was tested towards synthetic and real biotechnological samples giving demonstrating its feasibility to replace traditional quantification techniques.

7.3. Experimental section

7.3.1. Materials and chemicals

All chemicals were commercially available and were used without further purification. Barium chloride dihydrate (99%, $BaCl_2 \cdot 2H_2O$), sodium hydroxide (97%, NaOH), hydrochloric acid (37%, HCl), ethanol (96%, CH_3CH_2OH), sodium sulfate (99%, Na_2SO_4) and methylthymol blue sodium salt (98%, $C_{37}H_{40}N_2Na_4O_{13}S$) were purchased from SigmaAldrich.

All chemicals were commercially available and were used without further purification. Polylactic acid (PLA) filament (2.98 mm) was purchased from Fundació DCIM (Spain).

7.3.2. Sulfate standard and chromogenic reagent preparation

Aqueous solutions were prepared employing deionized Milli-Q water (180 MΩ·cm^{-1}). Stock solution of sulfate (1000 mg/L) was prepared by dissolving 1.481 g of Na_2SO_4 in 1 L of water. Solution used for pH modification was prepared by weighting 1.5 g of NaOH in 250 mL of water. Two separate solutions were prepared for the chromogenic reagent. First, 0.3428 g of $BaCl_2{\cdot}2H_2O$ ($5.6{\cdot}10^{-3}$ M) were dissolved in 250 mL of water. Second, methylthymol blue solution was prepared by weighting 0.1188 g of $C_{37}H_{40}N_2Na_4O_{13}S$ in 25 mL of $BaCl_2$ solution, then, 4 mL of 1 M HCl were added and 70 mL of water. Finally, ethanol was added until de the 250 mL mark. Final concentration of BaH_4MTB was $5.6{\cdot}10^{-4}$ M.

7.3.3. Spiked and real samples

Synthetic samples were prepared by adding K_2HPO_4 (200 mg·L^{-1}) and NH_4Cl (300 mg·L^{-1}) which are present in biotechnological reactors. Moreover, the study of the interference of the presence of glycerol was carried out by comparing the response of synthetic samples with (1000 mg·L^{-1}) and without glycerol. Real samples were collected from the outlet of a continuous stirred tank reactor containing sulfide-oxidizing microorganism.

7.3.4. Sensing working principle

The sensing working principle relied on a colorimetric change caused by the displacement of barium by its precipitation with sulfate in a barium ion-containing complex in acid medium and its subsequent change of pH to basic medium. The well-known methylthymol blue method is based on three consecutive reactions:

$$Ba^{2+} + H_4MTB_2^{2-} \Leftrightarrow BaH_4MTB \quad \text{(a)}$$

$$BaH_4MTB + SO_4^{2-} \rightarrow BaSO_4(s) + H_4MTB^{2-} + BaH_4MTB \quad \text{(b)}$$

$$H_4MTB^{2-} + BaH_4MTB + 8OH^- \rightarrow MTB^{6-} + BaMTB^{4-} + 8H_2O \quad \text{(c)}$$

First reaction (a) constitutes the formation of the barium complex with methylthymol blue (BaH_4MTB); complexation of barium takes place in acid media. This reaction is performed outside of the 3D-printed microfluidic platforms. The barium displacement by precipitation in the presence of sulfate (b) takes place on acid conditions and finally the pH conditioning in basic medium to be able to readout in the optimal wavelength. Stages (b) and (c) and detection step take place on microfluidic platform.

7.3.5. Microfluidic platforms fabrication

Generally, microfluidic scaffolds were designed with the 3D modeling software Fusion360. 3D models were then transformed into a printable file using slicer Cura and printed by BCN3D Sigma printer using PLA. In the case of the readout platform, two glass slides (the ones use in optical microscopy) were cut to fit the defined spot and glued with a resin. The first proof of concept was to design and build separately each of the microfluidic platforms necessary to carry out the analysis: reaction chamber, pH conditioner and measurement cell (readout). The final goal is integrating them all in a single platform.

7.3.6. Equipment

Initially, preliminary assays to determine the optimal wavelength of the light-emitting diode (LED) were conducted using a PerkinElmer (Lambda 25 model) spectrophotometer. Ion chromatography experiments were performed with conductivity detection using a Dionex ICS-2000 equipment with an IonPac AS18 column and an IonPac AG18 pre-column (ThermoScientific, USA).

7.3.7. Experimental setup

A rFIA system was chosen for its adequacy to be used for the automatization of sulfate ion analysis. In this particular case, the amount of sample is enormous and have to be diluted; therefore, rFIA system was chosen to reduce reagent waste. Figure 7.1 show the full experimental setup (reagents, fluid management, 3D-printed microfluidic platforms and data acquisition). The liquid management setup consists of an external peristaltic pump (Minipuls

3, Gilson) equipped with 1.14 mm internal diameter Tygon®tubing (Ismatec). Omnifit (1106 model) 6-way valve was used for reagent injection. Three consecutive 3D-printed microfluidic platform were used to provide the analytical reactions required in the assay. The first platform (reaction chamber) comprises a mixing path of 375 μL in which takes place reaction (b). The second platform (pH conditioner) has a volume of 300 μL in which a NaOH solution is mixed to modify the pH of the measuring solution; reaction (c). Finally, the last platform (readout) has a tear z-shaped optical chamber of 15 μL for readout purposes. Detection system was coupled to the detection platform which contained a light-emitting diode (LED orange, λ=607 nm Kingbright) with a power supply of 5 V and a Hamamatsu photodetector connected to homemade Labview software by an acquisition card NI USB-6009 (National Instruments). To simplify data acquisition, the experimental values were registered as potential and were not transformed into absorbance. Then, higher absorbance values correspond to more negative potentials and lower absorbance values with higher potentials.

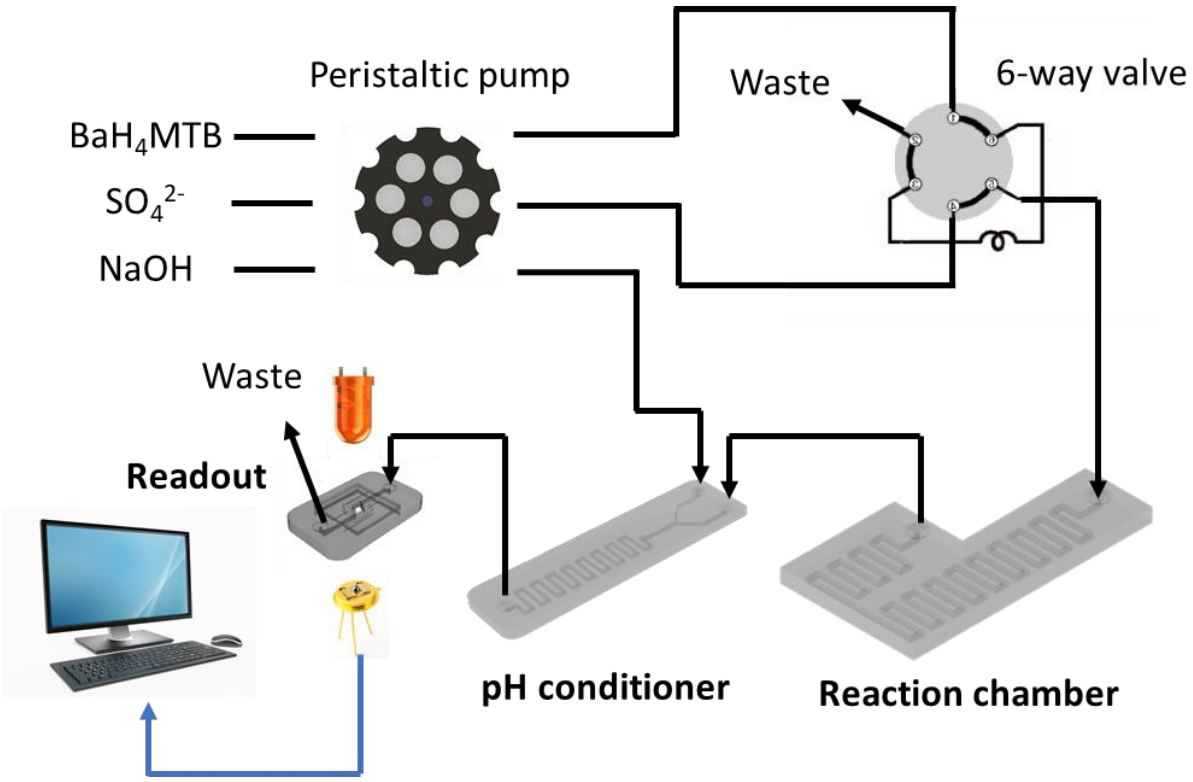

Figure 7.1. Scheme of the elements involved in the rFIA of sulfate

7.3.8. Sampling

Biotechnological samples were collected from the outlet sampling port of a 2 L upflow anaerobic sludge blanket reactor (UASB) which biologically oxidizes sulfur to sulfate and is used for treatment of a highly sulfide concentrated effluent. Samples from the reactor were filtered through a Millex 0.45 μm filter and conditioned by dilution with twice concentrated SAOB (1:1).

7.4. Results and discussion

The first step after producing the 3D-printed microfluidic platforms is to find the appropriate absorption wavelength for the assay and define the optimal LED to use. Therefore, a brief test doing a calibration with a spectrophotometer was carried out. Figure 7.2A shows the absorption spectrum of the complex with different concentrations of sulfate; elucidating that in this case a working wavelength of ~610 nm corresponding to an orange LED must be chosen.

The following step was to optimize the molar relation of $[Ba^{2+}]/[MTB^{6-}]$. This study has been used was spectrophotometer in batch conditions. Three different ratios were studied maintaining the same $[Ba^{2+}]$ ($5.6 \cdot 10^{-4}$ M) and increasing $[MTB^{6-}]$ ($5.6 \cdot 10^{-4}$ M, $1.1 \cdot 10^{-3}$ M and $2.24 \cdot 10^{-3}$ M); resulting in three relations evaluated 1:1, 1:2 and 1:4. The experiment consisted on injecting each one of the ratios in two extreme standard carriers (0 and 3000 $mg \cdot L^{-1}$) of the operational range concentrations of the reactor, to find the one that presents higher potential difference. Figure 7.2B demonstrate that the higher potential difference is achieved when using the 1:1 ratio. Therefore, 1:1 ratio will present the higher sensitivity and was chosen as the optimal.

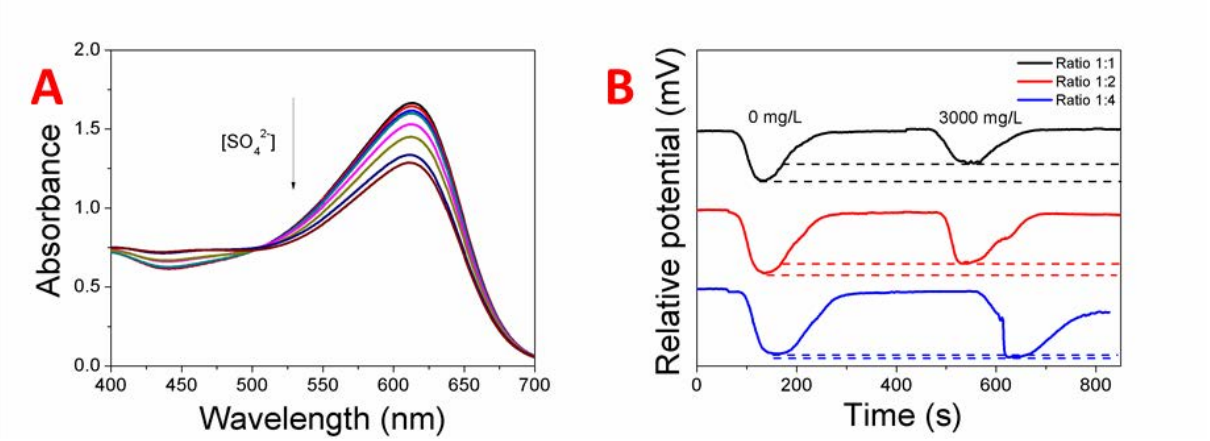

Figure 7.2. UV-Vis Absorption spectra of the chromogenic reagent produced by the presence of several sulfate ion concentrations (0, 25, 50, 100, 150, 500 and 1000 mg·L^{-1}) (A). Chromogenic reagent ratio study (1:1, 1:2 and 1:4); potential differences recorded by changing the sulfate concentration (0 and 3000 mg/L of sulfate ion).

Once the reagent ratio has been optimized, the influence of each flow assembly was studied to determine its efficiency in the reaction degree and effect in the dispersion process, and therefore the assay. Generally, injection volume, reaction chamber volume and flow rate were the features studied. The optimization method used was the univariate method. In this scenario, several initial conditions were fixed and afterwards each one was optimized until the desired sensitivity, limit of detection and linear range were achieved.

First, injection volume, which constitutes the amount of chromogenic reagent that will react with sulfate will be studied. Three different volumes were tested for this purpose (100, 150 and 200 μL). The difference in absolute value between the peak height of the 0 mg·L^{-1} (blank) and the peak height of a defined sulfate ion concentration was used as analytical signal to define the calibration plot points. Hence, the corresponding calibration plots for each injection volume are shown in Figure 7.3A. Each case presents significative differences in terms of sensitivity and linear range. The higher sensitivity was achieved in the case of an injection volume of 150 μL (considering the calibration curve was forced in all cases to the 50 mg·L^{-1} concentration point). Therefore, 150 μL was set as the optimized value for the injection volume.

The next step was to optimize the reaction chamber volume. Three different microfluidic mixers with 250, 375 and 500 μL were fabricated and tested to find the optimal one. In all cases the linear range obtained was within 10 to 80 mg·L^{-1} sulfate ion concentration. However, the 375 μL reaction chamber presented the higher sensitivity and was set as the optimal. This fact

can be explained by a compromise between reaction time and dispersion. Small reaction chambers do not let enough time to react sulfate ion with BaH_4MTB (reaction b in acid medium) whereas big reaction chambers present enough reaction time but also increases the dispersion BaH_4MTB that has not reacted with sulfate ion and therefore the signal would decreased. Hence, the optimal volume is somewhere in the middle of both situations.

To conclude the optimization, a brief study of the flowrate was carried out. Figure 7.3C shows the time trace of the injection at different flowrates (6, 8 and 10 $\mu L \cdot s^{-1}$). The slower flowrate presented higher dispersion and lower signal were obtained and highest analysis time is required, whereas the dispersion obtained at 8 and 10 $\mu L \cdot s^{-1}$ shows a higher Gaussian-like shape. Therefore, the highest flowrates were further studied by doing a calibration plot. Both flowrates presented the same results in terms of linear range and sensitivity thus 8 $\mu L \cdot s^{-1}$ was chosen to avoid more reagents waste and minimize reagent consumption.

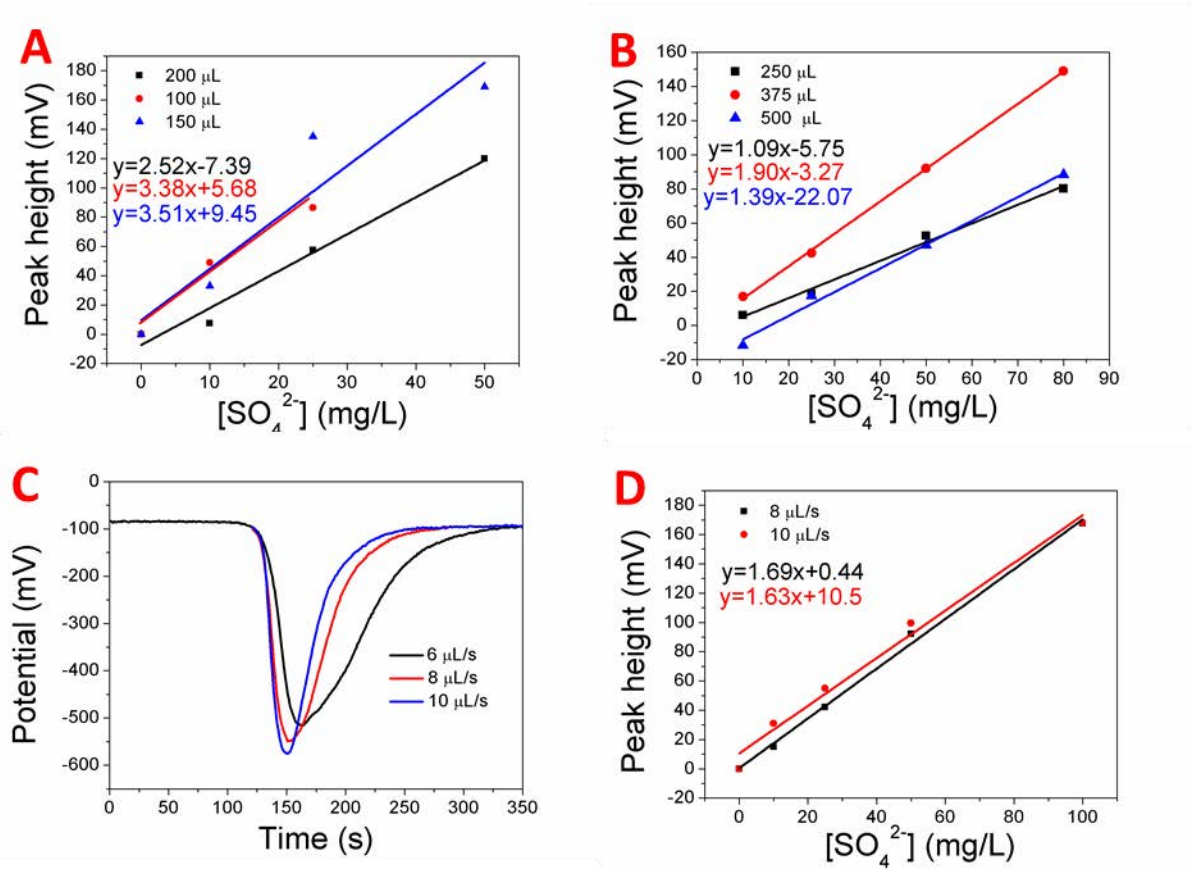

Figure 7.3. Optimization studies of the sulfate microanalyzer setup. Injection volume calibration plot obtained for 100, 150 and 200 µL (A), reaction chamber volume calibration plot obtained for 250, 375 and 500 µL (B), flowrates shape for xxx sulfate ion concentration (C) and calibration plot obtained for 8 and 10 µL/s (D).

To sum up, the optimized parameters obtained were 1:1 $[Ba^{2+}]/[MTB^{6-}]$ ratio ($5.6 \cdot 10^{-4}$ M) and for experimental operation parameters: 150 μL, 375 μL and 8 $\mu L \cdot s^{-1}$ for injection volume, reaction chamber volume and flowrate, respectively. To evaluate the final analytical features a calibration plot has been done under optimal conditions. Figure 7.4A shows an example of the potential recorded by the system demonstrating the well-defined peaks obtained. Additionally, reproducibility (in different days) and repeatability (in same day) were measured to validate the analytical system. Repeatability was measured in terms of repeating the calibration curve during 5 consecutive days for n=2 measurements for each sulfate ion concentration analyze in a day and ensure a low standard deviation of each one of the concentrations points of the plot. This calibration (Figure 7.4B) exhibits a linear range of 10-80 $mg \cdot L^{-1}$ a sensitivity of 1.76 $mV \cdot L \cdot mg^{-1}$ and a limit of detection of 8 $mg \cdot L^{-1}$. On the other hand, repeatability studies were performed by pumping 50 and 80 $mg \cdot L^{-1}$ of sulfate 5 consecutive times demonstrating the high repeatability of the system (Figure 7.4C).

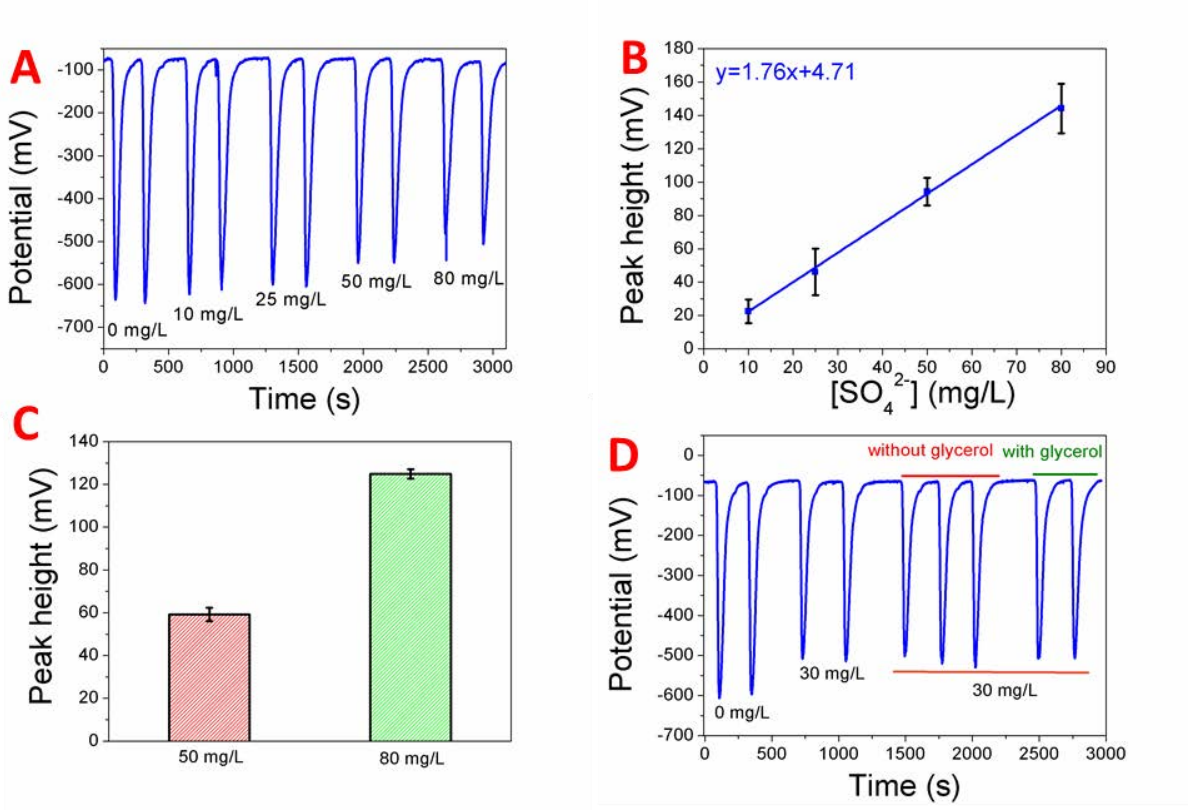

Figure 7.4. Potential record measured during a calibration (n=2; A), calibration plot obtained during by repeating the assay during 5 consecutive days (B) (n=2) repeatability study at two concentrations (n=5; C) and the study of the presence of glycerol in synthetic samples (D).

In conclusion, the 3D-printed systems were successfully fabricated, and the setup parameters were well-defined. The performance of the sulfate ion analyzer was tested towards real

samples. Two approaches of experiments were carried out to test its analytical performance. The first one was to use synthetic samples containing 200 $mg \cdot L^{-1}$ K_2HPO_4 and 300 $mg \cdot L^{-1}NH_4Cl$ with (1000 $mg \cdot L^{-1}$) and without glycerol as biotechnological reactor samples because glycerol is C source from biomass, example in Figure 7.4D. Results showed that significant recovery rates of 80-101% were achieved (Table 7.1). Moreover, it was demonstrated that there is no clear effect or trend when glycerol is present in the matrix. The second approach was to directly measure real samples extracted from a UASB reactor and compare the results with ionic chromatography. Results showed that the sulfate ion concentrations of each sample found with both methods did not differ significantly at a confidence level of 95% (details in statistics section). Overall, the developed 3D-printed sulfate microanalyzer demonstrated the potential to be used alternatively to the standard methodology of measuring sulfate ion (ionic chromatography) in a cheaper manner.

Table 7.1. Spiked synthetic samples analyses. Study of the potential interferences of glycerol.

	Without glycerol		**With glycerol**	
Spiked concentration ($mg \cdot L^{-1}$)	**Mean concentration of 3 measures ($mg \cdot L^{-1}$)**	**Recovery rate (%)**	**Mean concentration of 3 measures ($mg \cdot L^{-1}$)**	**Recovery rate (%)**
10	8.8±0.4	88%	8.0±0.2	80%
30	29±1	95%	30.3±0.2	101%

Table 7.2. UASB reactor samples. Comparison between the sulfate ion concentrations obtained with the ionic chromatography and the proposed 3D-printed system.

	Ionic chromatography	**3D-printed system**	
Sample	**Concentration obtained ($mg \cdot L^{-1}$)**	**Mean concentration of 5 measures ($mg \cdot L^{-1}$)**	**Standard deviation ($mg \cdot L^{-1}$)**
Reactor 1	108	109	±3
Reactor 2	143	146	±3
Reactor 3	182	184	±6
Reactor 4	208	209	±8
Reactor 5	104	104	±3

7.5. Statistics

Comparison of the performance of the 3D-printed sulfate analyzer against ionic chromatography was done following the procedure described in Quantitative Chemical Analysis, Daniel C. Harris, W. H. Free man and Company, California (2009). This comparison experiment was done measuring sulfate ion in diverse samples (n=5), by triplicate. Then, the mean value and the standard deviations are calculated and compared with a standard value given with no standard deviation by a standard technique.

Thus, calculate the mean value and add and subtract the confidence interval (Table 7.3).

If the mean standard value lies between both calculated values your method does not differ significantly from the method used to get the mean standard value.

Table 7.3. Comparison of the ion chromatography value with the experimental range obtained.

Ion chromatography value ($mg \cdot L^{-1}$)	**Experimental range ($mg \cdot L^{-1}$)**
108	106-112
143	143-149
182	178-190
208	201-217
104	101-107

In all cases, it is demonstrated that there are no significantly differences in sulfate concentration obtained by both methods.

7.6. Conclusions

A set of 3D-printed microfluidic platforms with integrated optical detection of sulfate by rFIA have been fabricated. The detection working principle relies on the well-known methyl thymol blue method, which consist of the displacement of barium from a chromophore by its precipitation in the presence of sulfate. Moreover, relevant parameters such as, $[Ba^{2+}]/[MTB^{6-}]$ ratio, injection volume, reaction chamber volume and flowrate were optimized achieving a linear range of 10-80 $mg \cdot L^{-1}$ sulfate ion concentration, a sensitivity of 1.76 $mV \cdot L \cdot mg^{-1}$ and a limit of detection of 8 $mg \cdot L^{-1}$. Finally, the sulfate microanalyzer was tested towards synthetic samples spiked with glycerol and real samples coming from a UASB reactor and the result showed no significant differences with the standard sulfate ion quantification technique (ionic chromatography). The combination of the described platforms has become a huge step towards the autonomous tracking of sulfate in biotechonological reactors replacing more expensive quantification methodologies and personnel.

Finally, once the viability of the proposed analyzer has been demonstrated two challenges could be proposed as future works. On the one hand integrate the 3 independent platforms into a single one. On the other hand, carry out an exhaustive study of possible interferences present in the samples with different complex matrices to analyze.

7.7. References

(1) Blázquez, E.; Gabriel, D.; Baeza, J. A.; Guisasola, A. Evaluation of Key Parameters on Simultaneous Sulfate Reduction and Sulfide Oxidation in an Autotrophic Biocathode. *Water Res*. **2017**, *123*, 301–310.

(2) Muyzer, G.; Stams, A. J. M. The Ecology and Biotechnology of Sulphate-Reducing Bacteria. *Nat. Rev. Microbiol*. **2008**, *6* (6), 441–454.

(3) Liamleam, W.; Annachhatre, A. P. Electron Donors for Biological Sulfate Reduction. *Biotechnol. Adv*. **2007**, *25* (5), 452–463.

(4) Fritz, J. S.; Freeland, M. Q. Direct Titrimetric Determination of Sulfate. *Anal. Chem*. **1954**, *26* (10), 1593–1595.

(5) Sörbo, B. Sulfate: Turbidimetric and Nephelometric Methods. *Methods Enzymol*. **1987**, *143* (1966), 3–6.

(6) Nor, A. S. M.; Faramarzi, M.; Yunus, M. A. M.; Ibrahim, S. Nitrate and Sulfate Estimations in Water Sources Using a Planar Electromagnetic Sensor Array and Artificial Neural Network Method. *IEEE Sens. J*. **2015**, *15* (1), 497–504.

(7) Rull-Barrull, J.; D'Halluin, M.; Le Grognec, E.; Felpin, F. X. Chemically-Modified Cellulose Paper as Smart Sensor Device for Colorimetric and Optical Detection of Hydrogen Sulfate in Water. *Chem. Commun*. **2016**, *52* (12), 2525–2528.

(8) Zhao, D.; Chen, C.; Lu, L.; Yang, F.; Yang, X. A Label-Free Colorimetric Sensor for Sulfate Based on the Inhibition of Peroxidase-like Activity of Cysteamine-Modified Gold Nanoparticles. *Sensors Actuators, B Chem*. **2015**, *215*, 437–444.

(9) Mulik, J.; Puckett, R.; Williams, D.; Sawicki, E. Ion Chromatographic Analysis Of Sulfate And Nitrate In Ambient Aerosols. *Anal. Lett*. **1976**, *9* (7), 653–663.

(10) Conboy, J. J.; Henion, J. D.; Martin, M. W.; Zweigenbaum, J. A. Ion Chromatography/Mass Spectrometry for the Determination of Organic Ammonium and Sulfate Compounds. *Anal. Chem*. **1990**, *62* (8), 800–807.

(11) Ganjali, M. R.; Shirvani-Arani, S.; Nourozi, P.; Salimzadeh, D.; Faal-Rastegar, M.; Moghimi, A. A Novel Sulfate Polymeric Membrane Sensor Based on a New Bis-Pyrylium Derivative. *Electroanalysis* **2004**, *16* (12), 1009–1013.

(12) Morigi, M.; Scavetta, E.; Berrettoni, M.; Giorgetti, M.; Tonelli, D. Sulfate-Selective Electrodes Based on Hydrotalcites. *Anal. Chim. Acta* **2001**, *439* (2), 265–272.

(13) Lomako, S. V.; Astapovich, R. I.; Nozdrin-Plotnitskaya, O. V.; Pavlova, T. E.; Lei, S.; Nazarov, V. A.; Okaev, E. B.; Rakhman'ko, E. M.; Egorov, V. V. Sulfate-Selective

Electrode and Its Application for Sulfate Determination in Aqueous Solutions. *Anal. Chim. Acta* **2006**, *562* (2), 216–222.

(14) Colovos, G.; Panesar, M. R.; Parry, E. P. Linearizing the Calibration Curve in Determination of Sulfate by the Methylthymol Blue Method. *Anal. Chem.* **1976**, *48* (12), 1693–1696.

(15) Adamski, J. M.; Villard, S. P. Application of the Methylthymol Blue Sulfate Method to Water and Wastewater Analysis. *Anal. Chem.* **1975**, *47* (7), 1191–1194.

(16) Madsen, B. C.; Murphy, R. J. Flow Injection and Photometric Determination of Sulfate in Rainwater with Methylthymol Blue. *Anal. Chem.* **1981**, *53* (12), 1924–1926.

(17) *Standard Methods for the Examination of Water and Wastewater*; American Water Works Association, Ed.; Washington DC, 1999.

(18) Rechberger, P. H. B. and H. *Practical Handbook of Material Flow Analysis*; Ecomed: Florida, 2004.

(19) Pol, R.; Céspedes, F.; Gabriel, D.; Baeza, M. Microfluidic Lab-on-a-Chip Platforms for Environmental Monitoring. *TrAC - Trends Anal. Chem.* **2017**, *95*, 62–68.

(20) Nge, P. N.; Rogers, C. I.; Woolley, A. T. Advances in Microfluidic Materials, Functions, Integration, and Applications. *Chem. Rev.* **2013**, *113* (4), 2550–2583.

(21) Koesdjojo, M. T.; Tennico, Y. H.; Remcho, V. T. Fabrication of a Microfluidic System for Capillary Electrophoresis Using a Two-Stage Embossing Technique and Solvent Welding on Poly(Methyl Methacrylate) with Water as a Sacrificial Layer. *Anal. Chem.* **2008**, *80* (7), 2311–2318.

(22) Geissler, M.; Roy, E.; Diaz-Quijada, G. A.; Galas, J. C.; Veres, T. Microfluidic Patterning of Miniaturized DNA Arrays on Plastic Substrates. *ACS Appl. Mater. Interfaces* **2009**, *1* (7), 1387–1395.

(23) Baeza, M.; López, C.; Alonso, J.; López-Santín, J.; Álvaro, G. Ceramic Microsystem Incorporating a Microreactor with Immobilized Biocatalyst for Enzymatic Spectrophotometric Assays. *Anal. Chem.* **2010**, *82* (3), 1006–1011.

(24) Yap, Y. C.; Guijt, R. M.; Dickson, T. C.; King, A. E.; Breadmore, M. C. Stainless Steel Pinholes for Fast Fabrication of High-Performance Microchip Electrophoresis Devices by CO2 Laser Ablation. *Anal. Chem.* **2013**, *85* (21), 10051–10056.

(25) Gross, B.; Lockwood, S. Y.; Spence, D. M. Recent Advances in Analytical Chemistry by 3D Printing. *Anal. Chem.* **2017**, *89* (1), 57–70.

(26) Au, A. K.; Huynh, W.; Horowitz, L. F.; Folch, A. 3D-Printed Microfluidics. *Angew. Chemie - Int. Ed.* **2016**, *55* (12), 3862–3881.

(27) Bhattacharjee, N.; Urrios, A.; Kang, S.; Folch, A. The Upcoming 3D-Printing Revolution in Microfluidics. *Lab Chip* **2016**, *16* (10), 1720–1742.

(28) He, Y.; Wu, Y.; Fu, J. Z.; Gao, Q.; Qiu, J. J. Developments of 3D Printing Microfluidics and Applications in Chemistry and Biology: A Review. *Electroanalysis* **2016**, *28* (8), 1658–1678.

CHAPTER 8

Versatile 3D-printed platform for nitrite ion analyses using a smartphone

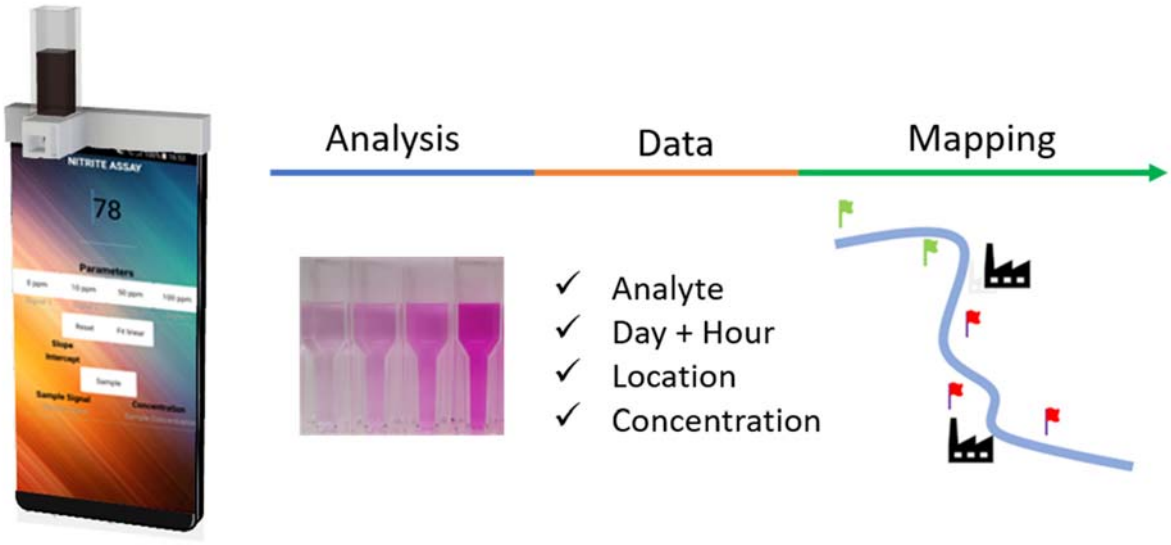

8.1. Foreword

On the last stages of this PhD thesis a new project, which intended to provide biotechnological reactor for waste water treatment; involving the well-known nitrogen cycle species started. Therefore, the tracking of ammonia, nitrite and nitrate ions became also and important task to complete by the analytical point of view. Considering that the Griess-Ilosvay reaction is the basis of the diverse standard methods for nitrite ion quantification in multiple cases and the research group experience, we recovered that previous applications and did a brainstorm. Nowadays, is common to produce sensors or sensing platforms that take advantage of smartphones and with the availability of a 3D printer, a scaffold that could help with nitrite ion quantification might be easy to develop. Moreover, with a little effort and patience, the programming skills required to develop a smartphone application were also achieved. The first experiments to test the analytical behavior and the comparison with a colorimeter were done by the undergraduate student Laura Diez during her summer stay.

8.2. Introduction

Nitrogen is a crucial element present in several chemical states in many freshwater and marine ecosystems.[1,2] Nitrogen presence in its different forms is controlled by the well-known nitrogen cycle, which spreads nitrogen among air and water to achieve an equilibrium. However, the anthropogenic activities such as the use of industrial fertilizers, automotive emissions, industrial production and waste water have dramatically contributed to the disruption of the nitrogen cycle.[3,4] Nitrite ion constitutes an intermediate in the oxidation of ammonia ion to nitrate ion becoming the most toxic nitrogen specie soluble in water.[5,6] Nitrite ion converts haemoglobin to methemoglobin (changes iron oxidation state), which is unable to bind oxygen causing aquatic organism to suffer hypoxia and perish.[7] Moreover, organism decomposition lead to an increase of nitrate causing eutrophication (i.e. overgrowth of bacteria and algae caused by an increment of nutrients). This fact is aggravated by the addition of nitrate ion (from fertilizers) causing extra growth of aquatic organism reducing the dissolved oxygen in water and finally extinguishing the ecosystem.

Production of hand-held and accurate sensing platform to constantly determine the concentration of such potential contaminants (*e.g.* nitrate and phosphate ions) has become a global concern. Scientist have been developing strategies for determination of nitrogen-based compound for the past 30 years. In the case of nitrite ion, the most common analysis performed to determine its concentrations is the well-known Griess-Ilosvay reaction. This prompt reaction takes place in two different consecutive steps. First, a formation of a diazonium salt in the presence of nitrite in acid media. Then, the diazonium salt and *N*-(1-Naphthyl)ethylenediamine dihydrochloride are coupled forming the chromogenic prove (azo dye formed) which presents a strong pink coloration. Other optical alternatives have also been developed by the scientific community. For instance, Wang et. al. [8] developed a spectrofluorometric method to determine nitrite in food. Another optical approach was reported by Li et. al.[9] in which nitrite was used as optical quencher of a rhodamine-decorated magnetic silica nanoparticle. On the other hand, electrochemical sensors have also been proposed. Mehmeti et. al.[10] developed an amperometric sensor for nitrite determination based on nanoribbons whereas Mani et. al.[11] developed another amperometric sensor based on reduced graphene oxide. Other proposed electrochemical alternatives are the use of nanoparticles as electrocatalyst.[12] Although many efforts have been

invested on finding novel approaches for nitrite ion quantification, the traditional optical-based Griess-Ilosvay method still remains as the worldwide standard.

Traditionally, optical measurements were carried out in laboratory facilities using bulky and expensive equipment such as spectrophotometers or colorimeters. With the recent miniaturization revolution and the incredible improvement in electronics, the laboratory equipment has been reduced drastically. Nowadays, several hand-held spectrophotometers/colorimeters can be purchased in the most common online websites at a relative low cost. Nonetheless, the trend nowadays is to substitute any laboratory equipment for a smartphone. Smartphone are not only available in everyone's pocket but also give a lot of versatility. For instance, with the required knowledge they can be adjusted to perform optical and even electrochemical measurements. Moreover, their tremendous features allow them to integrate several analytical steps, such as data acquisition, data treatment and data transfer allowing them to substitute the commonly required trained person. In the past few years scientists have widely exploited smartphones for many diverse analytical applications.[13,14,15] In most of the cases the smartphone devices work taking a picture with the camera and use a complex graphic design software (build up into a smartphone application) to determine the standard or sample concentration or carry out other kind of determination.[16,17,18,19] As an example, Berg et. al.[20] created a hand-held microplate reader to be used for enzyme-linked immunosorbent assays. Another interesting system was developed by Oncescu et. al. which constitutes a point-of-care system for determination of cholesterol at home.

Although the majority of sensor development that use a smartphone as readout are based on the camera, now few works have changed the trend to the use of the ambient light sensor (ALS) of the smartphone.[21] ALS is located at the top front corner of the smartphones and is commonly used to optimize the energy consumption (modifying the screen brightness depending on light intensity received). This integrated sensor presents a resemblance with the human eye with a spectrophotometric response ranging from 350 to 650 nm, making it perfect for coloured-based assays.[22] Moreover, as it can be set to constantly record light, it opens a brand new interesting potential application for monitoring purposes overcoming the smartphone camera-based sensors.

Herein, the ALS sensor was exploited to be used for the quantification of nitrite ion in real samples. Griess-Ilosvay reaction was chosen for its simplicity as the standard method for nitrite ion determination. First, prior analyses were conducted to determine the optimal absorption pattern of the azo dye formed between nitrite ion and the chromogenic reagent and chose the specific light-emitting diode (LED). Then, the response behavior of the ALS was studied, and a smartphone application was developed in concordance. The application allows to determine different analytes concentration and was developed to work in two different conditions; benchtop and field analyses. Moreover, is able to send automatically all the data recorded to an online database improving tracking the analyses later on. Finally, the potential of this methodology for nitrite ion quantification by optical readout was tested with real samples in both condition and compared to the standard analysis methods.

8.3. Experimental section

8.3.1. Materials and chemicals

All chemicals were commercially available and were used without further purification. Phosphoric acid (98%, H_3PO_4), sulfanilamide (99%, $H_2NC_6H_4SO_2NH_2$), N-(1-Naphthyl)ethylenediamine dihydrochloride (98%, $C_{10}H_7NHCH_2CH_2NH_2 \cdot 2HCl$), potassium chloride (99%, KCl), calcium chloride di-hydrate (99%, $Ca_2Cl \cdot 2H_2O$), sodium nitrate (99%, $NaNO_3$) and sodium sulphate (99%, Na_2SO_4) were purchased from SigmaAldrich. Potassium nitrite (98 %, KNO_2) was purchased from Fluka. Polylac-tic acid (PLA) filament (2.98 mm) was purchased from Fundació DCIM.

8.3.2. Standard solutions preparation

Stock solution of potassium nitrite was prepared by dissolving 1.85 g/L in water (resulting in 1000 mg/L of nitrite ion). Standards were prepared by subsequent dilution of the stock to fit the required concentrations. Colorimetric probe for the determination of nitrite (Griess-Ilosvay reagent) was prepared by dissolving 0.25 g of N-(1-Naphthyl)ethylenediamine dihydrochloride and 2.5 g of sulfanilamide in 25 mL of phosphoric acid and finally add water until 250 mL mark.[23] All solutions were prepared using deionized Milli-Q water (18.0 $M\Omega \cdot cm^{-1}$).

8.3.3. Sensing principle and procedure

Determination of nitrite was performed following the well-known Griess-Ilosvay reaction (Figure 9.1A). First, a formation of a diazonium salt in the presence of nitrite and sulfanilamide takes place in acid medium. Then, the diazonium salt and N-(1-Naphthyl)ethylenediamine dihydrochloride are coupled forming a strong pink solution in acid medium.

Determination of nitrite ion in standards and real samples was conducted as follow. First, 1 mL of standards or samples was diluted with 1 mL of water inside a 3 mL conventional spectroscopy plastic cuvette. Second, 100 μL of the Griess-Ilosvay reagent was added and the solution was hand-stirred for 30 s. Finally, the standard or sample was inserted in the readout cavity after reaction step. To make liquid management accessible to non-trained personnel a commercially available fixed volume small-sized micropipettes were searched.[24]

8.3.4. Equipment used for analysis

Initial assays to determine the optimal wavelength of dye absorption were conducted using a PerkinElmer (Lambda 25 model) spectrophotometer. Samsung S8 (TMD4906, AMS AG company ALS sensor) was chosen as the standard smartphone for all the measurements regarding the 3D-printed proposed readout system. A Pharmacia LKB (Novaspec II model) colorimeter was used to compare the benchtop responses of the analyzed samples. Disposable spectrophotometric cuvettes of polystyrene (12.5 x 12.5 x 45 mm, BRAND GMBH) were used for all the colorimetric assays. Green LED of wavelength 525 nm was used as a soured light. An adapted charger working at 3 V and a 3 V lithium button cell battery were used as power supply for the LED for benchtop and field analyses, respectively. For real biotechnological samples ion chromatography was used as standard method. Ion chromatography experiments were performed with conductivity detection using a Dionex ICS-2000 equipment with an IonPac AS18 column and an IonPac AG18 pre-column (ThermoScientific, USA).

8.3.5. 3D-printed readout printing settings, scaffold design and colorimetric read explanation

3D-printed readout scaffold was designed with the 3D modeling software Fusion360. 3D model was then transformed into a printable file using slicer Cura and printed by BCN3D Sigma printer using PLA.

The design of the 3D-printed readout scaffold was performed to keep it as simple as possible (Figure 8.1B). Several designed cavities were placed to contain all the required elements to perform the assay. In terms of light emission, two cavities were design. The first one that perfectly fits a common light-emitting diode and the second one was thought to contain a 3 V lithium button cell battery. For the sample cavity, a standard hole for common spectrophotometric cuvettes was chosen. Finally, the last cavity was optimized to fit the smartphone. Is worth saying that each one of these spots can be easily modified to include different light and battery sources, sample containers and smartphones, which makes this technology appealing for this kind of prototyping purposes.

To determine the concentration of nitrite ion, the 3D-printed scaffold includes a straightforward pathway to allow light emission-sample-detector interactions (Figure 8.1C) alike spectrophotometers. In this case, the light emission is constituted by a green LED which emits in the monochromatic wavelength required in nitrite assay. On the other hand, the detector is the ALS placed on the top side of the smartphone which is commonly used to modify the brightness of the screen depending on the light conditions. The determination working principle will rely on the attenuation of a monochromatic light beam once travels across the defined sample pathlength (Beer-Lambert law).

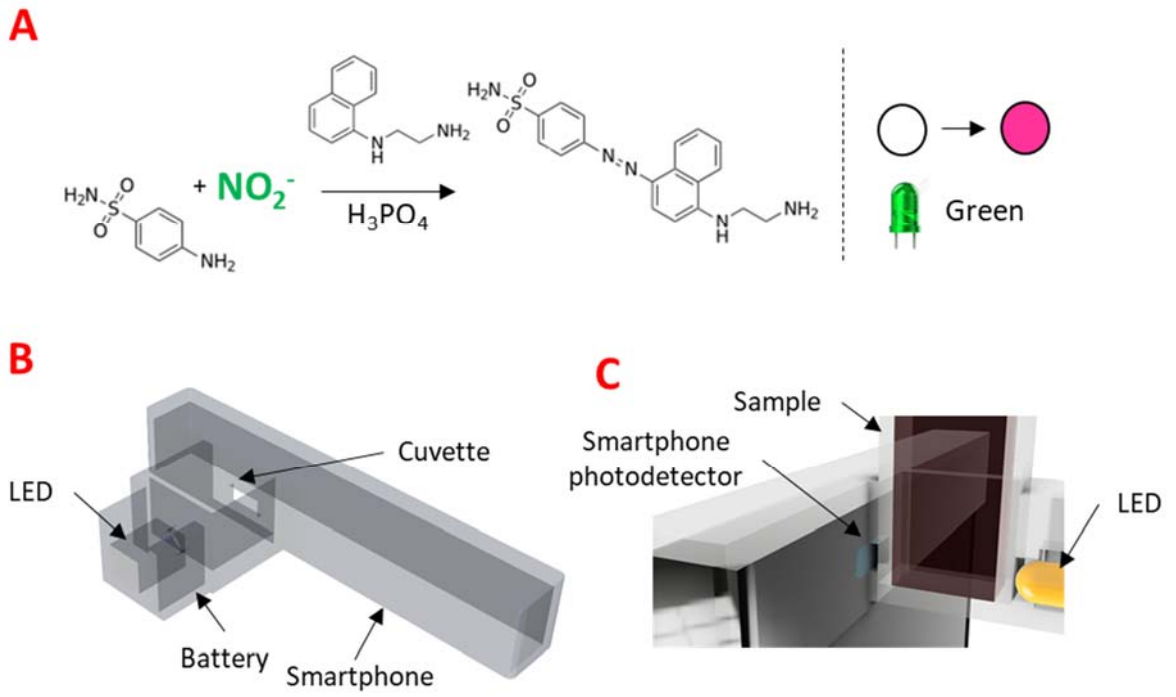

Figure 8.1. Schemes of the Griess-Ilosvay reaction used for nitrite ion quantification (A), 3D-printed readout scaffold (B), light emission source-sample-detector (C).

8.3.6. ALSens app development for Android

A smartphone application (app) named "ALSens" was developed to optimize the quantification of nitrite ion in different biotechnological/environmental samples. The app was developed with the help of a free cloud-based online platform (AppyBuilder) which allows the developing of mobile apps with almost no programming knowledge.[25] ALSens app was designed to be used for any kind of colorimetric assay. The flowchart of ALSens is showed in Figure 8.2. To begin with, the first display that is shown is to determine the target analyte that is going to be used (Figure 8.2A) and by pressing the selected molecule a new screen pops-up. As the application was designed to be used in any required situation, this new screen (Figure 8.2B) allows to choose the two most common situations.

In the case of working in benchtop conditions (working in a daily routine quality control alike lab) a new screen will appear with the following sections (Figure 8.2C, from top to bottom): At the top of the screen the analyte being assessed will be displayed followed by a "Sample" ID textbox which helps tracking the analysis later. A big number in the middle of the

screen displays online the light intensity (in lux units). Four different buttons with the standard concentration are used to define each one of the points of the calibration curve which their corresponding light intensity will be displayed in the textbox underneath. Each one of the points can be redone by pressing again or reset everyone pressing “Reset” button. Once the standard light intensities are set the slope and the intercept will appear after clicking in “Fit linear”. Furthermore, a notification will appear if the “Sample ID” textbox is empty to remind the user to fill it. Finally, by placing the sample and pushing “Sample” button the sample signal and the analyte concentration will be displaced, and the information will be sent to an online database.

In the case of working in field conditions (doing measurements outside of a laboratory facility) a new screen will appear with the following sections (Figure 8.2D, from top to bottom): Once again at the top of the screen the analyte being assessed will be displayed and a big number in the middle of the screen displays online the light intensity. In field analyses as they are done in uncomfortable conditions (there will be no table, chair and less equipment available) only two different buttons with the standard concentration are used to define each one of the points of the calibration curve with their corresponding intensities. Also, each one of the points can be redone by pressing again or reset everyone pressing “Reset” button. Once the two-point standard light intensities are set, the slope and the intercept will appear after clicking in “Fit linear”. Upon selecting “Fit linear” one or two notifications will appear. The first notification which will always appear, is a bare reminder to turn on location on the device. The second notification will only appear if the slope and the intercept are higher/lower than 3-fold their standard deviation. Finally, the sample signal and the analyte concentration will be displaced after pushing “Sample” button, and the information will be sent to an online database.

So far, the flowchart in the smartphone device has been shown. Interestingly, with this app, once the assay is finished, all the data is sent it to an online database (google drive excel fusion table) that can be accessible and/or editable by chosen users. This not only helps the transfer and sharing of information but also eliminates some possible human errors (e.g. mistakes in sample interpolation). Depending on the situation chosen (benchtop or field) different relevant parameters will be send to the database (Figure 8.2E).

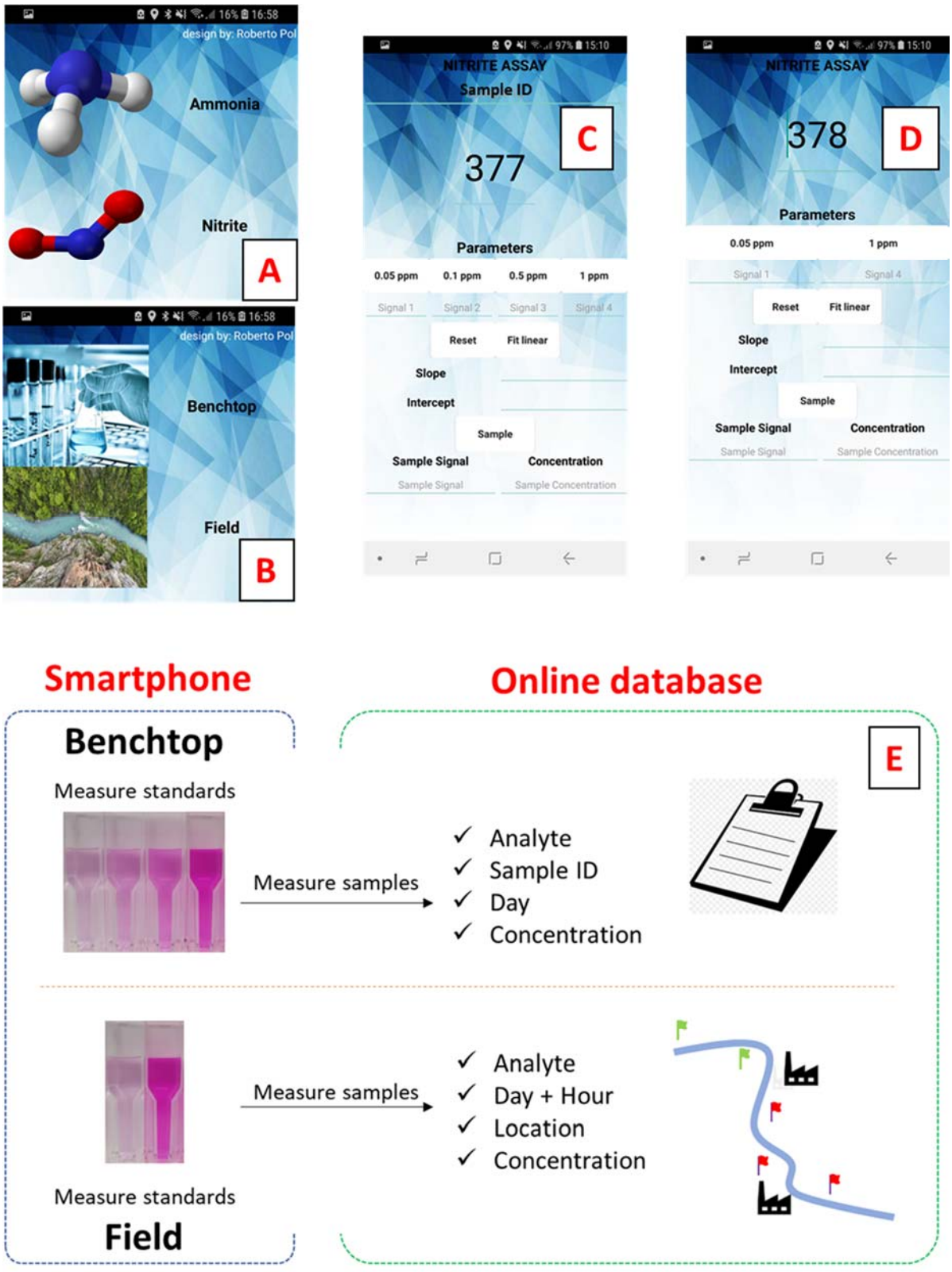

Figure 8.2. Smartphone application workflow (A-D): analyte selection (A), analysis condition (B) and calibration displays of benchtop and field analyses (C and D, respectively). Scheme describing the flowchart used by the application and information sent to the online database.

Is worth noting that to be able to setup the final workflow analyses of different analytes in the app, a prior study finding the optimal conditions (linear range and detection limit) must always be done first.

8.3.7. Sampling, spiking and determination in real samples.

River and sea water samples for benchtop analyses were collected following ISO 5667-6:2014 and ISO 5667-9:1992, respectively. Subsequently, both solutions were spiked with the same amount of NO_2^- (~2 ppm NO_2^-). Real samples were collected from a discontinuous stirred tank reactor studying a nitrification process.

8.4. Results and discussion

The first step after producing the 3D-printed readout scaffold is finding the required LED for the assay. Therefore, prior to start using the smartphone, a spectrophotometer must be used to find the absorption wavelength of the azo dye. Figure 8.3 shows the absorption spectrum of the azo dye for different concentrations of nitrite ion; elucidating that in this particular case a working wavelength of ~ 540 nm corresponding to a green LED have to be chosen.

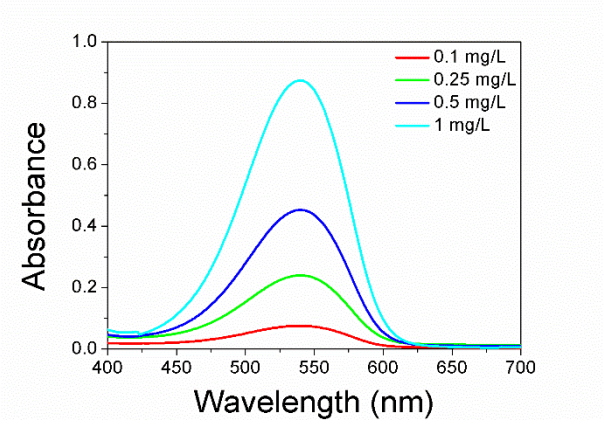

Figure 8.3. Absorption spectrum of the azo dye produced by several nitrite ion concentrations in the presence of the chromogenic reagent.

Understanding the working principle of the ALS sensors that are contained within the smartphones is the following step. Common spectrophotometers/colorimeters work measuring the differences of light transmitted (between a spectrophotometric blank and samples) that goes through a define pathway and giving a final value (commonly, absorbance). ALS sensor is

based on a light dependent resistor which works following the principle of photoconductivity. Photoconductivity is an optical phenomenon in which the material resistivity is reduced when light is absorbed by the material.[26] In the presence of light, electrons of the valence band jump to the conduction band increasing the number of charge carriers and therefore, decreasing the resistivity (Figure 8.4). The light intensity is expressed by the smartphone in lux units, which has an exponential-like proportion to the resistivity.[27]

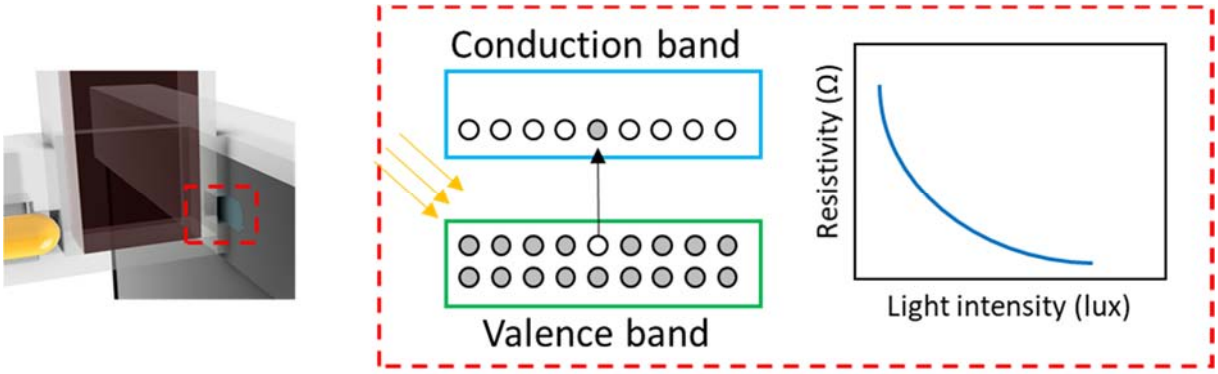

Figure 8.4. Schematic representation of the behavior of a photoconductive material and the relation between resistivity and light intensity measured in lux.

Considering the behavior of ALS sensor, the analytical response was studied to find the optimal mathematical transformation required to produce a calibration curve. Preliminary studies confirmed the exponential-like trend of the calibration (Figure 8.5A) therefore, the logarithm of the light intensity was chosen as the mathematical transformation to finally get a linear calibration curve (Figure 8.5B, n=3). The measuring system finally gave a linear response range of 0.05-1 mg/L exhibiting a sensitivity of -0.40±0.01 mg/L between 0.05 and 1.5 mg/L with a limit of detection of 0.01 mg/L (calculated by its definition)[28] and a square correlation coefficient of 0.9929. After this study, the application was then adapted to be used with four or two standards depending on the requirements of the assay and an equation (Equation 8.1) was set for the direct estimation of nitrite:

$$[\boldsymbol{NO_2^-}] = \frac{\boldsymbol{log(light\ intensity) - Intercept}}{\boldsymbol{-Slope}} \qquad \text{(Equation 8.1)}$$

In addition, interferences test was carried out using the most common present ions (K^+, Na^+, Ca^{2+}, Cl^-, NO_3^- and SO_4^{2-}) in environmental samples. Several ionic salts were directly added in high concentration (100 mg/L) and the response was measured. Result showed that no relevant

change in the response (higher than 3-folds the standard deviation of the blank) was found when the aforementioned ions are present (Figure 8.5C).

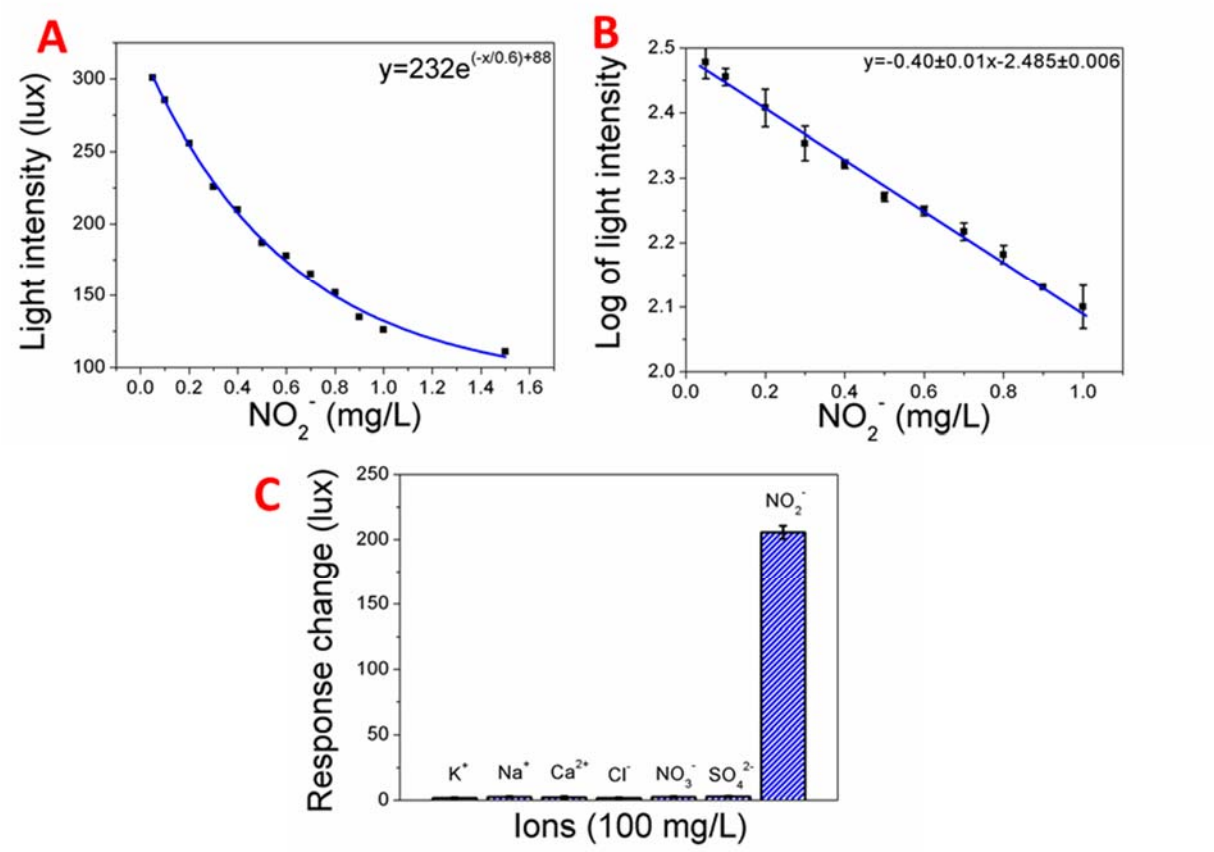

Figure 8.5. Direct nitrite calibration with the smartphone system (A). Calibration plot obtained using the smartphone (after the mathematical transformation, B) for nitrite (n=3) and interferences study of the most common ions found in environmental samples (C).

Taking advantage of the use of cuvettes as sample holder, the same cuvettes were also placed in a commercial colorimeter to test the differences between the readout of both devices. The only relevant difference between both readout systems is in terms of sensitivity in which the colorimeter presented 2-folds the sensitivity of the smartphone (Figure 8.6). Overall, considering that smartphones are present in routinely life, are available to everyone and the application allows data tracking and transfer, their potential usage excels over common colorimeters.

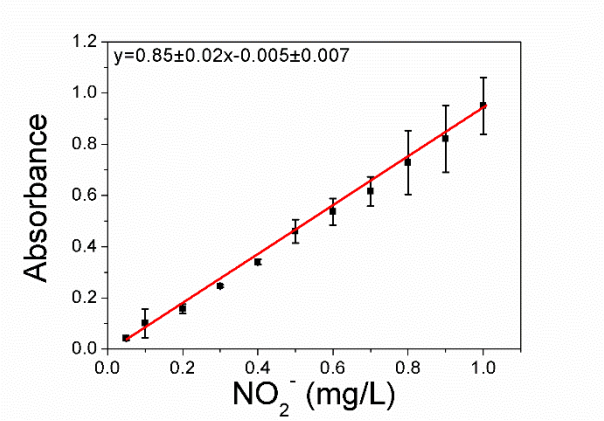

Figure 8.6. Calibration plot obtained using the colorimeter for several nitrite concentrations (n=3).

Once the smartphone system is properly validated and the modifications are set in the application (linear range, individual value limits, concentration equation…) the system was tested with completely different real samples to showcase its potential. First, benchtop analyses were performed. As environmental matrices water from river, sea and from a home aquarium were collected (river and sea were spiked with a known nitrite concentration). The spiked samples were prepared alike and measured with the two systems (smartphone and colorimeter). In this case, two different detectors were tested. Figure 8.7A shows the comparison between the nitrite concentrations obtained by the smartphone (blue) and the colorimeter (red). Result showed that the concentration obtained by both readout devices do not present differences and the device presented recovery rates of 78% and 84%, and the colorimeter presented 86% and 90% for river and sea-spiked samples, respectively (Table 8.1). Moreover, river and sea samples were also analyzed without spiking and the results showed concentrations below the limit of detection.

Tracking nitrite concentration is crucial to ensure the water quality of home aquarium systems and avoid fish decease. Therefore, nitrite concentration from three different home aquariums were measured using the proposed analytical system. Only one of the aquariums which was recently set (it requires ~20 days for bacteria to eliminate nitrite) presented relevant nitrite ion concentration.

Summarizing, the use of ALS demonstrates to be able to give reliable results competing with a common colorimeter in daily laboratory routines. On the other hand, the performance was

further tested against the standard methodology to quantify nitrite ion, ionic chromatography. Samples from a respirometer were measured by both methods (ALS smartphone and ionic chromatography) and compared. In this case, two analytical methods using different detection techniques were tested. Results demonstrated that there were no significant differences and showcased the potential use of this methodology to replace expensive and conventional analytical methodologies or standard methods.

Table 8.1. Comparison between the results obtained by the smartphone and the colorimeter for different samples (n=3) for same spiked samples analyzers.

Sample	Smartphone concentration (mg/L)	Recovery rate (%)	Colorimeter Concentration (mg/L)	Recovery rate (%)
River	0.193±0.003	78%	0.216±0.006	86%
Sea	0.210±0.004	84%	0.225±0.003	90%
Aq. 1	0.282±0.003	-	0.265±0.004	-
Aq. 2	Below LOD	-	Below LOD	-
Aq. 3	Below LOD	-	Below LOD	-

Finally, the feasibility of using this system for remote field analyses was also tested. Samples were collected and analyzed in-situ throughout a Ripoll river stretch (Figure 8.7C, Table 8.2). All field samples were spiked with a known nitrite concentration and analyzed by triplicate. In most cases the nitrite ion amount found was in correlation with the spiked (0.25 mg/L, Figure 8.7D). Nonetheless, one sample presented a higher relevant amount (sample was collected from a fountain next to the river). This sample was also analyzed without spiking and the results were also positive. However, no coloration was observed by naked eye (probably dispersed particles or microorganism dispersed the light causing interferences, which could be solved by filtering the sample with a syringe filter). Thanks to the use of a smartphone all the data analyzed (analyte, day, hour, location and concentration) was automatically recorded and sent to an online database.

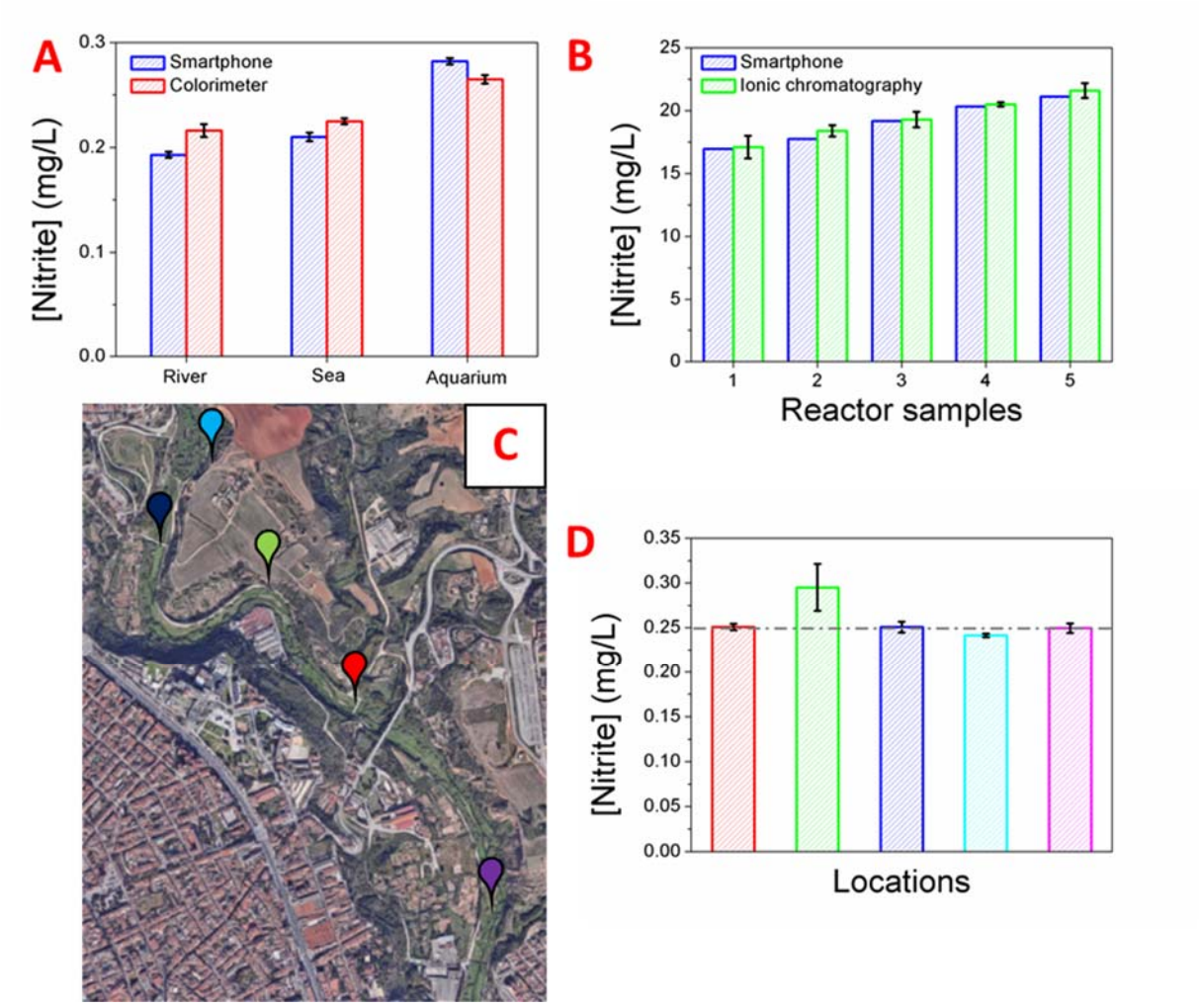

Figure 8.7. Real sample analyses. Nitrite ion concentration estimated by both readout platforms (A); smartphone (blue) and colorimeter (red) by two different detectors. Nitrite ion concentration estimated by two different analytical methods (B); smartphone (blue) and ionic chromatography (green). Ripoll river map with sample locations (C) and analysis results (D); histogram bar color agrees with map color.

Overall, a 3D-printed scaffold and ALSens application were developed to take advantage of smartphones as portable readout platforms for the quantification of nitrite ion in different required situations. Both, scaffold and smartphone application can be easily modified to cover a wide variety of optical-based analyses and adapt the system to other analytes. The analytical system has demonstrated its feasibility to replace conventional expensive equipment such as spectrophotometer and ionic chromatography. Moreover, its user-friendly design allows unskilled personnel to perform assays which extends its potential use for at home analyses (e.g. aquarium water quality or swimming pools control). Finally, in terms of price, the proposed readout platform (less 1€,considering that everyone has a smartphone) constitutes a relevant decrease of analysis equipment cost (hand-held colorimeter, 250-1500 €).

8.5. Statistics

Comparison of the performance of the smartphone ALS against the colorimeter and the ionic chromatograph was done following the procedure described in Quantitative Chemical Analysis, Daniel C. Harris, W. H. Free man and Company, California (2009). This comparison experiment was done measuring NO_2^- in multiple samples by both methods.

First, the difference between the two results for each sample is calculated (Table 9.2).

Table 9.2. Concentration values obtained by different measurement equipment or methods and the difference between them.

Samples	**Smartphone (mg/L)**	**Colorimeter (mg/L)**	**Difference**
River	0.193	0.216	0.023
Sea	0.21	0.225	0.015
Aquarium	0.282	0.265	-0.017
Mean	-	-	0.007
Standard deviation	-	-	0.021
Samples	**Smartphone (mg/L)**	**Ionic chromatography (mg/L)**	**Difference**
Reactor 1	16.96	17.1	-0.14
Reactor 2	17.75	18.4	-0.65
Reactor 3	19.2	19.3	-0.1
Reactor 4	20.34	20.5	-0.16
Reactor 5	21.13	21.4	-0.27
Mean	-	-	0.26
Standard deviation	-	-	0.22

Second, the mean value (**0.007/0.26**) and the standard deviation (**0.021/0.22**) of the differences is calculated, then t value is calculated with the following formula:

$$t_{calculated} = \frac{|\bar{d}|}{S_d}\sqrt{n}$$

Where $|\bar{d}|$ is the absolute value of the mean differences, S_d is the standard deviation of the differences and n is the number of samples measured.

If the t calculated (**0.6/2.63**) is lower than the t tabulated (**4.303/2.77**) the methods do not present significant differences.

8.6. Conclusion

The potential of the smartphone ALS was spotted. Ad-vantage of the versatility of 3D printing technology was explored to fabricate a 3D-printed readout scaffold adapt-able to fit a defined smartphone. The sensing system for nitrite ion quantification exhibited a sensitivity of -0.40 L/mg in an environmental relevant linear range of 0.05-1 mg/L and with a limit of detection of 0.01 mg/L. The readout platform was tested with real-spiked environmental samples giving reliable result in concordance with old-fashion equipment. Furthermore, the application was step-wise modified to finally work in different required analyses conditions; benchtop and field. A river walk measuring at several spots the spiked nitrite ion concentration demonstrated the massive potential of smartphone for field screening applications. Moreover, it is important to consider that by simply changing the readout platform size, the LED and/or reagents other relevant optical-based detected analytes can be measured and other smartphones or sample holders can be used.

8.7. References

(1) Tamm, C. O. *Nitrogen in Terrestrial Ecosystems*; 1991.

(2) Elser, J. J.; Bracken, M. E. S.; Cleland, E. E.; Gruner, D. S.; Harpole, W. S.; Hillebrand, H.; Ngai, J. T.; Seabloom, E. W.; Shurin, J. B.; Smith, J. E. Global Analysis of Nitrogen

and Phosphorus Limitation of Primary Producers in Freshwater, Marine and Terrestrial Ecosystems. *Ecol. Lett.* **2007**, *10* (12), 1135–1142.

(3) Gruber, N.; Galloway, J. N. An Earth-System Perspective of the Global Nitrogen Cycle. *Nature* **2008**, *451* (7176), 293–296.

(4) Galloway, J. D.; Townsend, A. R.; Erisman, J. W.; Bekunda, M.; Cai, Z.; Freney, J. R.; Martinelli, L. a; Seitzinger, S. P.; Sutton, M. a. Transformation of the Nitrogen Cycle. *Science (80-.).* **2008**, *320*, 889–892.

(5) Vinegar, P. I. N. The Toxicology of Nitrates and Nitrites with Particular Reference to the Potability of Water Supplies. *Analyst* **1961**, *86*, 517–519.

(6) Swann, P. F. The Toxicology of Nitrate, Nitrite and n-Nitroso Compounds. *J. Food Agric.* **1975**, *26*, 1761–1770.

(7) Lewis, W. M.; Morris, D. P. Toxicity of Nitrite to Fish: A Review. *Trans. Am. Fish. Soc.* **1986**, *115*, 183–195.

(8) Wang, Q.; Ma, S.; Huang, H.; Cao, A.; Li, M.; He, L. Highly Sensitive and Selective Spectrofluorimetric Determination of Nitrite in Food Products with a Novel Fluorogenic Probe. *Food Control* **2016**, *63*, 117–121.

(9) Li, X.; Zhu, Y.; Ma, Y.; Ren, H.; Wu, D.; Yang, Y.; Shao, Y.; Wei, X.; Zhao, J. Nitrite Optical Sensing from Core-Shell Structured Nanosensors Functionalized with Rhodamine Molecules. *J. Lumin.* **2018**, *200*, 225–232.

(10) Mehmeti, E.; Stanković, D. M.; Hajrizi, A.; Kalcher, K. The Use of Graphene Nanoribbons as Efficient Electrochemical Sensing Material for Nitrite Determination. *Talanta* **2016**, *159*, 34–39.

(11) Mani, V.; Periasamy, A. P.; Chen, S. M. Highly Selective Amperometric Nitrite Sensor Based on Chemically Reduced Graphene Oxide Modified Electrode. *Electrochem. commun.* **2012**, *17* (1), 75–78.

(12) Rastogi, P. K.; Ganesan, V.; Krishnamoorthi, S. A Promising Electrochemical Sensing Platform Based on a Silver Nanoparticles Decorated Copolymer for Sensitive Nitrite Determination. *J. Mater. Chem. A* **2014**, *2* (4), 933–943.

(13) Roda, A.; Michelini, E.; Zangheri, M.; Di Fusco, M.; Calabria, D.; Simoni, P. Smartphone-Based Biosensors: A Critical Review and Perspectives. *TrAC - Trends Anal. Chem.* **2016**, *79*, 317–325.

(14) Yang, K.; Peretz-Soroka, H.; Liu, Y.; Lin, F. Novel Developments in Mobile Sensing Based on the Integration of Microfluidic Devices and Smartphones. *Lab Chip* **2016**, *16*

(6), 943–958.

(15) Kassal, P.; Steinberg, M. D.; Steinberg, I. M. Wireless Chemical Sensors and Biosensors: A Review. *Sensors Actuators, B Chem.* **2018**, *266*, 228–245.

(16) Álvarez-Diduk, R.; Orozco, J.; Merkoçi, A. Paper Strip-Embedded Graphene Quantum Dots: A Screening Device with a Smartphone Readout. *Sci. Rep.* **2017**, *7* (1), 1–9.

(17) Lin, Y.; Gritsenko, D.; Feng, S.; Teh, Y. C.; Lu, X.; Xu, J. Detection of Heavy Metal by Paper-Based Microfluidics. *Biosens. Bioelectron.* **2016**, *83*, 256–266.

(18) Wang, H.; Li, Y. J.; Wei, J. F.; Xu, J. R.; Wang, Y. H.; Zheng, G. X. Paper-Based Three-Dimensional Microfluidic Device for Monitoring of Heavy Metals with a Camera Cell Phone. *Anal. Bioanal. Chem.* **2014**, *406* (12), 2799–2807.

(19) Zhu, H.; Sencan, I.; Wong, J.; Dimitrov, S.; Tseng, D.; Nagashima, K.; Ozcan, A. Cost-Effective and Rapid Blood Analysis on a Cell-Phone. *Lab Chip* **2013**, *13* (7), 1282–1288.

(20) Berg, B.; Cortazar, B.; Tseng, D.; Ozkan, H.; Feng, S.; Wei, Q.; Chan, R. Y. L.; Burbano, J.; Farooqui, Q.; Lewinski, M.; et al. Cellphone-Based Hand-Held Microplate Reader for Point-of-Care Testing of Enzyme-Linked Immunosorbent Assays. *ACS Nano* **2015**, *9* (8), 7857–7866.

(21) Dutta, S. Point of Care Sensing and Biosensing Using Ambient Light Sensor of Smartphone: Critical Review. *TrAC - Trends Anal. Chem.* **2019**, *110*, 393–400.

(22) Schmitz, T. Advantages of Packaging a Proximity Sensor with an Ambient Light Sensor https://www.digikey.com/en/articles/techzone/2012/aug/advantages-of-packaging-a-proximity-sensor-with-an-ambient-light-sensor.

(23) *Standard Methods for the Examination of Water and Wastewater*; American Water Works Association, Ed.; Washington DC, 1999.

(24) Small micropipettes https://www.indiamart.com/proddetail/mini-pen-pipette-15135410173.html.

(25) Appybuilder https://appybuilder.com/.

(26) Joshi, N. V. *Photoconductivity*; New York, 1970.

(27) Bose, A.; Sarkar, S.; Das, S. Helianthus – a Low Cost High Efficient Solar Tracking System Using AVR Microcontroller. *Int. J. Sci. Eng. Res.* **2012**, *3* (10), 1–6.

(28) Definition of limit of detecion https://goldbook.iupac.org/html/L/L03540.html.

CHAPTER 9

Conclusions

9.1. Conclusions

9.1.1. General conclusion about printing technologies

One-line pitch conclusion: In the near future, printing technologies will replace conventional fabrication methodologies of sensing platforms.

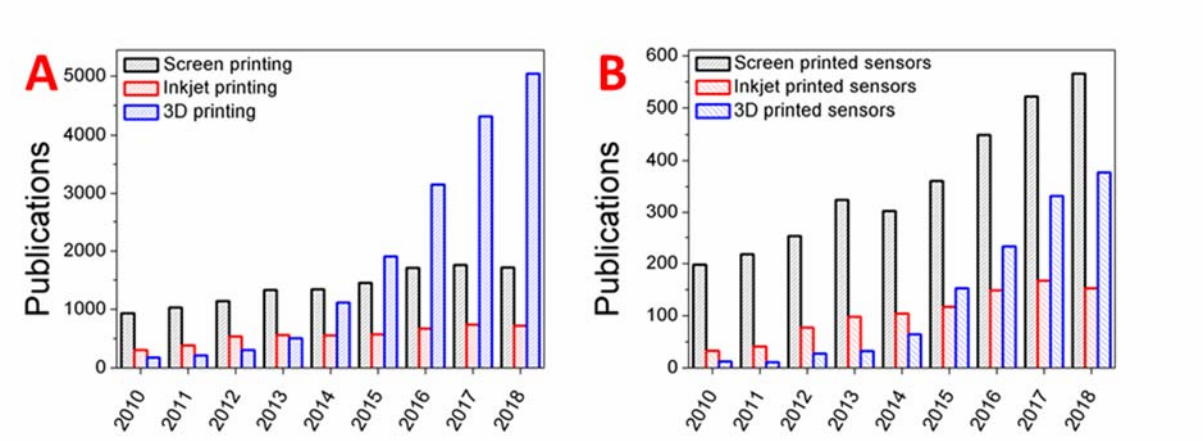

Figure 9.1. Publications per year of screen printing, inkjet printing and 3D printing (A). Publications per year of screen-printed sensors, inkjet-printed sensors and 3D-printed sensors (B).

Over the years, screen printing technique has been stablished as the commercial fabrication alternative to old-fashion bulky sensors. Several companies have emerged that are based on the fabrication and sold-out of this kind of sensors. Inkjet printing appeared several years ago; it becomes a substitute for screen-printed sensors with the advantage of avoiding the use of a mask and reduce waste. Although, inkjet printing presents great advantages compared with screen printing, their possibility to establish this technology for industrial purposes remains challenging considering the drawbacks presented by the ink stability. On the other hand, in the last years the appearance of 3D printing has constituted a paradigm shift in the production of functional parts replacing almost any other fabrication methodology. Scientific publications per year convey the future trend of printing techniques (Figure 9.1A) and their potential application in the analytical field (Figure 9.1B). In technological terms, 3D printing technology excels compared with its counterparts as its potential to be used in any required situation makes it suitable to be applied in any scientific or technical field. However, considering the trend in sensor production, screen-printed sensors will remain as the most published ones for at least five years until 3D-printed sensors exceed them.

9.1.2. Specific conclusions

Considering the experience gained throughout the experiments performed, some relevant specific conclusions were obtained:

- Specific requirements of monitoring devices have pushed the scientific community to propose novel fabrication methodologies. Unaddressed technological gaps found in traditional fabrication methods would be filled with printing technologies such as screen printing, inkjet printing and 3D printing. Printing technologies will solve the problems that environmental monitoring face and will become the standard technology to produce autonomous full deployable systems at a low cost.

- Second kind sulfide-selective electrodes have demonstrated their potential application in biotechnological and environmental fields. Moreover, they have shown good analytical behavior presenting Nernstian response when fabricated by screen printing and inkjet printing technologies with no relevant interferences found.

- Sulfide-selective electrode based on second-kind metallic electrode were able to be fabricated by two methodologies. Silver sulfide electrodeposition on top a silver layer or long-term deposition under basic conditions.

- Although inkjet printing technology is commonly used to produce disposable sensors, it has been demonstrated that inkjet-printed sensors can be used during routine assay up to 15 days. Moreover, if sensors are stored under certain required conditions they can be used for long periods of time.

- 3D printing technology allows to modify *in situ* the mask of screen-printed electrodes. Furthermore, the mask can also be used as electrode holder making this technology more suitable and easier to use than conventional screen printers.

- Thanks to the high versatility of 3D printing technology different platforms with different purposes can be fabricated at a really low cost. It has been extensively demonstrated its potential to produce relevant microfluidic platforms. In fact, it has also demonstrated its

potential to integrate electrochemical and optical detection therein a microfluidic platform. Besides, has been also exploited for the fabrication of bare holders (electrochemical cells, cuvette holders, optical alignments, etc).

- Traditional sensing principles/methodologies used in this work (second-kind electrodes, methyl thymol blue method and Griess-Ilosvay reaction) have demonstrated to be adaptable to new printing technologies and present reliable results in the quantification of biotechnological/environmental relevant chemical parameters.

- The combination of devices produced by means of printing technologies alongside with the development of personalized applications to use smartphones as readout platforms will suddenly change the stablished mindset in analytical chemistry.

9.1.3. Future perspective

Considering the unexplored potential of printing technologies, there is still a lot of work to do in the sensors and actuators field. First, there are many research laboratories that are producing new inks and filaments with different properties (mechanical, chemical and electrical) to reach new possible applications (*e.g.* graphene and graphite-based filaments have been recently developed for production of 3D-printed conductive devices). Second, the combination of two printing technologies will allow autonomous fabrication of full functional devices. For instance, the device itself can be fabricated by means of 3D printing whereas the electronic parts could be included by inkjet printing. Finally, new architectures of devices that could not be afforded until the appearance of this technologies have to come to the fore.

ANNEX

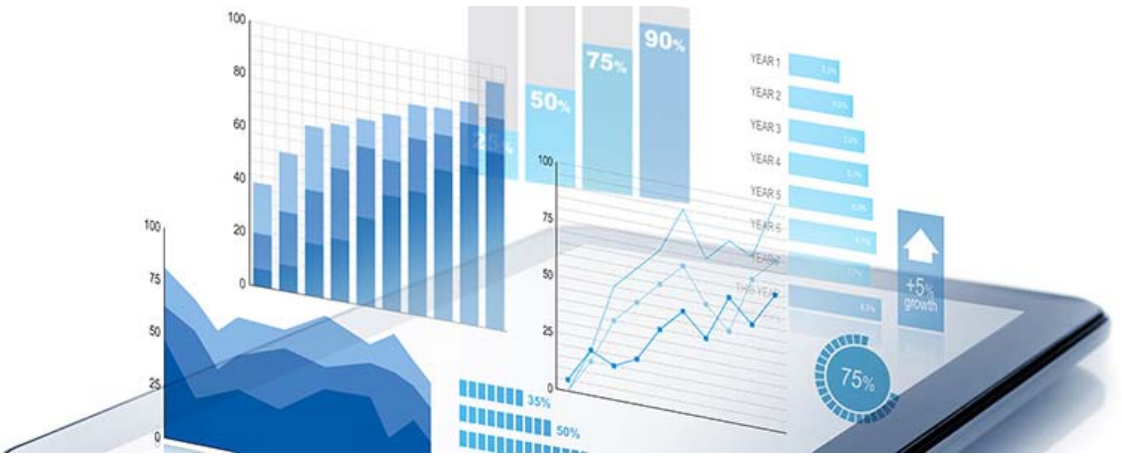
100
80
60
40
20
0
50%
75%
90%
YEAR 1
YEAR 2
YEAR 3
YEAR 4
YEAR 5
YEAR 6
100
75
50
25
0
35%
50%
75%

A.1. Statistics

All experiments suffer from some sort of variability. Thus, no experimental value can be drawn with certainty. Statistics help us to whether accept the obtain results or not. In this section we will discuss how to compare values obtained by the fabricated microfluidic devices *vs* a standard method.[1]

A.1.1. Mean and standard deviation

There are two equations (Equation A.1 and A.2) that will be used constantly across this section:

$$\boldsymbol{Mean} = \overline{\boldsymbol{x}} = \frac{\sum \boldsymbol{x_i}}{\boldsymbol{n_i}} \qquad \text{(Equation A.1)}$$

$$\boldsymbol{Standard\ deviation} = \boldsymbol{s_x} = \sqrt{\frac{\sum(\boldsymbol{x_i}-\overline{\boldsymbol{x}})^2}{\boldsymbol{n-1}}} \qquad \text{(Equation A.2)}$$

Where $\mathbf{x_i}$ are the measured values, $\mathbf{n_i}$ the number of times measured.

A.1.2. Means compared by t test

In analytical chemistry field we use the "t test" to compare a set of measurements with another to determine if they can be considered the same. Analytical chemist work under the hypothesis that two mean values that come from different set of measurements do not present significant differences. In this scenario, there are three cases that are handled in different manners:

A.1.2.1. Comparing measured result with a "known" value

A sample is measured several times. Then, the mean value and the standard deviations are calculated and compared with a mean standard value given with no standard deviation.

Calculate the mean value and add and subtract the confidence interval (Equation A.3). If the mean standard value lies between both calculated values your method does not differ significantly from the method used to get the mean standard value.

$$\bar{\boldsymbol{x}} + \frac{\boldsymbol{ts}}{\sqrt{\boldsymbol{n}}}, \bar{\boldsymbol{x}} - \frac{\boldsymbol{ts}}{\sqrt{\boldsymbol{n}}} \qquad \text{(Equation A.3)}$$

Where $\bar{\boldsymbol{x}}$ is the mean value, **t** is the tabulated **t student** value for n-1 degrees of freedom defined for a given confidence level, s is the standard deviation and n is the number of measures.

A.1.2.2. Comparing replicate measurements

A sample is measured several times with two different methods that give two means with their respective standard deviations.

First, F test (Equation A.4) tells whether two standard deviations significantly different from each other.

$$F_{calculated} = \frac{s_1^2}{s_2^2}, \quad s_1 > s_2 \qquad \text{(Equation A.4)}$$

Then two different cases can happen:

- **Both methods have the same precision:** if the F calculated is lower than the F tabulated both standard deviations obtained do not present significant differences.

  For two sets of data consisting of n_1 and n_2 measurements (with averages $\bar{x}_1 - \bar{x}_2$) we calculate a value of **t** with the following equation (Equation A.5):

$$t_{calculated} = \frac{|\bar{x}_1 - \bar{x}_2|}{S_{pooled}} \sqrt{\frac{n_1 n_2}{n_1 + n_2}} \qquad \text{(Equation A.5)}$$

  Where $|\bar{\boldsymbol{x}}_{\boldsymbol{1}} - \bar{\boldsymbol{x}}_{\boldsymbol{2}}|$ is the absolute value of the difference and $\mathbf{S_{pooled}}$ is a pooled standard deviation making use of both sets of data (Equation A.6):

$$S_{spooled} = \sqrt{\frac{s_1^2(n_1-1)+s_2^2(n_2-1)}{n_1+n_2-2}} \qquad \text{(Equation A.6)}$$

If the $\boldsymbol{t_{calculated}}$ is lower than the $\boldsymbol{t_{tabulated}}$ both results obtained do not present significant differences.

- **Both methods have different precision:** if the F calculated is higher than the F tabulated both standard deviations obtained present significant differences.

For two sets of data consisting of n_1 and n_2 measurements (with averages $\bar{x}_1 - \bar{x}_2$) we calculate a value of **t** with the following equation (Equation A.7):

$$t_{calculated} = \frac{|\bar{x}_1-\bar{x}_2|}{\sqrt{\frac{s_1^2}{n_1}+\frac{s_2^2}{n_2}}} \qquad \text{(Equation A.7)}$$

Then, $\boldsymbol{t_{calculated}}$ is compared with the $\boldsymbol{t_{tabulated}}$ with the following degrees of freedom (Equation A.8):

$$\boldsymbol{Degrees\ of\ freedom} = \frac{(s_1^2/n_1)+(s_2^2/n_2)^2}{\left(\frac{(s_1^2/n_1)^2}{n_1+1}+\frac{(s_2^2/n_1)^2}{n_2+1}\right)} - 2 \qquad \text{(Equation A.8)}$$

A.1.2.3. Comparing individual differences

Several samples are measured by two methods with no replicates. First, calculate de difference between both values measured with the two methods by each one of the samples and calculate the mean and standard deviation of these values.

Then we calculate a value of t with the following equation (Equation A.9):

$$t_{calculated} = \frac{|\bar{d}|}{s_d}\sqrt{n} \qquad \text{(Equation A.9)}$$

Where $|\bar{d}|$ is the absolute value of the mean differences, S_d is the standard deviation of the differences and **n** is the number of samples measured.

A.2. References

(1) Harris, D. *Quantitative Chemical Analysis*; California, 2009.